Title
Investigating the Neural Circuit for Carbon Dioxide Avoidance Behavior in Caenorhabditis elegans

Author
Carrillo, Mayra

Publication Date
2015

Peer reviewed|Thesis/dissertation

UNIVERSITY OF CALIFORNIA

Los Angeles

Investigating the Neural Circuit for Carbon Dioxide Avoidance Behavior in *Caenorhabditis elegans*

A dissertation submitted in partial satisfaction of the requirements for the degree of Doctor of Philosophy in Microbiology, Immunology, and Molecular Genetics

by

Mayra Alejandra Carrillo

2015

ABSTRACT OF THE DISSERTATION

Investigating the Neural Circuit for Carbon Dioxide Avoidance Behavior in *Caenorhabditis elegans*

by

Mayra Alejandra Carrillo

Doctor of Philosophy in Microbiology, Immunology, and Molecular Genetics

University of California, Los Angeles, 2015

Professor Elissa A. Hallem, Chair

Carbon dioxide (CO_2) is a byproduct of oxidative metabolism that can be sensed by different species including mammals, insects, and nematodes and can lead to both physiological and behavioral responses. In the free-living nematode *Caenorhabditis elegans* the behavioral response can be either avoidance or neutral to CO_2, indicating that the behavior is flexible. In this thesis, I investigated the neural basis of behavioral flexibility. We found that the CO_2 circuit can be modulated by diverse sensory neurons that respond to ambient oxygen (O_2), temperature, and food odor. Additionally, we identified two interneurons downstream of the CO_2-sensing BAG neurons, AIY and RIG, that have opposing roles in CO_2-evoked responses. A decrease in AIY activity and an increase in RIG activity promote appropriate avoidance behavior to CO_2 levels. Our results show that just like thermosensory and oxygen circuits, the CO_2 circuit can exhibit a network of multisensory integration to enable animals to generate flexible behaviors to changing environments.

The dissertation of Mayra Alejandra Carrillo is approved.

David G. Brooks

Peter J. Bradley

Alvaro Sagasti

Elissa A. Hallem, Committee Chair

University of California, Los Angeles

2015

DEDICATION

I dedicate this dissertation to my parents Pedro and Aurora Carrillo, and to all my friends and family. I thank them for all their support during graduate school. I would also like to dedicate this to all my past mentors and science teachers who inspired me to pursue a career in science. Mike Reynolds, Kent Smith, Victor and Brenna Tam, Robb Pagarigan, Raymond Wong, Brian Weist, and others. Thank you guys for giving me the opportunity to learn from you.

TABLE OF CONTENTS

LIST OF FIGURES

ACKNOWLEDGMENTS

First, I would like to acknowledge my PI Elissa Hallem for being a wonderful and excellent mentor. I hope I can inspire younger generations to become excited about science as she has inspired me. I would also like to acknowledge Manon L. Guillermin, my partner in crime, for equally contributing to this work, especially generating transgenic lines and calcium imaging data. This project would not be close to where it is now if it wasn't for her contributions.

I would like to acknowledge my funding sources, the NSF Graduate Research Fellowship and the Eugene Cota-Robles Fellowship for supporting me throughout graduate school. I would also like to thank the Hallem lab members for the feedback on this project and overall being the best group of people with restricted dietary needs anyone can ever work with. Thank you guys for being so awesome. I especially like to extend my gratitude to the members of my committee for giving valuable feedback on my progress and on this project.

Chapter 1 is a version of Carrillo, M.A. and Hallem, E.A. (2015) Gas sensing in nematodes. Mol. Neurobiol. 51: 919-931. Permission was granted by publisher for use in this thesis

Chapter 2 is a version of Carrillo, M.A., Guillermin, M.L., Rengarajan, S., Okubo, R.P., and Hallem, E.A. (2013). O_2-sensing neurons control CO_2 response in *C. elegans*. J. Neurosci. 33, 9675–9683.

Chapter 3 is in preparation for publication.

Chapter 4 is a version of Peña, J.M., Carrillo, M.A., and Hallem, E.A. (2015) Variation in the susceptibility of *Drosophila* to different entomopathogenic nematodes. Infect. Immun. 83, 1130-1138.

VITA

Education:

Bachelor of Science in Biological Sciences from University of California, Irvine, Irvine, CA.

September 2007 - June 2010

Associate of Arts in Liberal Arts from Los Angeles Mission College, Sylmar, CA

September 2000 - June 2003.

Academic Honors and Awards:

National Science Foundation Predoctoral Fellowship, 2010

Eugene Cota-Robles Fellowship, 2010

Sigma Xi Poster Presentation Award in Cell Biology, 2009

Dean's Honor List, University of California Irvine, 2008

Publications:

Peña, J.M., Carrillo, M.A., and Hallem, E.A. (2015) Variation in the susceptibility of *Drosophila* to different entomopathogenic nematodes. Infect. Immun. 83, 1130-1138.

Carrillo, M.A. and Hallem, E.A. (2015) Gas sensing in nematodes. Mol. Neurobiol. 51: 919-931

Carrillo, M.A., Guillermin, M.L., Rengarajan, S., Okubo, R.P., and Hallem, E.A. (2013). O_2-sensing neurons control CO_2 response in *C. elegans*. J. Neurosci. 33, 9675–9683.

Smith, K.A., Meisenburg, B.L., Tam, V.L., Pagarigan, R.R., Wong, R., Joea, D.K., Lantzy, L., Carrillo, M.A., Gross, T.M., Malyankar, U.M., et al. (2009). Lymph node- targeted

immunotherapy mediates potent immunity resulting in regression of isolated or metastatic human papillomavirus-transformed tumors. Clin. Cancer Res. 15, 6167–6176.

Wong, R.M., Smith, K.A., Tam, V.L., Pagarigan, R.R., Meisenburg, B.L., Quach, A.M., Carrillo, M.A., Qiu, Z., and Bot, A.I. (2009). TLR-9 signaling and TCR stimulation co- regulate CD8(+) T cell-associated PD-1 expression. Immunol. Lett. 127, 60–67.

Presentations:

Peña, J.M., Carrillo, M.A., and Hallem, E.A. Immune response of Drosophila to entomopathogenic nematode infection. Presented at the Southern California Eukaryotic Pathogens Symposium, UC Riverside 2014.

Carrillo, M.A., Guillermin, M.L., Rengarajan, S., Okubo, R.P., and Hallem, E.A. O2- sensing neurons control CO2 response in C. elegans. Presented at the 19th International *C. elegans* meeting, UCLA 2013.

Carrillo, M.A. Investigating the regulation of carbon dioxide response in *C. elegans*. Worm Club Meeting, UCLA 2013.

Carrillo, M.A. Investigating the regulation of carbon dioxide response in *C. elegans*. Synapse to Circuit seminar, UCLA 2012.

Carrillo, M.A., Sharp, K., Bardwell, L. The role of docking sites in yeast MAPK cascade signaling specificity. Sigma Xi Annual Meeting and International Research Conference, Houston 2009

Chapter 1:

Introduction

Mol Neurobiol
DOI 10.1007/s12035-014-8748-z

Gas Sensing in Nematodes

M. A. Carrillo · E. A. Hallem

Received: 11 April 2014 / Accepted: 7 May 2014

Abstract Nearly all animals are capable of sensing changes in environmental oxygen (O_2) and carbon dioxide (CO_2) levels, which can signal the presence of food, pathogens, conspecifics, predators, or hosts. The free-living nematode *Caenorhabditis elegans* is a powerful model system for the study of gas sensing. *C. elegans* detects changes in O_2 and CO_2 levels and integrates information about ambient gas levels with other internal and external cues to generate context-appropriate behavioral responses. Due to its small nervous system and amenability to genetic and genomic analyses, the functional properties of its gas-sensing microcircuits can be dissected with single-cell resolution, and signaling molecules and natural genetic variations that modulate gas responses can be identified. Here, we discuss the neural basis of gas sensing in *C. elegans,* and highlight changes in gas-evoked behaviors in the context of other sensory cues and natural genetic variations. We also discuss gas sensing in other free-living nematodes and parasitic nematodes, focusing on how gas-sensing behavior has evolved to mediate species-specific behavioral requirements.

Keywords Oxygen (O_2) response · Carbon dioxide (CO_2) response-aerotaxis · Chemotaxis · Nematodes · Gas sensing

Introduction

Nearly all animals are capable of sensing changes in environmental concentrations of oxygen (O_2) and carbon dioxide (CO_2). Aerobic organisms require O_2 for cellular respiration and emit CO_2 as a by-product of respiration. Fluctuations in ambient O_2 or CO_2 levels can signal the presence of food, pathogens, conspecifics, predators, or hosts. Moreover, prolonged exposure to hypoxia, hyperoxia, or hypercapnia can result in cell damage, altered neural activity, and ultimately death [1–4]. Thus, the ability to respond appropriately to changes in environmental O_2 and CO_2 levels is essential for survival. *Caenorhabditis elegans* is a powerful system for the study of the neural basis of gas sensing. It displays robust responses to both O_2 and CO_2. Moreover, it has a small nervous system composed of 302 neurons and approximately 6,500 synaptic connections [5, 6], and is amenable to precise circuit manipulation due to its optical transparency, stereotyped anatomy, and extensive genetic and genomic toolkits. The molecular pathways that regulate circuit function and the general principles of circuit design are in many cases conserved between mammals and nematodes [7–9]. A better understanding of gas-sensing circuits in *C. elegans* is likely to enhance our understanding of similar circuits in the mammalian brain.

M. A. Carrillo · E. A. Hallem (✉)
Department of Microbiology, Immunology, and Molecular Genetics, University of California, Los Angeles, Los Angeles, CA 90095, USA
e-mail: ehallem@microbio.ucla.edu

Published online: 08 June 2014

The Neural Basis of O_2 Response by *C. elegans*

Behavioral Responses of *C. elegans* to O_2

C. elegans is capable of surviving at a wide range of O_2 concentrations. For example, worms of all developmental stages can survive for up to 24 h under anoxic conditions, although movement and development cease [10]. Worms can also survive for multiple generations at 100 % O_2 [10]. Under hypoxic conditions, worms cease feeding and move away from a food source [10]. Thus, worms appear to forgo food and initiate exploratory behavior in an attempt to meet their O_2 requirements.

C. elegans also exhibits aerotaxis behavior. When wild-type N2 animals are removed from food and placed in an O_2

gradient ranging from 0 % O_2 to 21 % O_2, they migrate to 5–12 % O_2, with approximately 10 % O_2 being the preferred concentration [11–13] (Fig. 1a). Aerotaxis is modulated by the presence of food such that the hyperoxia avoidance exhibited by N2 animals off food is greatly reduced in the presence of food [11, 12] (Fig. 1a). O_2 response is also modulated by hypoxia, since worms cultured at 1 % O_2 prefer lower O_2 concentrations and exhibit hyperoxia avoidance even in the presence of food [13, 15]. Thus, aerotaxis behavior is plastic and can be modulated by environmental conditions.

Molecular and Cellular Basis of O_2 Response

O_2 is sensed by a distributed network of sensory neurons. The primary O_2-sensing neurons are the AQR, URX, and BAG neurons in the head and the PQR neuron in the tail [11, 14, 16]. The processes of the AQR, URX, and PQR neurons are directly exposed to the pseudocoelomic body fluid, while the processes of the BAG neurons terminate at the tip of the nose but are not directly exposed to the external environment [5]. A number of other sensory neurons also contribute to O_2-evoked behaviors, including the putative O_2-sensing neurons SDQ, ALN, PLN; the nociceptive neurons ASH and ADL; and the serotonergic neuron ADF [12, 17].

O_2 detection is mediated by a family of soluble guanylate cyclases (sGCs) and the cGMP-gated cation channel TAX-2/TAX-4 [11, 13, 14, 18]. The sGCs are expressed in O_2-sensing neurons [11–14, 16, 18] and multiple lines of evidence indicate that they function as O_2 receptors: GCY-35 directly binds O_2 [11], the expression of GCY-35 and GCY-36 in the AWB olfactory neuron is sufficient to convert AWB into an O_2-sensing neuron [13], and GCY-35 and GCY-36 are required for hyperoxia avoidance [11, 12]. Different sGCs in *C. elegans* are expressed in different subsets of O_2-sensing neurons and mediate distinct O_2 responses. For example, URX neurons are activated by increasing O_2 levels and require GCY-35 and GCY-36, while BAG neurons are activated by decreasing O_2 levels and require GCY-31 and GCY-33 [14] (Fig. 1b). Misexpression of GCY-35 in BAG neurons lacking *gcy-31* and *gcy-33* causes them to be activated by O_2 increases, indicating that it is the sGC rather than the neuron that determines O_2 response specificity [14]. sGCs also function as O_2 receptors in the fruit fly *Drosophila melanogaster* [19]; thus, the molecular basis of O_2 detection appears to be conserved in nematodes and insects.

The response of AQR, PQR, and URX to O_2 increases involves both phasic and tonic components. In response to an increase in ambient O_2 from 7 to 21 %, these neurons exhibit

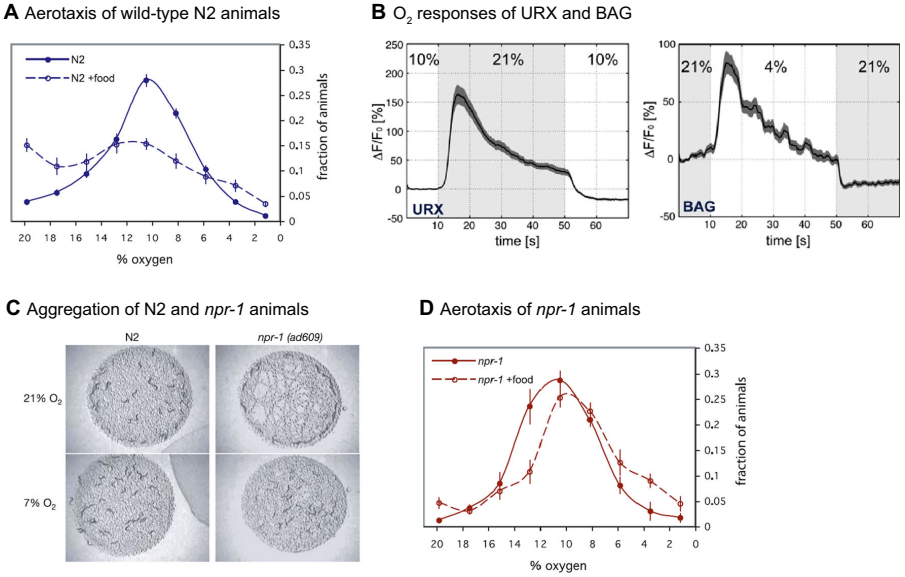

Fig. 1 Responses of *C. elegans* to O_2. **a** Aerotaxis of wild-type N2 animals. Animals tested off food migrate to 10 % O_2, while animals tested on food no longer display hyperoxia avoidance. Reproduced from Chang et al., 2006 [12]. **b** Responses of URX and BAG neurons to changes in O_2 levels. URX neurons respond to O_2 increases, while BAG neurons respond to O_2 decreases. Neural activity was monitored using the calcium indicator G-CaMP. Reproduced with permission from Zimmer et al., 2009 [14]. **c** Aggregation of N2 and *npr-1(lf)* animals. N2 animals exhibit solitary feeding and distribute over the surface of a bacterial lawn at both high and low O_2. *npr-1(lf)* animals exhibit aggregation and bordering at high O_2, but solitary feeding at low O_2, reproduced with permission from Gray et al., 2004 [11].**d** Aerotaxis of *npr-1(lf)* animals. *npr-1(lf)* animals Respond similarly to O_2 both on and off food. Reproduced from Chang et al., 2006 [12]

an initial peak of activation followed by sustained activity that lasts until O_2 levels drop [20, 21]. The tonic activity of these neurons results in sustained changes in downstream interneurons and sustained behavioral responses. For example, high O_2 results in high tonic activity of the downstream RMG and AUA interneurons and rapid movement on food, while low O_2 results in low activity of RMG and AUA and slow movement on food [20]. Thus, *C. elegans* can modify its behavior according to changes in ambient O_2 through tonically signaling sensory neurons.

Context-dependent modulation of O_2 response occurs via a number of different signaling pathways. For example, the hyperoxia avoidance on food exhibited by worms cultivated under hypoxic conditions is mediated by hypoxia inducible factor-1 (HIF-1), since *hif-1* mutants cultivated at low O_2 do not show hyperoxia avoidance on food [15]. Moreover, activation of the HIF-1 pathway by hypoxia appears to reconfigure the O_2 circuit such that only a subset of the neurons involved in O_2 response under normoxic conditions remain involved in O_2 response under hypoxic conditions [13, 15]. Food also modulates the O_2 circuit via TGF-β and serotonin signaling pathways [12]. Animals that lack the TGF-β gene *daf-7* show robust hyperoxia avoidance on and off food, suggesting that TGF-β signaling is required for the suppression of hyperoxia avoidance on food in N2 animals [12]. *daf-7* mutants also show increased expression of the tryptophan hydroxylase gene *tph-1*, which is required for serotonin biosynthesis [22], in the ADF neurons. Overexpression of *tph-1* in ADF neurons in N2 animals results in hyperoxia avoidance on food, suggesting that *daf-7* suppresses hyperoxia avoidance on food by inhibiting serotonin production in ADF neurons [12]. However, the precise mechanisms by which these signaling pathways reconfigure the O_2 circuit remain to be elucidated.

Regulation of O_2 Response by *npr-1*

O_2 response is also regulated by the polymorphic neuropeptide receptor NPR-1, a G protein-coupled receptor homologous to the mammalian neuropeptide Y (NPY) receptor [23]. The N2 wild-type laboratory strain contains a high-activity allele of *npr-1*, while the Hawaii (HW) strain and other wild isolates contain a low-activity allele of *npr-1* [23, 24]. Animals with the *npr-1(N2)* allele are solitary feeders that disperse on a bacterial lawn, while animals with the *npr-1(HW)* allele or an *npr-1* loss-of-function (*lf*) allele are social feeders that aggregate around the border of a bacterial lawn [11, 23] (Fig. 1c). NPR-1 regulates aggregation and bordering via the O_2 circuit, since *npr-1(lf)* animals exhibit solitary feeding at low O_2 and *gcy-35*; *npr-1(lf)* animals exhibit solitary feeding at both high and low O_2 [11, 13, 17, 18] (Fig. 1c). *npr-1(lf)* animals also exhibit robust hyperoxia avoidance on food (Fig. 1d), and ablation of the O_2-sensing AQR, PQR, and URX neurons in *npr-1(lf)* animals abolishes hyperoxia avoidance [11, 12]. Thus, NPR-1 regulates aggregation, bordering, and aerotaxis by modulating the activity of the O_2 circuit.

Aggregation behavior is controlled not only by the O_2-sensing neurons but also by the nociceptive ASH and ADL neurons and the pheromone-sensing ASK neurons [7, 17, 25]. URX, ASH, ADL, and ASK form gap junctions with a pair of interneurons called the RMG neurons [5, 6]. NPR-1 acts in RMG to decrease its activity, which in turn modulates sensory neuron activity and promotes solitary feeding [7]. Thus, NPR-1 coordinately regulates the activity of multiple classes of chemosensory neurons to control aggregation behavior.

Regulation of O_2 Response by *glb-5*

O_2-evoked behavior is also controlled by the polymorphic neuroglobin gene *glb-5,* which regulates responses to small changes in ambient O_2 levels [24, 26]. HW animals and most other wild isolates contain a high-activity allele of *glb-5*, whereas N2 animals and a few wild isolates contain a low-activity allele of *glb-5* [24, 26]. Animals containing the *glb-5(HW)* and *npr-1(HW)* alleles show a dramatic reduction in crawling speed as O_2 levels drop from 21 to 19.2 %, whereas animals containing the *glb-5(N2)* allele and either the *npr-1(HW)* allele or the *npr-1(N2)* allele do not [26]. GLB-5 is expressed in O_2-sensing neurons and increases their calcium responses to small changes in O_2. For example, URX neurons of animals containing the *glb-5(HW)* and *npr-1(HW)* alleles are significantly activated by O_2 increases from 20 to 21 %, whereas URX neurons of animals containing the *glb-5(N2)* and *npr-1(HW)* alleles are not [24]. Thus, GLB-5 acts in the O_2-sensing neurons to sensitize animals to small changes in ambient O_2 [24, 26].

The Neural Basis of CO_2 Response by *C. elegans*

Behavioral Responses of *C. elegans* to CO_2

Two types of behavioral assays have been used to assay the response of *C. elegans* to environmental CO_2. In an acute CO_2 assay, the head of an individual animal is exposed to a CO_2 stimulus, and the animal is given 4 s to respond [27–31]. In a CO_2 chemotaxis assay, a population of animals is allowed to navigate in a CO_2 gradient, and the distribution of animals at the end of the assay is determined [31–33]. Both assays indicate that *C. elegans* responds robustly to CO_2. In the acute assay, exposure of a forward-moving animal to CO_2 causes the animal to reverse directions [27–31]. In the chemotaxis assay, animals migrate away from the CO_2 source, indicating they are repelled by CO_2 [31–33] (Fig. 2a). *C. elegans* adults respond to CO_2 concentrations as low

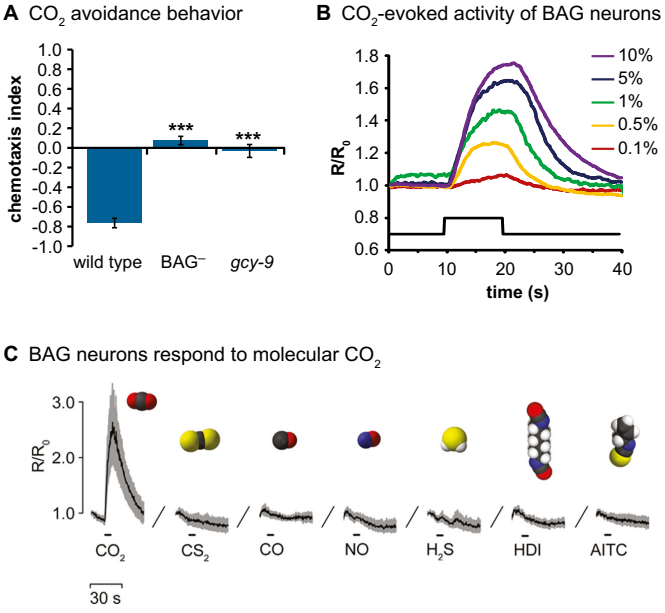

Fig. 2 Responses of *C. elegans* to CO_2. **a** Wild-type N2 animals avoid CO_2 in a chemotaxis assay, while BAG-ablated animals and *gcy-9* mutant animals do not respond to CO_2. Reproduced from Carrillo et al., 2013 [31]. **b** BAG neurons respond to CO_2 across concentrations. Neural activity was monitored using the calcium indicator yellow cameleon YC3.60. Reproduced from Hallem et al., 2011 [28]. **c** BAG neurons respond to molecular CO_2 but do not respond to other small molecules. Reproduced with permission from Smith et al., 2013 [34]

as 1 %, indicating that even low levels of CO_2 are sufficient to evoke an avoidance response [27, 32].

The response of *C. elegans* adults to CO_2 is modulated by nutritional status: well-fed animals avoid CO_2 on and off food, while food-deprived animals suppress CO_2 avoidance and become slightly attracted to CO_2 [27, 32]. The response of *C. elegans* to CO_2 is also dependent on the life stage of the animal. Under unfavorable environmental conditions such as the absence of food, *C. elegans* arrests development at the dauer larval stage [35]. Unlike adults, *C. elegans* dauers are strongly attracted to CO_2 [36]. Thus, CO_2 response depends on nutritional status and developmental stage.

Molecular and Cellular Basis of CO_2 Response

CO_2 response is mediated primarily by the BAG neurons in the head. BAG-ablated adults and dauers do not respond to CO_2 in multiple assays [27, 28, 31, 36] (Fig. 2a). Calcium imaging studies have revealed that BAG neurons are activated by CO_2 across concentrations, suggesting they are CO_2-detecting sensory neurons [28, 33] (Fig. 2b). The interneurons that are required downstream of BAG for CO_2-evoked behavior have not yet been identified.

CO_2 detection by BAG neurons is mediated by a cGMP signaling pathway that includes the receptor guanylate cyclase GCY-9 and the cGMP-gated cation channel TAX-2/TAX-4 [27–29, 32, 33] (Fig. 2a). GCY-9 appears to be expressed primarily in BAG neurons [29-30] and is sufficient to confer CO_2-evoked calcium responses on other sensory neurons that use cGMP signaling, suggesting it is a CO_2 receptor [29]. A receptor guanylate cyclase, GC-D, has also been implicated in CO_2 sensing in rodents [37–39], suggesting that similar mechanisms of CO_2 detection operate in mammals.

A recent study examined the response properties of isolated BAG neurons in cell culture and found that they respond to CO_2, thus confirming that the CO_2-evoked activity of BAG neurons is cell-intrinsic [34]. BAG neurons are activated by both molecular CO_2 and acid in a *gcy-9*-dependent manner. Bicarbonate and other small molecules such as carbon monoxide, carbon disulfide, and nitric oxide do not activate BAG neurons [34] (Fig. 2c). Thus, the BAG neurons appear to be specific detectors of CO_2, acid, and O_2.

The extent to which sensory neurons other than BAG contribute to CO_2-evoked behavior in *C. elegans* remains unclear. In some studies, BAG-ablated animals retained some responsiveness to CO_2, suggesting that other neurons can mediate CO_2 response under certain assay conditions [33, 40]. In these studies, the AFD thermosensory neurons, ASE gustatory neurons, and O_2-sensing AQR, PQR, and URX neurons also contributed to CO_2 avoidance. Animals lacking these neurons showed decreased CO_2 avoidance, and expressing the cGMP-gated cation channel subunit gene *tax-2* in these neurons in a *tax-2* mutant background partially rescued the CO_2 avoidance defect of *tax-2* mutants [33]. The AFD and ASE neurons were also found to respond to CO_2 by calcium imaging. AFD neurons showed a small decrease in

calcium levels upon CO_2 exposure and a stronger phasic increase in calcium levels upon CO_2 removal, while the ASE neurons showed a small tonic response to CO_2 [33] (Fig. 3a–c). Moreover, the behavioral response to low CO_2 concentrations was modulated by temperature. For example, compared to animals cultivated at 22 °C and assayed at 22 °C, animals cultivated at 22 °C and assayed at 15 °C showed a more robust response to 1 % CO_2, while animals cultivated at 15 °C and assayed at 22 °C showed a reduced response [40] (Fig. 3d). Cultivation at 15 °C also altered the calcium response of AFD neurons [40] (Fig. 3e), suggesting that the altered response properties of AFD may contribute to the temperature-dependent regulation of CO_2 response. However, other studies using different imaging conditions have not observed CO_2-evoked activity in AFD and ASE [29, 31, 34], and thus, the precise role of these neurons in mediating CO_2 response remains unclear.

Nutritional status modulates CO_2 avoidance via the insulin and TGF-β pathways. Adults that lack the insulin receptor gene *daf-2* or the TGF-β gene *daf-7* do not avoid CO_2 [27, 32], suggesting that activity of both pathways in well-fed adults is required for CO_2 avoidance. Moreover, mutation of downstream effectors of insulin and TGF-β signaling restores CO_2 avoidance to starved animals [27]. The BAG neurons of *daf-2* and *daf-7* mutants respond normally to CO_2, indicating that insulin and TGF-β signaling are not required for CO_2 detection [28]. The mechanism by which they regulate activity of the CO_2 circuit to confer plasticity in response to nutritional cues remains unclear.

CO_2 Response is Regulated by *npr-1*, *glb-5*, and Ambient O_2

CO_2 response is regulated by *npr-1* and ambient O_2 levels [27, 31, 32, 40]. Animals containing the *npr-1(N2)* allele avoid CO_2 regardless of ambient O_2 levels, whereas animals containing the *npr-1(HW)* or *npr-1(lf)* alleles avoid CO_2 at low O_2 but are neutral to CO_2 at high O_2 [31, 40] (Fig. 4a). The fact that the HW allele of *npr-1* is the natural variant [24] suggests that regulation of CO_2 response by O_2 is likely to occur in natural populations.

At the circuit level, NPR-1 acts in the O_2-sensing URX neurons to regulate CO_2 response [31, 40] (Fig. 4a–c). In *npr-1(lf)* animals, URX neurons are tonically active at high O_2 and their activity inhibits CO_2 avoidance. In N2 animals, NPR-1 reduces URX neuron activity, and thereby enables CO_2 avoidance [31, 40]. Mutation of the O_2 receptor gene *gcy-35* restores CO_2 response to *npr-1(lf)* animals at high O_2, indicating that the activation of URX by high O_2 is required for inhibition of CO_2 avoidance [31]. Two FMRFamide-like neuropeptide genes that express in URX, *flp-8* and *flp-19*, are required for the inhibition of CO_2 avoidance in *npr-1* animals [31] (Fig. 4b). Taken together, these results suggest a model in

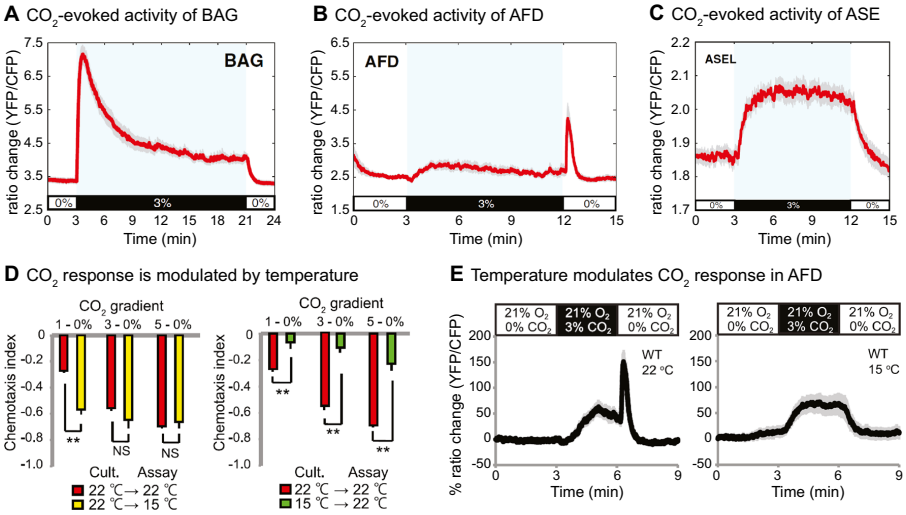

Fig. 3 CO_2 response by *C. elegans* is modulated by temperature. **a**–**c** Responses of BAG, AFD, and ASE neurons to CO_2. Under at least some imaging conditions, AFD neurons respond to CO_2 removal and ASE neurons respond to CO_2 addition. The CO_2-evoked responses of AFD and ASE are smaller than the CO_2-evoked responses of BAG. Reproduced with permission from Bretscher et al., 2011 [33]. **d** CO_2 chemotaxis behavior can be modulated by cultivation temperature. Reproduced from Kodama-Namba et al., 2013 [40]. **e** Temperature modulates CO_2 response in AFD by eliminating the response to CO_2 removal. Reproduced from Kodama-Namba et al., 2013 [40]

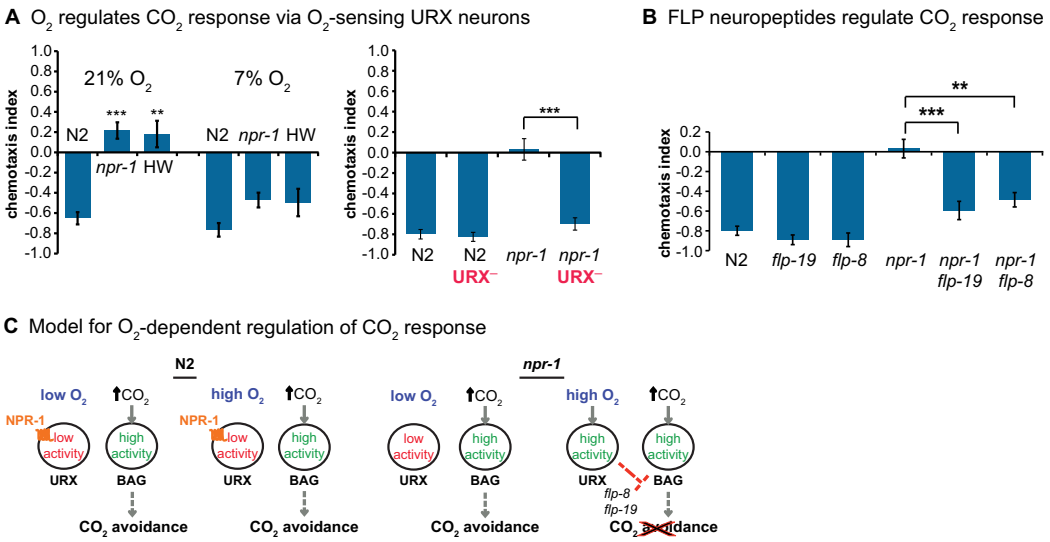

Fig. 4 CO_2 response by *C. elegans* is modulated by ambient O_2. **a** O_2 regulates CO_2 response via the URX neurons. *npr-1(lf)* and HW animals do not avoid CO_2 at 21 % O_2 but avoid CO_2 at 7 % O_2 (*left*). *npr-1(lf)* animals lacking URX neurons (as well as AQR and PQR neurons) avoid CO_2 at 21 % O_2 (*right*). **b** Neuropeptide signaling regulates CO_2 avoidance. Mutation of the URX-expressed neuropeptide genes *flp-8* and *flp-19* restores CO_2 avoidance to *npr-1(lf)* animals. **c** A model for O_2-dependent regulation of CO_2 response. In N2 animals, NPR-1 maintains URX in a low activity state, thus enabling CO_2 avoidance. In *npr-1(lf)* animals, reduced URX activity at low O_2 allows CO_2 avoidance, while increased URX activity at high O_2 blocks CO_2 avoidance. FLP-8 and FLP-19 neuropeptides may mediate inhibition of CO_2 avoidance by URX. Reproduced from Carrillo et al., 2013 [31]

which URX neurons inhibit CO_2 avoidance at high O_2 via a neuropeptide signaling pathway (Fig. 4c). The RIA interneurons, which are downstream of both BAG and URX [5, 6], display CO_2-evoked activity and are required for O_2-dependent regulation of CO_2 response at low but not high CO_2 levels [40]. Thus, URX may modulate CO_2 response at least in part via the RIA interneurons.

The *glb-5* locus also regulates CO_2 response. Animals containing the *glb-5(HW)* allele in the *npr-1(lf)* background show enhanced CO_2 avoidance relative to *npr-1(lf)* animals at both high and low O_2 concentrations [40]. In addition, animals containing the *glb-5(HW)* and *npr-1(lf)* alleles show reduced URX neuron activity relative to *npr-1(lf)* animals in response to an increase from 7 % O_2 to 21 % O_2 [40]. These results raise the possibility that GLB-5 enhances CO_2 avoidance by reducing URX neuron activity at high O_2, thereby reducing URX-mediated inhibition of the CO_2 circuit.

Physiological Responses of *C. elegans* to Hypoxia, Hyperoxia, and Hypercapnia

Exposure to hypoxia, hyperoxia, and hypercapnia elicits physiological as well as behavioral changes. The responses of *C. elegans* to prolonged hypoxia and hyperoxia have been reviewed elsewhere [41–44], so we focus here on physiological responses to hypercapnia. Long-term exposure to CO_2 levels above 9 % slows development, reduces fertility, and increases lifespan [45, 46]. CO_2-induced lifespan extension appears to be independent of insulin signaling, since *daf-2* mutants show an increased lifespan in the presence of 19 % CO_2 [45]. Lifespan may be regulated in part by the BAG neurons, since BAG-ablated animals have slightly increased lifespans relative to wild-type animals [46]. The reduction in fertility induced by elevated CO_2 levels appears to be due in part to the activation of the c-Jun N-terminal kinase (JNK) signaling pathway, since it can be partly rescued by mutation of the JNK homolog genes *jnk-1* and *kgb-2* [47]. Thus, conserved signaling pathways operate in *C. elegans* to mediate the long-term physiological effects of hypercapnia.

Development of Gas-Sensing Neurons in *C. elegans*

The gas-sensing neurons are specified by a network of transcription factors that include the aryl hydrocarbon receptor AHR-1, the ETS (E-twenty six)-domain winged helix-turn-helix protein ETS-5, and the SoxD transcription factor EGL-13. Development of the O_2-sensing URX, AQR, and PQR neurons requires AHR-1 and its transcriptional partner, the

aryl hydrocarbon receptor associated protein AHA-1 [48, 49]. The *ahr-1* and *aha-1* genes are coexpressed in O_2-sensing neurons, and mutating them suppresses the aggregation behavior of *npr-1* animals, suggesting they are required for proper function of O_2-sensing neurons. Moreover, AHR-1 regulates sGC expression in O_2-sensing neurons, indicating that it is required for their normal differentiation [48, 49].

Development of the O_2-/CO_2-sensing BAG neurons requires ETS-5 [29, 30]. The *ets-5* gene is expressed in BAG neurons [28–30] and is required for the expression of the BAG-specific gene battery, including the CO_2 receptor gene *gcy-9* and the O_2 receptor genes *gcy-31* and *gcy-33* [29, 30]. *ets-5* mutants do not show CO_2-evoked calcium responses in BAG and do not display behavioral responses to CO_2 [29, 30]. Thus, ETS-5 is required for normal differentiation of BAG neurons.

A third transcription factor required for gas neuron development is the SoxD transcription factor EGL-13 [50]. *egl-13* is expressed in BAG and URX neurons, and is required for the expression of the terminal gene batteries of both neuron classes as well as for behavioral responses to changes in O_2 and CO_2 levels. Expression of *egl-13* is regulated by ETS-5 in BAG neurons and AHR-1 in URX neurons, and EGL-13 acts in partially parallel pathways with ETS-5 or AHR-1 to control BAG or URX neuron cell fate, respectively. Thus, EGL-13 acts in combination with neuron-specific transcription factors to specify the distinct fates of O_2- and CO_2-sensing neurons [50]. Whether homologs of these transcription factors control the development of gas-sensing neurons in other organisms remains to be determined.

Ecological Implications of Gas Sensing in *C. elegans*

C. elegans and other *Caenorhabditis* species colonize fallen rotting fruit and stems of herbaceous plants, where they feed and proliferate in large numbers [51]. In this environment, nematodes are likely to encounter fluctuating levels of O_2 and CO_2 while foraging for food. *C. elegans* exhibits foraging decisions, selecting high-quality food and moving away from bacteria that are difficult to eat [52]. A number of recent studies have provided insight into how gas sensing regulates foraging behavior.

As described above, the *npr-1* gene regulates O_2 and CO_2 response as well as foraging behavioral traits such as aggregation and bordering [11, 13, 17, 18, 23, 27, 32]. *npr-1* also regulates food leaving, a behavior in which an animal migrates away from an existing bacterial food source [53–56]. *npr-1(HW)* animals show a higher rate of food leaving than *npr-1(N2)* animals [53–56]. NPR-1 acts in the RMG interneurons to regulate food leaving, indicating that the same circuit that regulates O_2 response, pheromone response, and aggregation also regulates food leaving [7, 57]. Aggregation, bordering, and food leaving are all increased at high O_2 in *npr-1(lf)* animals [11, 56, 57], and food leaving is increased at high CO_2 in N2 animals [56]. Moreover, food leaving by *npr-1(lf)* animals is reduced by mutation of the O_2 receptor gene *gcy-35,* indicating a direct link between food leaving and gas sensing [56]. Thus, multiple aspects of foraging are regulated by gas sensing.

Another regulator of foraging is the naturally polymorphic gene *tyra-3*, which encodes a catecholamine G protein-coupled receptor [57]. The *tyra-3* gene regulates food-leaving behavior: N2 animals have lower food-leaving rates than HW animals, and this variation is due in part to the fact that N2 animals express higher levels of *tyra-3* than HW animals. Rescue experiments revealed that *tyra-3* acts in the BAG and ASK sensory neurons to regulate food leaving. Ablation of the BAG neurons in N2 animals increased food leaving, indicating that BAG neuron activity suppresses food leaving. These results suggest that high levels of *tyra-3* suppress food leaving in part by increasing BAG neuron activity [57].

In a different study using a different food-leaving assay, ablation of BAG neurons was found to have the opposite effect: BAG-ablated animals showed reduced food leaving relative to wild-type N2 animals, suggesting that BAG activity promotes food leaving [56]. Similarly, animals lacking the ASE neurons or AQR, PQR, and URX neurons showed reduced food leaving, suggesting that these neurons also promote food leaving. Moreover, animals lacking both AFD and BAG showed wild-type food-leaving behavior, and animals lacking both AFD and ASE showed a less severe food-leaving phenotype than animals lacking ASE alone [56]. These results suggest that AFD antagonizes BAG and ASE to inhibit food leaving [56]. Thus, the combined activity of multiple gas-detecting sensory neurons may regulate the decision about when to leave an existing food supply in search of new resources. However, the mechanism by which these neurons regulate food leaving, and in particular the mechanism by which the BAG neurons can apparently have opposite effects on food leaving [56, 57], remains unclear.

In the microenvironments of fallen rotting fruit and stems, *C. elegans* lives in close association with microbial food sources, arthropod and nematode predators, and bacterial and fungal pathogens [51]. CO_2 response may contribute to the detection of food, predators, and pathogens. CO_2 avoidance by well-fed animals may help them escape predation by other aerobic organisms, while the downregulation of CO_2 avoidance in starved animals may facilitate food finding at the expense of increased predation risk. *C. elegans* dauers are thought to form phoretic relationships with arthropods that enable long-range migration to more favorable environmental niches [58, 59], and CO_2 attraction may help dauers locate potential arthropod carriers. However, the precise role of CO_2 response in shaping interactions with other aerobic organisms remains to be determined.

Gas Sensing in Other Free-Living Nematodes

CO_2 response, but not O_2 response, has been examined in a number of other free-living nematodes. In an acute CO_2 assay, adults of the necromenic species *Pristionchus pacificus* reverse in response to CO_2 at a rate comparable to that of *C. elegans* N2 animals [27]. By contrast, *Panagrellus redivivus* adults show a lower rate of reversals in response to CO_2, while adults of the *Caenorhabditis* species *Caenorhabditis briggsae* and *Caenorhabditis angaria* show little or no CO_2 response [27]. Whether *C. briggsae* and *C. angaria* respond to CO_2 at low ambient O_2, like *C. elegans* HW animals [31, 40], has not yet been examined. The responses of the dauer larvae of these species to CO_2 have also not yet been investigated. The distantly related marine nematode *Adoncholaimus thalassophygas* is attracted to CO_2 [60], demonstrating that CO_2 response varies greatly across nematode species.

The neural basis of CO_2 response is at least partly conserved in other free-living nematodes, since CO_2 response by *P. pacificus* also requires BAG neurons [27]. Neurons anatomically analogous to the gas-sensing BAG and URX neurons have been identified in two distantly related nematodes, the fungal feeder *Aphelenchus avenae* and the microbial feeder *Acrobeles complexus* [61, 62], suggesting that the neural basis of gas sensing may be conserved among phylogenetically distant species.

Gas Sensing in Parasitic Nematodes

O_2 response by parasitic nematodes has not yet been examined. However, significant progress has been made in understanding CO_2 response both in harmful parasitic nematodes of animals and plants, and in beneficial insect-parasitic nematodes.

CO_2 Response by Entomopathogenic Nematodes

Entomopathogenic nematodes (EPNs) in the genera *Heterorhabditis*, *Steinernema, and Oscheius* are soil-dwelling lethal parasites of insects that are often called beneficial nematodes due to their utility as biocontrol agents for insect pests [63, 64]. The infective stage of EPNs is a developmentally arrested third larval stage called the infective juvenile (IJ), which is analogous to the dauer stage of *C. elegans* [65]. CO_2 is a robust attractant for all EPN IJs that have so far been examined [36, 66–69] (Fig. 5a). CO_2 also stimulates jumping, a host-seeking behavior exhibited by some *Steinernema* species in which the IJ stands on its tail, curls into a loop, and propels itself into the air to attach to passing hosts [36, 68]. Removing CO_2 from host odor eliminates or greatly reduces attraction to host odor, indicating that CO_2 is an essential host odor cue for EPNs [68, 70] (Fig. 5b). EPNs are also attracted to a diverse array of other host- and plant-emitted odorants [36, 68, 71–74], and CO_2 acts synergistically with some of these odorants to attract EPNs [75]. Thus, EPNs use CO_2 in combination with other odorants to locate hosts. BAG neurons are required for CO_2 attraction and CO_2-evoked jumping in EPNs [36] (Fig. 5c), indicating that BAG neurons mediate CO_2 response in both parasitic and free-living nematodes regardless of whether CO_2 is an attractive or repulsive cue.

CO_2 Response by Plant-Parasitic Nematodes

Plant-parasitic nematodes are major agricultural pests worldwide, causing over 100 billion dollars of agricultural losses each year [76]. Plant roots undergo respiration and exude CO_2 into the rhizosphere [77], and many plant-parasitic nematodes are thought to use CO_2 to locate plant hosts [78]. Phylogenetically diverse plant-parasitic species, such as *Meloidogyne incognita, Rotylenchulus reniformis*, and *Ditylenchus phyllobius*, are attracted to CO_2 [69, 79]. Plant-parasitic nematodes are also attracted to a number of other plant-emitted volatiles [80]. Thus, like EPNs, they appear to rely on CO_2 in combination with host-specific odorants for host detection. The neural basis of chemosensation in plant-parasitic nematodes has not yet been investigated.

CO_2 Response by Mammalian-Parasitic Nematodes

Human-parasitic nematodes infect over a billion people worldwide and are responsible for some of the most common neglected tropical diseases [81], while livestock-parasitic nematodes are a major cause of food and economic loss worldwide [76]. Different species of mammalian-parasitic nematodes rely on different strategies for host infection: some infect by skin penetration, some are passively ingested, and some are transmitted by an insect intermediate vector [76]. For example, the human threadworm *Strongyloides stercoralis* and the human hookworms *Necator americanus* and *Ancylostoma duodenale* are skin-penetrating species that infect as IJs [65, 82]. By contrast, the human and ruminant parasite *Trichostrongylus colubriformis* and the ruminant parasite *Haemonchus contortus* are passively ingested as IJs [83, 84], while the human-parasitic giant roundworm *Ascaris lumbricoides* is ingested as eggs and hatches into the infective larvae inside the host [76].

CO_2 plays an important role in the development of some mammalian-parasitic species. CO_2 stimulates egg hatching in passively ingested species such as *A. lumbricoides* and the cat parasite *Toxocara mystax* [85, 86]. CO_2 also stimulates IJ recovery, the process whereby IJs resume development once inside a host, in passively ingested species such as *T. colubriformis* and *H. contortus* [86–89]. In addition to being a developmental cue, CO_2 is also a

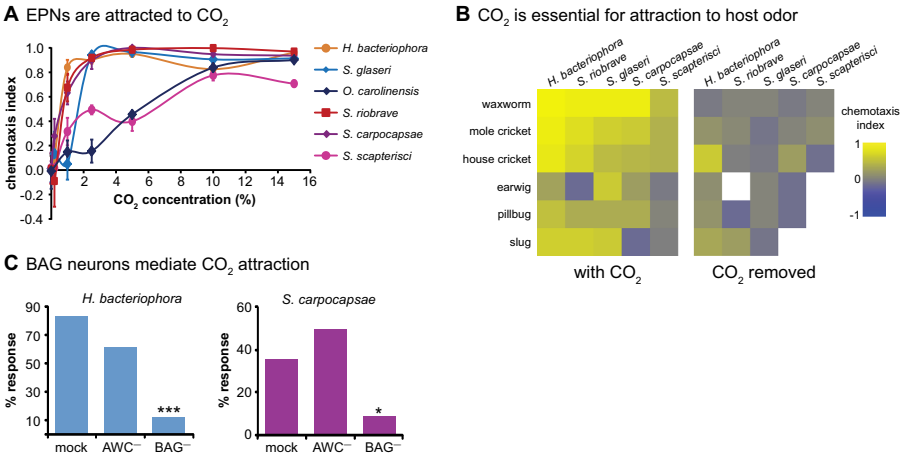

Fig. 5 CO_2 response by entomopathogenic nematodes (EPNs). **a** EPNs are attracted to CO_2 across concentrations in a CO_2 chemotaxis assay. Reproduced from Dillman et al., 2011 [68]. **b** CO_2 is essential for attraction to host odor. EPNs are strongly attracted to the odor of potential hosts in a host chemotaxis assay (*left heatmap*). Chemically removing CO_2 from host odor using soda lime eliminates or greatly reduces attraction to potential hosts (*right heatmap*). *White boxes* indicate EPN-host combinations that were not tested in the absence of CO_2 because the potential host was not attractive even in the presence of CO_2. Reproduced from Dillman et al., 2011 [68]. **c** BAG neurons are required for CO_2 attraction. Laser ablation of BAG neurons in the EPNs *Heterorhabditis bacteriophora* and *Steinernema carpocapsae* eliminates CO_2 attraction. By contrast, the ablation of a different neuron type, AWC, does not affect CO_2 attraction. Reproduced from Hallem et al., 2011 [36]

behavioral cue for at least some mammalian-parasitic nematodes. For example, exposure to CO_2 stimulates nictation in the skin-penetrating dog hookworm *Ancylostoma caninum* [90]. CO_2 exposure also increases crawling in *A. caninum* and *S. stercoralis* and decreases crawling in *H. contortus* [91]. Whether mammalian-parasitic nematodes are attracted or repelled by CO_2 in a chemotaxis assay remains to be determined. In addition, the neural basis of CO_2 response in mammalian-parasitic nematodes has not yet been investigated.

Conclusions and Future Directions

In summary, nematodes detect environmental gases and integrate information about ambient gas levels with information about food availability and nutritional status to generate context-dependent behavioral responses. Both the signaling pathways that mediate O_2 and CO_2 detection, and the signaling pathways that modulate O_2- and CO_2-evoked behaviors, are conserved in other organisms. Thus, a better understanding of gas sensing in nematodes may illuminate general principles of gas sensing across phyla.

An important focus for future research will be elucidating the neural circuitry that operates downstream of the gas-detecting sensory neurons to mediate gas-evoked behaviors. In order to understand the neural basis of gas sensing, it will be essential to not only identify the downstream circuits for O_2- and CO_2-evoked behaviors but also characterize the real-time dynamics of the gas-sensing microcircuits in response to fluctuating levels of ambient O_2 and CO_2. Recent technical advances in high-speed imaging have made it possible to image from many neurons in the same worm simultaneously [92–94], or from a few neurons in multiple behaving worms simultaneously [95]. A recent proof-of-concept study used wide-field temporal focusing to image the activity of 69 neurons simultaneously in response to changes in O_2 levels [94], paving the way for more detailed systems-level dynamic analyses of the gas-sensing microcircuits. The molecular and cellular mechanisms by which these microcircuits are modulated to generate context-dependent behaviors can then be elucidated.

Context-dependent modulation of CO_2 response occurs in insects as well as nematodes, and a number of recent studies have provided insight into the neural basis for this context-dependent modulation. For example, *D. melanogaster* is repelled by CO_2 when walking but attracted to CO_2 in flight, a valence change that is modulated by octopamine signaling [96, 97]. Nutritional status also modulates CO_2 response in insects such that CO_2-evoked behavior depends on both the presence of food odorants and starvation state [98–101]. For example, fed flies are repelled by the combination of CO_2 and vinegar, while starved flies are significantly less repelled [101]. Moreover, the mushroom bodies are required for CO_2 response in starved, but not fed flies, indicating that distinct neural circuits mediate CO_2 response in a context-dependent manner [101]. Whether similar mechanisms mediate context-dependent changes in CO_2 response in *C. elegans* remains to be determined.

Another important focus for future work will be elucidating the functional properties of gas-sensing circuits in other nematode species. Nematodes provide a powerful system for comparative studies of neural circuit function. Despite differences in body size and lifestyle among species, neural anatomy is often conserved down to the single neuron level [61, 62, 102–104]. For example, analogous sensory neurons are required for thermosensation in *C. elegans, A. caninum*, and *H. contortus* [105, 106]. This conservation of neural anatomy makes it feasible to investigate how sensory circuits evolve in species with diverse lifestyles and ecological niches to support species-specific behaviors. Studies of nematodes other than *C. elegans* were previously limited by the lack of genetic and genomic tools. However, many nematodes now have sequenced genomes [107], and techniques for genetic transformation and gene modification have been successfully applied to a number of different species [108–111]. These recent technical advances pave the way for comparative analyses of gas-sensing circuits in free-living and parasitic nematodes, which will provide important insights into the evolution of gas sensing and the neural basis of sensory behaviors.

Finally, parasitic nematodes of animals and plants are a major cause of morbidity, mortality, and economic loss worldwide. Current drugs used to treat nematode infections are inadequate due to toxicity, increasing drug resistance, and high rates of reinfection [112]. A better understanding of how nematodes respond to O_2 and CO_2 may enable the development of traps, repellents, or other novel strategies for preventing harmful nematode infections.

Acknowledgments We thank Manon Guillermin, Sophie Rengarajan, Kristen Yankura, and Michelle Castelletto for the helpful comments on the manuscript. M.A.C. is a National Science Foundation Graduate Research Fellow and a Eugene V. Cota-Robles Fellow. E.A.H. is a MacArthur Fellow, a McKnight Scholar, a Rita Allen Foundation Scholar, and a Searle Scholar.

References

1. Bonora M, Boule M (1994) Effects of hypercapnia and hypoxia on inspiratory and expiratory diaphragmatic activity in conscious cats. J Appl Physiol 77(4):1644–1652. doi:10.1203/01.PDR.0000117841.81730.2B
2. Mortola JP, Lanthier C (1996) The ventilatory and metabolic response to hypercapnia in newborn mammalian species. Respir Physiol 103(3):263–270
3. Vovk A, Cunningham DA, Kowalchuk JM, Paterson DH, Duffin J (2002) Cerebral blood flow responses to changes in oxygen and carbon dioxide in humans. Can J Physiol Pharmacol 80(8):819–827
4. Azzam ZS, Sharabi K, Guetta J, Bank EM, Gruenbaum Y (2010) The physiological and molecular effects of elevated CO_2 levels. Cell Cycle 9(8):1528–1532. doi:10.4161/cc.9.8.11196
5. White JG, Southgate E, Thomson JN, Brenner S (1986) The structure of the nervous system of the nematode *Caenorhabditis elegans*. Phil Trans R Soc Lond B 314(1165):1–340
6. Varshney LR, Chen BL, Paniagua E, Hall DH, Chklovskii DB (2011) Structural properties of the *Caenorhabditis elegans* neuronal network. PLoS Comput Biol 7(2): e1001066. doi:10.1371/journal.pcbi.1001066
7. Macosko EZ, Pokala N, Feinberg EH, Chalasani SH, Butcher RA, Clardy J, Bargmann CI (2009) A hub-and-spoke circuit drives pheromone attraction and social behaviour in *C. elegans*. Nature 458(7242):1171–1175. doi:10.1038/nature07886
8. Chalasani SH, Chronis N, Tsunozaki M, Gray JM, Ramot D, Goodman MB, Bargmann CI (2007) Dissecting a circuit for olfactory behaviour in *Caenorhabditis elegans*. Nature 450(7166):63–70
9. Taghert PH, Nitabach MN (2012) Peptide neuromodulation in invertebrate model systems. Neuron 76(1):82–97. doi:10.1016/j.neuron.2012.08.035
10. Van Voorhies WA, Ward S (2000) Broad oxygen tolerance in the nematode *Caenorhabditis elegans*. J Exp Biol 203(Pt 16):2467–2478
11. Gray JM, Karow DS, Lu H, Chang AJ, Chang JS, Ellis RE, Marletta MA, Bargmann CI (2004) Oxygen sensation and social feeding mediated by a *C. elegans* guanylate cyclase homologue. Nature 430(6997):317–322
12. Chang AJ, Chronis N, Karow DS, Marletta MA, Bargmann CI (2006) A distributed chemosensory circuit for oxygen preference in *C. elegans*. PLoS Biol 4(9):e274
13. Cheung BH, Cohen M, Rogers C, Albayram O, de Bono M (2005) Experience-dependent modulation of *C. elegans* behavior by ambient oxygen. Curr Biol 15(10):905–917
14. Zimmer M, Gray JM, Pokala N, Chang AJ, Karow DS, Marletta MA, Hudson ML, Morton DB, Chronis N, Bargmann CI (2009) Neurons detect increases and decreases in oxygen levels using distinct guanylate cyclases. Neuron 61:865–879
15. Chang AJ, Bargmann CI (2008) Hypoxia and the HIF-1 transcriptional pathway reorganize a neuronal circuit for oxygen-dependent behavior in *Caenorhabditis elegans*. Proc Natl Acad Sci U S A 105(20):7321–7326. doi:10.1073/pnas.0802164105
16. Coates JC, de Bono M (2002) Antagonistic pathways in neurons exposed to body fluid regulate social feeding in *Caenorhabditis elegans*. Nature 419(6910):925–929
17. Rogers C, Persson A, Cheung B, de Bono M (2006) Behavioral motifs and neural pathways coordinating O_2 responses and aggregation in *C. elegans*. Curr Biol 16(7):649–659
18. Cheung BH, Arellano-Carbajal F, Rybicki I, de Bono M (2004) Soluble guanylate cyclases act in neurons exposed to the body fluid to promote *C. elegans* aggregation behavior. Curr Biol 14(12): 1105–1111
19. Derbyshire ER, Marletta MA (2012) Structure and regulation of soluble guanylate cyclase. Annu Rev Biochem 81:533–559. doi:10.1146/annurev-biochem-050410-100030
20. Busch KE, Laurent P, Soltesz Z, Murphy RJ, Faivre O, Hedwig B, Thomas M, Smith HL, de Bono M (2012) Tonic signaling from O_2 sensors sets neural circuit activity and behavioral state. Nat Neurosci 15(4):581–591. doi:10.1038/nn.3061
21. Couto A, Oda S, Nikolaev VO, Soltesz Z, de Bono M (2013) In vivo genetic dissection of O_2-evoked cGMP dynamics in a *Caenorhabditis elegans* gas sensor. Proc Natl Acad Sci U S A 110(35):E3301–E3310. doi:10.1073/pnas.1217428110
22. Sze JY, Victor M, Loer C, Shi Y, Ruvkun G (2000) Food and metabolic signalling defects in a *Caenorhabditis elegans* serotonin-synthesis mutant. Nature 403(6769):560–564
23. de Bono M, Bargmann CI (1998) Natural variation in a neuropeptide Y receptor homolog modifies social behavior and food response in *C. elegans*. Cell 94(5):679–689
24. McGrath PT, Rockman MV, Zimmer M, Jang H, Macosko EZ, Kruglyak L, Bargmann CI (2009) Quantitative mapping of a digenic behavioral trait implicates globin variation in

C. elegans sensory behaviors. Neuron 61(5):692–699. doi:10.1016/j.neuron.2009.02.012
25. de Bono M, Tobin DM, Davis MW, Avery L, Bargmann CI (2002) Social feeding in *Caenorhabditis elegans* is induced by neurons that detect aversive stimuli. Nature 419(6910):899–903
26. Persson A, Gross E, Laurent P, Busch KE, Bretes H, de Bono M (2009) Natural variation in a neural globin tunes oxygen sensing in wild *Caenorhabditis elegans*. Nature 458(7241):1030–1033. doi:10.1038/nature07820
27. Hallem EA, Sternberg PW (2008) Acute carbon dioxide avoidance in *Caenorhabditis elegans*. Proc Natl Acad Sci U S A 105(23):8038–8043
28. Hallem EA, Spencer WC, McWhirter RD, Zeller G, Henz SR, Ratsch G, Miller DM, Horvitz HR, Sternberg PW, Ringstad N (2011) Receptor-type guanylate cyclase is required for carbon dioxide sensation by *Caenorhabditis elegans*. Proc Natl Acad Sci U S A 108(1):254–259. doi:10.1073/pnas.1017354108
29. Brandt JP, Aziz-Zaman S, Juozaityte V, Martinez-Velazquez LA, Petersen JG, Pocock R, Ringstad N (2012) A single gene target of an ETS-family transcription factor determines neuronal CO_2-chemosensitivity. PLoS ONE 7(3):e34014. doi:10.1371/journal.pone.0034014
30. Guillermin ML, Castelletto ML, Hallem EA (2011) Differentiation of carbon dioxide-sensing neurons in *Caenorhabditis elegans* requires the ETS-5 transcription factor. Genetics 189(4):1327–1339. doi:10.1534/genetics.111.133835
31. Carrillo MA, Guillermin ML, Rengarajan S, Okubo R, Hallem EA (2013) O_2-sensing neurons control CO_2 response in *C. elegans*. J Neurosci 33:9675–9683. doi:10.1523/JNEUROSCI.4541-12.2013
32. Bretscher AJ, Busch KE, de Bono M (2008) A carbon dioxide avoidance behavior is integrated with responses to ambient oxygen and food in *Caenorhabditis elegans*. Proc Natl Acad Sci U S A 105(23):8044–8049
33. Bretscher AJ, Kodama-Namba E, Busch KE, Murphy RJ, Soltesz Z, Laurent P, de Bono M (2011) Temperature, oxygen, and salt-sensing neurons in *C. elegans* are carbon dioxide sensors that control avoidance behavior. Neuron 69(6):1099–1113. doi:10.1016/j.neuron.2011.02.023
34. Smith ES, Martinez-Velazquez L, Ringstad N (2013) A chemoreceptor that detects molecular carbon dioxide. J Biol Chem 288(52):37071–37081. doi:10.1074/jbc.M113.517367
35. Hu PJ (2007) Dauer. In WormBook, www.WormBook.org. doi:10.1895/wormbook.1.144.1
36. Hallem EA, Dillman AR, Hong AV, Zhang Y, Yano JM, DeMarco SF, Sternberg PW (2011) A sensory code for host seeking in parasitic nematodes. Curr Biol 21(5):377–383. doi:10.1016/j.cub.2011.01.048
37. Hu J, Zhong C, Ding C, Chi Q, Walz A, Mombaerts P, Matsunami H, Luo M (2007) Detection of near-atmospheric concentrations of CO_2 by an olfactory subsystem in the mouse. Science 317(5840):953–957
38. Sun L, Wang H, Hu J, Han J, Matsunami H, Luo M (2009) Guanylyl Cyclase-D in the olfactory CO_2 neurons is activated by bicarbonate. Proc Natl Acad Sci U S A 106(6):2041–2046
39. Guo D, Zhang JJ, Huang XY (2009) Stimulation of guanylyl cyclase-D by bicarbonate. Biochemistry 48(20):4417–4422
40. Kodama-Namba E, Fenk LA, Bretscher AJ, Gross E, Busch KE, de Bono M (2013) Cross-modulation of homeostatic responses to temperature, oxygen and carbon dioxide in *C. elegans*. PLoS Genet 9(12):e1004011. doi:10.1371/journal.pgen.1004011
41. Rodriguez M, Snoek LB, De Bono M, Kammenga JE (2013) Worms under stress: *C. elegans* stress response and its relevance to complex human disease and aging. Trends Genet 29(6):367–374. doi:10.1016/j.tig.2013.01.010
42. Powell-Coffman JA (2010) Hypoxia signaling and resistance in *C. elegans*. Trends Endocrinol Metab 21(7):435–440. doi:10.1016/j.tem.2010.02.006
43. Pocock R (2011) Invited review: decoding the microRNA response to hypoxia. Pflugers Arch 461(3):307–315. doi:10.1007/s00424-010-0910-5
44. Gorr TA, Gassmann M, Wappner P (2006) Sensing and responding to hypoxia via HIF in model invertebrates. J Insect Physiol 52:349–364
45. Sharabi K, Hurwitz A, Simon AJ, Beitel GJ, Morimoto RI, Rechavi G, Sznajder JI, Gruenbaum Y (2009) Elevated CO_2 levels affect development, motility, and fertility and extend life span in *Caenorhabditis elegans*. Proc Natl Acad Sci U S A 106(10):4024–4029
46. Liu T, Cai D (2013) Counterbalance between BAG and URX neurons via guanylate cyclases controls lifespan homeostasis in *C. elegans*. EMBO J 32:1529–1542
47. Vadasz I, Dada LA, Briva A, Helenius IT, Sharabi K, Welch LC, Kelly AM, Grzesik BA, Budinger GR, Liu J, Seeger W, Beitel GJ, Gruenbaum Y, Sznajder JI (2012) Evolutionary conserved role of c-Jun-N-terminal kinase in CO_2-induced epithelial dysfunction. PLoS ONE 7(10):e46696. doi:10.1371/journal.pone.0046696
48. Qin H, Powell-Coffman JA (2004) The *Caenorhabditis elegans* aryl hydrocarbon receptor, AHR-1, regulates neuronal development. Dev Biol 270(1):64–75
49. Qin H, Zhai Z, Powell-Coffman JA (2006) The *Caenorhabditis elegans* AHR-1 transcription complex controls expression of soluble guanylate cyclase genes in the URX neurons and regulates aggregation behavior. Dev Biol 298(2):606–615
50. Gramstrup Petersen J, Romanos TR, Juozaityte V, Riveiro AR, Hums I, Traunmuller L, Zimmer M, Pocock R (2013) EGL-13/SoxD specifies distinct O_2 and CO_2 sensory neuron fates in *Caenorhabditis elegans*. PLoS Genet 9(5):e1003511. doi:10.1371/journal.pgen.1003511
51. Felix MA, Duveau F (2012) Population dynamics and habitat sharing of natural populations of *Caenorhabditis elegans* and *C. briggsae*. BMC Biol 10:59. doi:10.1186/1741-7007-10-59
52. Shtonda BB, Avery L (2006) Dietary choice behavior in *Caenorhabditis elegans*. J Exp Biol 209(Pt 1):89–102
53. Gloria-Soria A, Azevedo RB (2008) *npr-1* regulates foraging and dispersal strategies in *Caenorhabditis elegans*. Curr Biol 18(21):1694–1699. doi:10.1016/j.cub.2008.09.043
54. Styer KL, Singh V, Macosko E, Steele SE, Bargmann CI, Aballay A (2008) Innate immunity in *Caenorhabditis elegans* is regulated by neurons expressing NPR-1/GPCR. Science 322(5900):460–464. doi:10.1126/science.1163673
55. Reddy KC, Andersen EC, Kruglyak L, Kim DH (2009) A polymorphism in *npr-1* is a behavioral determinant of pathogen susceptibility in *C. elegans*. Science 323(5912):382–384. doi:10.1126/science.1166527
56. Milward K, Busch KE, Murphy RJ, de Bono M, Olofsson B (2011) Neuronal and molecular substrates for optimal foraging in *Caenorhabditis elegans*. Proc Natl Acad Sci U S A 108(51):20672–20677. doi:10.1073/pnas.1106134109
57. Bendesky A, Tsunozaki M, Rockman MV, Kruglyak L, Bargmann CI (2011) Catecholamine receptor polymorphisms affect decision-making in *C. elegans*. Nature 472(7343):313–318. doi:10.1038/nature09821
58. Lee H, Choi MK, Lee D, Kim HS, Hwang H, Kim H, Park S, Paik YK, Lee J (2012) Nictation, a dispersal behavior of the nematode *Caenorhabditis elegans,* is regulated by IL2 neurons. Nat Neurosci 15(1):107–112. doi:10.1038/nn.2975
59. Kiontke K, Sudhaus W (2006) Ecology of *Caenorhabditis* species. In WormBook, www.WormBook.org. doi:10.1895/wormbook.1.37.1

60. Riemann F, Schrage M (1988) Carbon dioxide as an attractant for the free-living marine nematode *Adoncholaimus thalassophygas*. Mar Biol 98:81–85
61. Bumbarger DJ, Crum J, Ellisman MH, Baldwin JG (2007) Three-dimensional fine structural reconstruction of the nose sensory structures of *Acrobeles complexus* compared to *Caenorhabditis elegans* (Nematoda: Rhabditida). J Morphol 268(8):649–663
62. Ragsdale EJ, Ngo PT, Crum J, Ellisman MH, Baldwin JG (2009) Comparative, three-dimensional anterior sensory reconstruction of *Aphelenchus avenae* (Nematoda: Tylenchomorpha). J Comp Neurol 517(5):616–632
63. Liu J, Poinar GO Jr, Berry RE (2000) Control of insect pests with entomopathogenic nematodes: the impact of molecular biology and phylogenetic reconstruction. Annu Rev Entomol 45:287–306
64. Dillman AR, Sternberg PW (2012) Entomopathogenic nematodes. Curr Biol 22(11):R430–R431. doi:10.1016/j.cub.2012.03.047
65. Crook M (2014) The dauer hypothesis and the evolution of parasitism: 20 years on and still going strong. Int J Parasitol 44:1–8
66. Gaugler R, LeBeck L, Nakagaki B, Boush GM (1980) Orientation of the entomogenous nematode *Neoaplectana carpocapsae* to carbon dioxide. Environ Entomol 9:649–652
67. O'Halloran DM, Burnell AM (2003) An investigation of chemotaxis in the insect parasitic nematode *Heterorhabditis bacteriophora*. Parasitology 127(Pt 4):375–385
68. Dillman AR, Guillermin ML, Lee JH, Kim B, Sternberg PW, Hallem EA (2012) Olfaction shapes host-parasite interactions in parasitic nematodes. Proc Natl Acad Sci U S A 109(35):E2324–E2333. doi:10.1073/pnas.1211436109
69. Robinson AF (1995) Optimal release rates for attracting *Meloidogyne incognita, Rotylenchulus reniformis,* and other nematodes to carbon dioxide in sand. J Nematol 27:42–50
70. Gaugler R, Campbell JF, Gupta P (1991) Characterization and basis of enhanced host-finding in a genetically improved strain of *Steinernema carpocapsae*. J Invertebr Pathol 57: 234–241
71. Rasmann S, Kollner TG, Degenhardt J, Hiltpold I, Toepfer S, Kuhlmann U, Gershenzon J, Turlings TC (2005) Recruitment of entomopathogenic nematodes by insect-damaged maize roots. Nature 434(7034):732–737
72. Ali JG, Alborn HT, Stelinski LL (2010) Subterranean herbivore-induced volatiles released by citrus roots upon feeding by *Diaprepes abbreviatus* recruit entomopathogenic nematodes. J Chem Ecol 36:361–368
73. Kollner TG, Held M, Lenk C, Hiltpold I, Turlings TC, Gershenzon J, Degenhardt J (2008) A maize (E)-beta-caryophyllene synthase implicated in indirect defense responses against herbivores is not expressed in most American maize varieties. Plant Cell 20(2):482–494. doi:10.1105/tpc.107.051672
74. Laznik Z, Trdan S (2013) An investigation on the chemotactic responses of different entomopathogenic nematode strains to mechanically damaged maize root volatile compounds. Exp Parasitol 134:349–355
75. Turlings TC, Hiltpold I, Rasmann S (2012) The importance of root-produced volatiles as foraging cues for entomopathogenic nematodes. Plant Soil 358:51–60
76. Jasmer DP, Goverse A, Smant G (2003) Parasitic nematode interactions with mammals and plants. Annu Rev Phytopathol 41:245–270
77. Philippot L, Raaijmakers JM, Lemanceau P, van der Putten WH (2013) Going back to the roots: the microbial ecology of the rhizosphere. Nat Rev Microbiol 11(11):789–799. doi:10.1038/nrmicro3109
78. Rasmann S, Ali JG, Helder J, van der Putten WH (2012) Ecology and evolution of soil nematode chemotaxis. J Chem Ecol. doi:10.1007/s10886-012-0118-6
79. Pline M, Dusenbery DB (1987) Responses of plant-parasitic nematode *Meloidogyne incognita* to carbon dioxide determined by video camera computer tracking. J Chem Ecol 13:873–888
80. Ali JG, Alborn HT, Stelinski LL (2011) Constitutive and induced subterranean plant volatiles attract both entomopathogenic and plant parasitic nematodes. J Ecol 99:26–35
81. Boatin BA, Basanez MG, Prichard RK, Awadzi K, Barakat RM, Garcia HH, Gazzinelli A, Grant WN, McCarthy JS, N'Goran EK, Osei-Atweneboana MY, Sripa B, Yang GJ, Lustigman S (2012) A research agenda for helminth diseases of humans: towards control and elimination. PLoS Negl Trop Dis 6(4):e1547. doi:10.1371/journal.pntd.0001547
82. Viney ME, Lok JB (2007) *Strongyloides* spp. In WormBook, www.WormBook.org. doi:10.1895/wormbook.1.141.1
83. Sutherland I, Scott I (2010) Gastrointestinal Nematodes of Sheep and Cattle: Biology and Control. John Wiley & Sons, Chichester
84. Veglia F (1915) The anatomy and life-history of *Haemonchus contortus* (Rud.). Rep Dir Vet Res 3–4:347–500
85. Fairbairn D (1961) The in vitro hatching of *Ascaris lumbricoides* eggs. Can J Zool 39:153–162
86. Rogers WP (1960) The physiology of infective processes of nematode parasite; the stimulus from the animal host. Proc R Soc Lond B 152:367–386
87. Sommerville RI (1964) Effect of carbon dioxide on the development of third-stage larvae of *Haemonchus contortus* in vitro. Nature 202:316–317
88. Silverman PH, Podger KR (1964) In vitro exsheathment of some nematode infective larvae. Exp Parasitol 15(4):314–324
89. Davey KG, Sommerville RI, Rogers WP (1982) The effect of ethoxyzolamide, an analogue of insect juvenile hormone, noradrenaline, and iodine on changes in the optical path difference in the excretory cells and oesophagus during exsheathment in *Haemonchus contortus*. Int J Parasitol 12: 509–513
90. Granzer M, Hass W (1991) Host-finding and host recognition of infective *Ancylostoma caninum* larvae. Int J Parasitol 21:429–440
91. Sciacca J, Forbes WM, Ashton FT, Lombardini E, Gamble HR, Schad GA (2002) Response to carbon dioxide by the infective larvae of three species of parasitic nematodes. Parasitol Int 51(1):53–62
92. Wu Y, Wawrzusin P, Senseney J, Fischer RS, Christensen R, Santella A, York AG, Winter PW, Waterman CM, Bao Z, Colon-Ramos DA, McAuliffe M, Shroff H (2013) Spatially isotropic four-dimensional imaging with dual-view plane illumination microscopy. Nat Biotechnol 31(11):1032–1038. doi:10.1038/nbt.2713
93. Wu Y, Ghitani A, Christensen R, Santella A, Du Z, Rondeau G, Bao Z, Colon-Ramos D,Shroff H (2011) Inverted selective plane illumination microscopy (iSPIM) enables coupled cellidentity lineaging and neurodevelopmental imaging in Caenorhabditis elegans. Proc Natl AcadSci USA 108 (43):17708–17713. doi:10.1073/pnas.1108494108
94. Schrodel T, Prevedel R, Aumayr K, Zimmer M, Vaziri A (2013) Brain-wide 3D imaging of neuronal activity in *Caenorhabditis elegans* with sculpted light. Nat Methods 10:1013–1020. doi:10.1038/nmeth.2637
95. Larsch J, Ventimiglia D, Bargmann CI, Albrecht DR (2013) High-throughput imaging of neuronal activity in *Caenorhabditis elegans*. Proc Natl Acad Sci U S A 110(45):E4266–E4273. doi:10.1073/pnas.1318325110
96. Suh GS, Wong AM, Hergarden AC, Wang JW, Simon AF, Benzer S, Axel R, Anderson DJ (2004) A single population of olfactory sensory neurons mediates an innate avoidance behaviour in *Drosophila*. Nature 431(7010):854–859
97. Wasserman S, Salomon A, Frye MA (2013) *Drosophila* tracks carbon dioxide in flight. Curr Biol 23(4):301–306. doi:10.1016/j.cub.2012.12.038

98. Turner SL, Ray A (2009) Modification of CO_2 avoidance behaviour in *Drosophila* by inhibitory odorants. Nature 461(7261):277–281. doi:10.1038/nature08295
99. Turner SL, Li N, Guda T, Githure J, Carde RT, Ray A (2011) Ultra-prolonged activation of CO_2-sensing neurons disorients mosquitoes. Nature 474(7349):87–91. doi:10.1038/nature10081
100. Faucher CP, Hilker M, de Bruyne M (2013) Interactions of carbon dioxide and food odours in *Drosophila:* olfactory hedonics and sensory neuron properties. PLoS ONE 8(2):e56361. doi:10.1371/journal.pone.0056361
101. Bracker LB, Siju KP, Varela N, Aso Y, Zhang M, Hein I, Vasconcelos ML, Grunwald Kadow IC (2013) Essential role of the mushroom body in context-dependent CO_2 avoidance in *Drosophila*. Curr Biol 23(13):1228–1234. doi:10.1016/j.cub.2013.05.029
102. Ashton FT, Li J, Schad GA (1999) Chemo- and thermosensory neurons: structure and function in animal parasitic nematodes. Vet Parasitol 84(3–4):297–316
103. Chaisson KE, Hallem EA (2012) Chemosensory behaviors of parasites. Trends Parasitol 28(10):427–436. doi:10.1016/j.pt.2012.07.004
104. Bumbarger DJ, Wijeratne S, Carter C, Crum J, Ellisman MH, Baldwin JG (2009) Three-dimensional reconstruction of the amphid sensilla in the microbial feeding nematode, *Acrobeles complexus* (Nematoda: Rhabditida). J Comp Neurol 512(2):271–281
105. Li J, Zhu X, Boston R, Ashton FT, Gamble HR, Schad GA (2000) Thermotaxis and thermosensory neurons in infective larvae of *Haemonchus contortus,* a passively ingested nematode parasite. J Comp Neurol 424(1):58–73
106. Bhopale VM, Kupprion EK, Ashton FT, Boston R, Schad GA (2001) *Ancylostoma caninum:* the finger cell neurons mediate thermotactic behavior by infective larvae of the dog hookworm. Exp Parasitol 97(2):70–76
107. Dillman AR, Mortazavi A, Sternberg PW (2012) Incorporating genomics into the toolkit of nematology. J Nematol 44:191–205
108. Lok JB (2012) Nucleic acid transfection and transgenesis in parasitic nematodes. Parasitology 139:574–588. doi:10.1017/S0031182011001387
109. Friedland AE, Tzur YB, Esvelt KM, Colaiacovo MP, Church GM, Calarco JA (2013) Heritable genome editing in *C. elegans* via a CRISPR-Cas9 system. Nat Methods 10(8):741–743. doi:10.1038/nmeth.2532
110. Lo TW, Pickle CS, Lin S, Ralston EJ, Gurling M, Schartner CM, Bian Q, Doudna JA, Meyer BJ (2013) Heritable genome editing using TALENs and CRISPR/Cas9 to engineer precise insertions and deletions in evolutionarily diverse nematode species. Genetics 195(2):331–348. doi:10.1534/genetics.113.155382
111. Chiu H, Schwartz HT, Antoshechkin I, Sternberg PW (2013) Transgene-free genome editing in *Caenorhabditis elegans* using CRISPR-Cas. Genetics 195(3):1167–1171. doi:10.1534/genetics.113.155879
112. Diawara A, Schwenkenbecher JM, Kaplan RM, Prichard RK (2013) Molecular and biological diagnostic tests for monitoring benzimidazole resistance in human soil-transmitted helminths. Am J Trop Med Hyg 88(6):1052–1061. doi:10.4269/ajtmh.12-0484

Chapter 2:

Oxygen sensing neurons control carbon dioxide response in *C. elegans*

This project was done in collaboration with another graduate student in the Hallem lab, Manon L. Guillermin.

O_2-Sensing Neurons Control CO_2 Response in *C. elegans*

Mayra A. Carrillo,* Manon L. Guillermin,* Sophie Rengarajan, Ryo P. Okubo, and Elissa A. Hallem
Department of Microbiology, Immunology, and Molecular Genetics, University of California, Los Angeles, Los Angeles, California 90095

Sensory behaviors are often flexible, allowing animals to generate context-appropriate responses to changing environmental conditions. To investigate the neural basis of behavioral flexibility, we examined the regulation of carbon dioxide (CO_2) response in the nematode *Caenorhabditis elegans*. CO_2 is a critical sensory cue for many animals, mediating responses to food, conspecifics, predators, and hosts (Scott, 2011; Buehlmann et al., 2012; Chaisson and Hallem, 2012). In *C. elegans*, CO_2 response is regulated by the polymorphic neuropeptide receptor NPR-1: animals with the N2 allele of *npr-1* avoid CO_2, whereas animals with the Hawaiian (HW) allele or an *npr-1* loss-of-function (*lf*) mutation appear virtually insensitive to CO_2 (Hallem and Sternberg, 2008; McGrath et al., 2009). Here we show that ablating the oxygen (O_2)-sensing URX neurons in *npr-1*(*lf*) mutants restores CO_2 avoidance, suggesting that NPR-1 enables CO_2 avoidance by inhibiting URX neurons. URX was previously shown to be activated by increases in ambient O_2 (Persson et al., 2009; Zimmer et al., 2009; Busch et al., 2012). We find that, in *npr-1*(*lf*) mutants, O_2-induced activation of URX inhibits CO_2 avoidance. Moreover, both HW and *npr-1*(*lf*) animals avoid CO_2 under low O_2 conditions, when URX is inactive. Our results demonstrate that CO_2 response is determined by the activity of O_2-sensing neurons and suggest that O_2-dependent regulation of CO_2 avoidance is likely to be an ecologically relevant mechanism by which nematodes navigate gas gradients.

Introduction

Animals from nematodes to humans respond to environmental gases, such as CO_2 and O_2. CO_2 is aversive for many free-living animals but attractive for many parasitic animals, which rely on CO_2 for host location (Luo et al., 2009; Chaisson and Hallem, 2012). O_2 increases or decreases can evoke avoidance responses in flies and nematodes (Chang et al., 2006; Morton, 2011) and alter foraging and feeding behaviors (Wingrove and O'Farrell, 1999; Cheung et al., 2005; Rogers et al., 2006; Vigne and Frelin, 2010). These responses are critical for survival: exposure to hypercapnia, hyperoxia, or hypoxia can result in reduced neural activity, cell cycle arrest, tumor formation, or death (Wingrove and O'Farrell, 1999; Harris, 2002; West, 2004; Langford, 2005).

The nematode *Caenorhabditis elegans* detects and responds to changes in environmental CO_2 and O_2 (Scott, 2011). *C. elegans* adults migrate away from a CO_2 source and toward ~10% O_2 (Gray et al., 2004; Bretscher et al., 2008; Hallem and Sternberg, 2008). However, CO_2 response can vary with developmental stage and environmental context. For example, CO_2 is repulsive for adults but attractive for dauer larvae (Hallem et al., 2011a), and the behavioral response to simultaneous changes in CO_2 and O_2 levels is indicative of an interaction between the responses to the two gases (Bretscher et al., 2008; McGrath et al., 2009).

The response of *C. elegans* to CO_2 and many other stimuli is regulated by NPR-1, a polymorphic neuropeptide receptor homologous to mammalian neuropeptide Y receptors (de Bono and Bargmann, 1998; Gray et al., 2004; Rogers et al., 2006; Bretscher et al., 2008; Hallem and Sternberg, 2008; Macosko et al., 2009; McGrath et al., 2009; Reddy et al., 2009). The N2 strain of *C. elegans* contains an *npr-1* allele that confers solitary feeding behavior, whereas the CB4856 Hawaiian (HW) strain contains an *npr-1* allele that confers social feeding behavior (de Bono and Bargmann, 1998). N2 animals respond strongly to CO_2 but weakly to O_2 on food, whereas HW animals appear relatively indifferent to CO_2 but respond strongly to O_2 on food (Gray et al., 2004; Bretscher et al., 2008; Hallem and Sternberg, 2008). NPR-1 is thought to act by repressing neural activity (Chang et al., 2006; Macosko et al., 2009).

To investigate the mechanisms of CO_2 response plasticity, we examined the regulation of CO_2 response by NPR-1. We show that HW and *npr-1*(*lf*) animals do not avoid CO_2 despite showing normal CO_2-evoked activity in BAG neurons. However, ablation of URX neurons in *npr-1*(*lf*) animals restores CO_2 avoidance, suggesting that NPR-1 enables CO_2 avoidance by decreasing URX activity. URX is activated by increases in ambient O_2 (Persson et al., 2009; Zimmer et al., 2009; Busch et al., 2012), and we show that its O_2-sensing ability is required to inhibit CO_2 avoidance. We also show that HW and *npr-1*(*lf*) animals avoid CO_2 under low O_2 conditions, when URX is inactive. Our results

Received Sept. 24, 2012; revised April 21, 2013; accepted April 27, 2013.

Author contributions: M.A.C., M.L.G., S.R., and E.A.H. designed research; M.A.C., M.L.G., S.R., R.P.O., and E.A.H. performed research; M.A.C., M.L.G., S.R., and E.A.H. analyzed data; M.A.C., M.L.G., and E.A.H. wrote the paper.

M.A.C. was supported by a National Science Foundation Graduate Research Fellowship (Grant No. DGE-0707424) and a Eugene V. Cota-Robles Fellowship. S.R. was supported by the National Institutes of Health National Institute of General Medical Sciences training Grant GM08042 and the UCLA-Cal Tech Medical Scientist Training Program. E.A.H. is a MacArthur Fellow, an Alfred P. Sloan Research Fellow, a Rita Allen Foundation Scholar, and a Searle Scholar. This work was supported by a National Institutes of Health R00 Grant to E.A.H (Grant No. R00-AI085107). We thank Cori Bargmann, Alon Zaslaver, Paul Sternberg, Jo Anne Powell-Coffman, Miriam Goodman, Maureen Barr, Ikue Mori, Mario de Bono, Shawn Lockery, Shohei Mitani, and the Caenorhabditis Genetics Center for *C. elegans* strains; Cori Bargmann, Alon Zaslaver, and Paul Sternberg for plasmids; Lars Dreier, Michelle Castelletto, Alvaro Sagasti, Doug Black, and Keely Chaisson for critical reading of this manuscript; and Joe Vanderwaart for insightful discussion of this manuscript.

The authors declare no competing financial interests.

*M.A.C. and M.L.G. contributed equally to this work.

Correspondence should be addressed to Dr. Elissa A. Hallem, University of California, Los Angeles, MIMG 237 BSRB, 615 Charles E. Young Drive East, Los Angeles, CA 90095. E-mail: ehallem@microbio.ucla.edu.

DOI:10.1523/JNEUROSCI.4541-12.2013

 0270-6474/13/339675-09$15.00/0

suggest that CO_2 avoidance is regulated by ambient O_2 via a pair of O_2-sensing neurons, allowing flexible responses to fluctuating levels of environmental gases.

Materials and Methods

Strains. C. elegans strains are listed in the order in which they appear in the figures. The following strains were used: N2 (Bristol); DA609 *npr-1(ad609);* CB4856 (Hawaiian); CX11697 *kyIs536[flp-17::p17 SL2 GFP, elt-2::mCherry]; kyIs538[glb-5::p12 SL2 GFP, elt-2::mCherry]*; EAH2 *gcy-9(tm2816)*; PS6416 *pha-1(e2123); syEx1206[gcy-33::G-CaMP3.0, pha-1(+)]*; EAH117 *npr-1(ad609); syEx1206[gcy-33::G-CaMP3.0, pha-1(+)]*; EAH119 *bruEx89[gcy-33::G-CaMP-3.0, ets-8::GFP]*; MT17148 *flp-21(ok889); flp-18(n4766)*; PR767 *ttx-1(p767)*; GN112 *pgIs2[gcy-8::caspase, unc-122::GFP]*; PR679 *che-1(p679)*; MT18636 *nIs326[gcy-33::YC3.60]; lin-15AB(n765)*; AX2047 *gcy-8::YC3.60, unc-122::dsRed*; XL115 *flp-6::YC3.60*; CX9592 *npr-1(ad609); kyEx2016[npr-1::npr-1 SL2 GFP, ofm-1::dsRed]*; CX9395 *npr-1(ad609); kyEx1965[gcy-32::npr-1 SL2 GFP, ofm-1::dsRed]*; CX9633 *npr-1(ad609); kyEx2096[flp-8::npr-1 SL2 GFP, ofm-1::dsRed]*; CX9396 *npr-1(ad609); kyEx1966[flp-21::npr-1 SL2 GFP, ofm-1::dsRed]*; CX9644 *npr-1(ad609); kyEx2107[ncs-1::npr-1 SL2 GFP, ofm-1::dsRed]*; CX7102 *lin-15(n765) qaIs2241[gcy-36::egl-1, gcy-35::GFP, lin-15(+)]*; CX7158 *npr-1(ad609) qaIs2241[gcy-36::egl-1, gcy-35::GFP, lin-15(+)]*; ZG629 *iaIs22[gcy-36::GFP, unc-119(+)]*; EAH80 *iaIs22[gcy-36::GFP, unc-119(+)]; npr-1(ad609)*; EAH106 *bruEx86[gcy-36::G-CAMP3.0, coel::RFP]*; EAH114 *npr-1(ad609)*; *bruEx86[gcy-36::G-CaMP3.0, coel::RFP]*; ZG24 *ahr-1(ia3)*; ZG624 *ahr-1(ia3); npr-1(ad609)*; CX6448 *gcy-35(ok769)*; CX7157 *gcy-35(ok769); npr-1(ad609)*; RB1902 *flp-19(ok2460)*; PT501 *flp-8(pk360)*; PT502 *flp-10(pk367)*; EAH123 *npr-1(ad609) flp-19(ok2460)*; EAH141 *npr-1(ad609) flp-8(pk360);* EAH140 *flp-10(pk367); npr-1(ad609);* PS5892 *gcy-33(ok232); gcy-31(ok296)*; EAH127 *gcy-33(ok232); gcy-31(ok296) lon-2(e678) npr-1(ad609).* In addition, CX7376 *kyIs511[gcy-36::G-CaMP, coel::GFP]* and EAH115 *kyIs511[gcy-36::G-CaMP, coel::GFP]; npr-1(ad609)* were used to confirm the results shown in Figure 5*A* with independent transgenes, and RB1903 *flp-19(ok2461)* and EAH139 *npr-1(ad609) flp-19(ok2461)* were used to confirm the results shown in Figure 5*C* with an independent deletion allele of *flp-19.* All transgenes were injected into N2, except *bruEx89*, which was injected into CB4856 to generate EAH119. EAH2 was derived from FX2816 by outcrossing to N2 for five generations. Nematodes were cultured on NGM plates containing *Escherichia coli* OP50 according to standard methods (Brenner, 1974). *C. elegans* dauer larvae were collected from the lids of plates from which the OP50 food source had been depleted ("starved plates") and stored in dH_2O at 15°C before use. All nematodes tested were hermaphrodites.

Generation of reporter transgenes and transgenic animals. To generate EAH119, the *gcy-33::G-CaMP3.0* construct from PS6416 was injected into CB4856 at 50 ng/μl along with *ets-8::GFP* at 50 ng/μl as a coinjection marker. To generate EAH106, a *gcy-36::G-CaMP3.0* transcriptional fusion construct was generated by amplifying a 1.0 kb region upstream of the start codon of the *gcy-36* gene from N2 genomic DNA using primers that included the following sequences: 5′-gatgttggtagatggggtttgga-3′ and 5′-aaattcaaacaagggctacccaaca-3′. The promoter fragment was then cloned into a modified Fire vector containing the G-CaMP3.0 coding region (Tian et al., 2009). The *gcy-36::G-CaMP3.0* construct was injected into N2 animals at a concentration of 25 ng/μl along with 50 ng/μl of *coel::RFP* as a coinjection marker.

Acute CO_2 avoidance assays. Acute CO_2 avoidance assays were performed as previously described (Hallem and Sternberg, 2008; Guillermin et al., 2011; Hallem et al., 2011b). Briefly, ~10–15 young adults were tested on 5 cm assay plates consisting of NGM agar seeded with a thin lawn of *E. coli* OP50 bacteria. Gas stimuli consisted of certified industrial mixes (Airgas or Air Liquide). CO_2 stimuli consisted of 10% CO_2, 10% O_2 (unless otherwise indicated), and the rest N_2. Control stimuli consisted of 10% O_2 (unless otherwise indicated) and the rest N_2. Two 50 ml gas-tight syringes were filled with gas: one with CO_2 and one without CO_2. The mouths of the syringes were connected to flexible PVC tubing attached to Pasteur pipettes, and gases were pumped through the Pasteur pipettes using a syringe pump at a rate of 1.5 ml/min. Worms were exposed to gases by placing the tip of the Pasteur pipette near the head of a forward-moving worm, and a response was scored if the worm reversed within 4 s. Gases were delivered blindly, and worms were scored blindly. An avoidance index was calculated by subtracting the fraction of animals that reversed to the air control from the fraction that reversed to the CO_2. Single-worm acute CO_2 avoidance assays were performed on L4 or young adult laser-ablated animals (see Fig. 3*C*) as described above, except that each animal was tested 12 times with >2 min between trials. For each animal, an avoidance index was calculated by subtracting the fraction of trials in which it reversed to the air control from the fraction of trials in which it reversed to the CO_2 stimulus. The avoidance index for each genotype or treatment was calculated as the mean avoidance index for each animal of the same genotype or treatment.

CO_2 chemotaxis assays. CO_2 chemotaxis assays were performed on young adults essentially as previously described (Bretscher et al., 2008). Briefly, animals were washed off plates and into a 65 mm Syracuse watch glass using M9 buffer. Animals were washed 3× with M9 and transferred from the watch glass to a 1 cm × 1 cm square of Whatman paper. Animals were then transferred from the filter paper to the center of a 9 cm NGM or chemotaxis plate (Bargmann et al., 1993). Gas stimuli were delivered to the plate though holes in the plate lids as previously described (Hallem et al., 2011a; Dillman et al., 2012), except at a flow rate of 2 ml/min. Assay plates were placed on a vibration-reducing platform for 20 min. The number of worms in a 2-cm-diameter circle centered under each gas inlet was then counted, except for Figures 1*B* and 2*A*, *B*, where the number of worms in an area comprising ~3/10 of the plate under each gas inlet was counted. The chemotaxis index was calculated as follows: (no. of worms at CO_2 − no. of worms at control)/(no. of worms at CO_2 + control). Two identical assays were always performed simultaneously with the CO_2 gradient in opposite directions on the two plates to control for directional bias resulting from room vibration; assays were discarded if the difference in the chemotaxis index for the two plates was ≥0.9 or if <7 worms moved into the scoring regions on one or both of the plates.

For CO_2 chemotaxis assays under different O_2 conditions, assays were performed as described above inside airtight canisters (OGGI; 13.3 cm × 10.1 cm) with four holes drilled into the lids to insert tubing for gas flow. One hole was used to establish the ambient O_2 level, two were used to establish the CO_2 gradient, and one was used as an exhaust. A gas mixture consisting of either 7% O_2 and the balance N_2, or 21% O_2 and the balance N_2, was pumped into the chamber at a rate of 2.5 L/min for 1 min and then 0.5 L/min for the duration of the assay. The CO_2 stimulus (10% CO_2, either 7% O_2 or 21% O_2, balance N_2) and control stimulus (7% O_2 or 21% O_2, balance N_2) were pumped into the chamber at a rate of 2 ml/min using a syringe pump, as described above. The assay duration was 25 min.

Dauer CO_2 chemotaxis assays were performed as previously described (Hallem et al., 2011a; Dillman et al., 2012). Briefly, assays were performed on chemotaxis plates (Bargmann et al., 1993). For each assay, ~50–150 dauers were placed in the center of the assay plate. Gas stimuli and gas delivery to the assay plate were as described above, and a chemotaxis index was calculated as described above.

Calcium imaging. Imaging was performed using the genetically encoded calcium indicators G-CaMP (Zimmer et al., 2009), G-CaMP3.0 (Tian et al., 2009), or yellow cameleon YC3.60 (Nagai et al., 2004). Young adult or L4 animals were immobilized onto a cover glass containing a 2% agarose pad made with 10 mM HEPES using Surgi-Lock 2oc instant tissue adhesive (Meridian). A custom-made gas delivery chamber was placed over the cover glass. Gases were delivered at a rate of 0.8–1 L/min. Gas delivery was controlled by a ValveBank4 controller (AutoMate Scientific). Imaging was performed on an AxioObserver A1 inverted microscope (Carl Zeiss) using a 40× EC Plan-NEOFLUAR lens, a Hamamatsu C9100 EM-CCD camera, and AxioVision software (Carl Zeiss). For YC3.60 imaging, the emission image was passed through a DV2 beam splitter (Photometrics) as previously described (Hallem et al., 2011b). Image analysis was performed using AxioVision software (Carl Zeiss) and Microsoft Excel. The mean pixel value of a background region of interest was subtracted from the mean pixel value of a region of interest containing the neuron soma. Fluorescence values were normalized to the average values obtained in the 4 s before CO_2 delivery. For YC3.60 im-

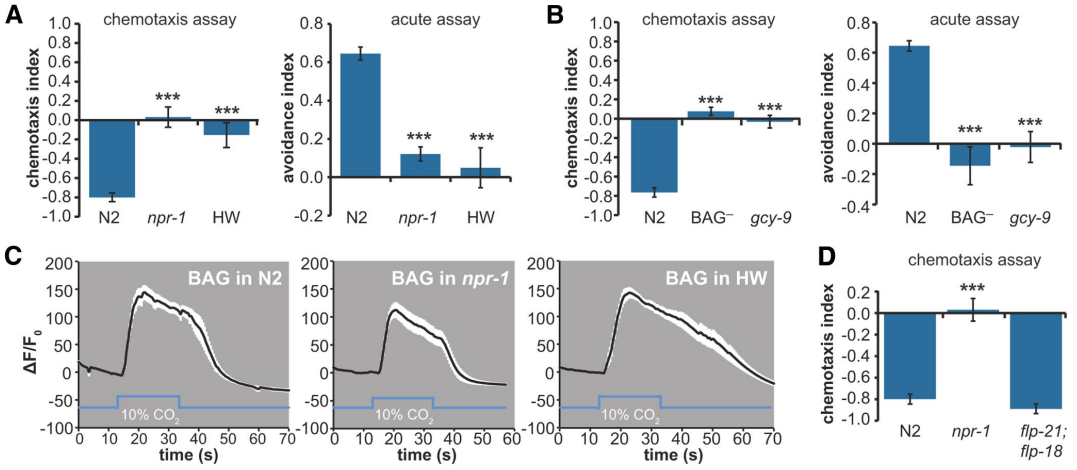

Figure 1. *npr-1* is required for CO_2 avoidance behavior but not CO_2 detection. ***A***, *npr-1* is required for CO_2 avoidance by adults. Left, CO_2 chemotaxis assay. Right, Acute CO_2 avoidance assay. *npr-1*(*lf*) and HW animals do not respond to CO_2 in either assay. ***$p < 0.001$, one-way ANOVA with Bonferroni post-test. $n = 6–9$ trials (chemotaxis assay) or 10–27 trials (acute assay) for each genotype. Error bars represent SEM. ***B***, Animals that lack BAG neurons and *gcy-9*(*tm2816*) mutant animals do not respond to CO_2. BAG-ablated animals express a transgene that specifically kills the BAG neurons (Zimmer et al., 2009; Hallem et al., 2011b). Left, CO_2 chemotaxis assay. Right, Acute CO_2 avoidance assay. The CO_2 stimulus was delivered in an airstream containing 10% O_2, which approximates the preferred O_2 concentration for *C. elegans* (Gray et al., 2004); the control airstream also contained 10% O_2. $n = 18$ or 19 trials (chemotaxis assay) or 4–27 trials (acute assay). ***$p < 0.001$, Kruskal–Wallis test with Dunn's post-test (chemotaxis assay) or one-way ANOVA with Bonferroni post-test (acute assay). Error bars represent SEM. ***C***, *npr-1* is not required for CO_2 detection by BAG neurons. BAG neuron cell bodies of N2 (left), *npr-1*(*lf*) (middle), and HW (right) animals respond to CO_2. Calcium increases were measured using the calcium indicator G-CaMP3.0. Black lines indicate average calcium responses; white shading represents SEM. Blue lines below the traces indicate the timing of the CO_2 pulse. The peak response amplitudes of all three genotypes were not significantly different (one-way ANOVA with Bonferroni post-test). The decay kinetics of all three genotypes were significantly different ($p < 0.001$ using a polynomial curve fit). However, these differences are not likely to be a result of differences at the *npr-1* locus because recordings from BAG neurons of N2 animals using G-CaMP3.0 showed different decay kinetics from BAG neurons of N2 animals using YC3.60 (Fig. 2*C*,*D*). ***D***, The NPR-1 ligands FLP-21 and FLP-18 are not required for CO_2 response. ***$p < 0.001$, one-way ANOVA with Bonferroni post-test. $n = 6–9$ animals for each genotype. Error bars represent SEM.

aging, the YFP/CFP ratio was calculated as previously described (Hallem et al., 2011b). Images were baseline corrected using a linear baseline correction. Traces with unstable baselines before the onset of the CO_2 stimulus were discarded.

Laser ablation. Ablations were performed on L2 and L3 animals as previously described (Hallem and Sternberg, 2008). Briefly, animals were mounted on glass slides for DIC microscopy on a pad consisting of 5% Noble agar in dH_2O with 5% sodium azide as anesthetic. Ablations were performed on a Zeiss AxioImager A2 microscope with an attached MicroPoint laser (Carl Zeiss). Neurons were ablated by focusing a laser microbeam on the cell. Mock-ablated animals were mounted similarly but were not subjected to a laser microbeam. Neurons were identified by both cell position and GFP expression. Loss of the ablated cell was confirmed by observing loss of fluorescence in the adult animal.

Fluorescence microscopy. Nematodes were anesthetized with 3 mM levamisole and mounted on a pad consisting of 5% Noble agar in dH_2O. Epifluorescence images were captured using a Zeiss AxioImager A2 microscope with an attached Zeiss AxioCam camera and Zeiss AxioVision software (Carl Zeiss). To quantify epifluorescence in Figure 4*D*, all images were taken with the same exposure time. Average pixel intensities in the region of interest were quantified using AxioVision software (Carl Zeiss). Relative intensities were normalized by setting the highest mean intensity value to 1.

Statistical analysis. Statistical analysis was performed using GraphPad Instat and Prism. All significance values reported are relative to the N2 control, unless otherwise indicated.

Results

NPR-1 regulates CO_2 avoidance behavior

To investigate the role of *npr-1* in mediating CO_2 response, we examined the CO_2-evoked behavior of N2, HW, and *npr-1*(*lf*) animals in both a chemotaxis assay and an acute avoidance assay. We found that N2 animals displayed robust CO_2 avoidance in both assays, whereas HW and *npr-1*(*lf*) animals were essentially unresponsive to CO_2 in both assays (Fig. 1*A*). Thus, the N2 allele of *npr-1* is required for the behavioral response to CO_2. CO_2 avoidance behavior also requires the CO_2-detecting BAG neurons and the receptor guanylate cyclase gene *gcy-9*, which encodes a putative receptor for CO_2 or a CO_2 metabolite (Fig. 1*B*) (Hallem and Sternberg, 2008; Hallem et al., 2011b; Brandt et al., 2012). To test whether *npr-1* is required for CO_2 detection, we imaged from BAG neurons using the genetically encoded calcium indicator G-CaMP3.0 (Tian et al., 2009). We found that the BAG neurons of N2, *npr-1*(*lf*), and HW animals all showed CO_2-evoked activity (Fig. 1*C*), suggesting that *npr-1* regulates the behavioral response to CO_2 downstream of the calcium response of BAG neurons. The *flp-21* and *flp-18* genes, which encode NPR-1 ligands, are not required for CO_2 avoidance, suggesting that other ligands are required for the regulation of CO_2 response by *npr-1* (Fig. 1*D*).

In addition to the BAG neurons, the salt-sensing ASE neurons and the temperature-sensing AFD neurons have been implicated in CO_2 detection and avoidance (Bretscher et al., 2011). However, we found that *che-1* mutant animals, which lack functional ASE neurons (Uchida et al., 2003), displayed normal CO_2 avoidance in both a chemotaxis assay and an acute assay (Fig. 2*A*) (Hallem and Sternberg, 2008). Both AFD-ablated animals and *ttx-1* mutant animals, which lack functional AFD neurons (Satterlee et al., 2001), showed defective CO_2 avoidance in a chemotaxis assay but not an acute assay (Fig. 2*A*) (Hallem and Sternberg, 2008). These results suggest that ASE neurons are not required for CO_2 avoidance under our assay conditions and that AFD neurons are required for some but not all CO_2-evoked be-

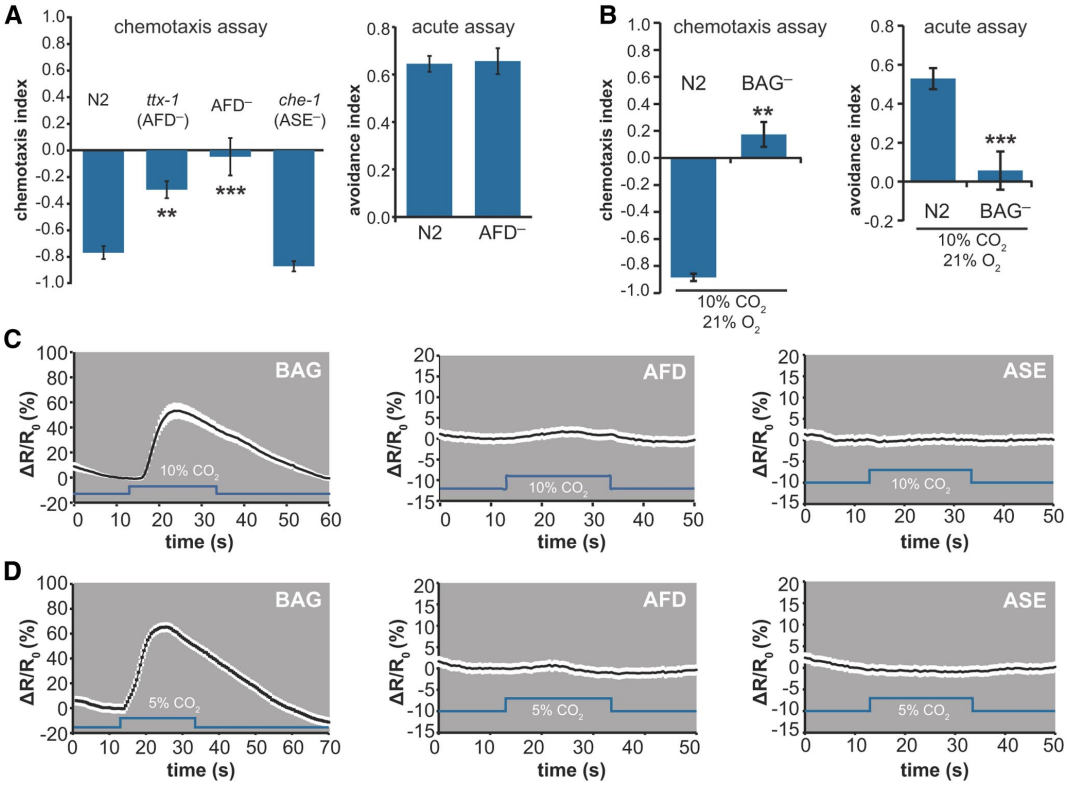

Figure 2. The role of AFD, ASE, and BAG neurons in CO_2 response. ***A***, Animals that lack functional ASE neurons respond normally to CO_2 in both a chemotaxis assay (left graph) and an acute avoidance assay (Hallem and Sternberg, 2008). Animals that lack functional AFD neurons respond normally to CO_2 in an acute avoidance assay (right) but not a chemotaxis assay (left). AFD-ablated animals (AFD^-) express a transgene that specifically kills the AFD neurons (Glauser et al., 2011). The *ttx-1* and *che-1* genes encode transcription factors that are required for normal development of the AFD and ASE neurons, respectively (Satterlee et al., 2001; Uchida et al., 2003; Hobert, 2010). $^{**}p < 0.01$, Kruskal–Wallis test with Dunn's post-test. $^{***}p < 0.001$, Kruskal–Wallis test with Dunn's post-test. $n = 10–18$ trials (chemotaxis assay) or $n = 9–27$ trials (acute assay) for each genotype. Error bars represent SEM. ***B***, Animals that lack BAG neurons do not respond to CO_2 when the CO_2 stimulus is delivered in an airstream containing 21% O_2, which approximates the atmospheric O_2 concentration. The control airstream also contained 21% O_2. $^{**}p < 0.01$, Mann–Whitney test. $^{***}p < 0.001$, one-way ANOVA with Bonferroni post-test. $n = 4–11$ trials (chemotaxis assay) or $n = 10–27$ trials (acute assay). Error bars represent SEM. ***C***, ***D***, Calcium responses of BAG, AFD, and ASE neurons to 10% CO_2 (***C***) and 5% CO_2 (***D***), measured using the ratiometric calcium indicator yellow cameleon YC3.60. Black lines indicate average calcium responses; white shading represents SEM. Blue lines below the traces indicate the timing of the CO_2 pulse. Calcium increases were observed in BAG neuron cell bodies but not AFD and ASE neuron cell bodies. $n = 5–13$ animals for each genotype.

haviors. By contrast, animals lacking BAG neurons showed a complete loss of CO_2 response in both assays, regardless of whether CO_2 was delivered in combination with 10% O_2, which approximates the preferred O_2 concentration of *C. elegans* (Gray et al., 2004), or 21% O_2, which approximates atmospheric O_2 concentration (Figs. 1*B* and 2*B*). We then imaged from BAG, ASE, and AFD neurons using the calcium indicator yellow cameleon YC3.60 (Nagai et al., 2004). We observed CO_2-evoked activity in BAG neurons but not AFD and ASE neurons in response to a 20 s pulse of either 5% or 10% CO_2 (Fig. 2*C*,*D*). Thus, BAG neurons are the primary sensory neurons that contribute to CO_2 response under our assay conditions.

NPR-1 regulates URX neuron activity to control CO_2 avoidance behavior

NPR-1 is not expressed in BAG neurons but is expressed in a number of other sensory neurons as well as some interneurons (Macosko et al., 2009). To identify the site of action for the regulation of CO_2 response by *npr-1*, we introduced the N2 allele of *npr-1* into *npr-1*(*lf*) mutants in different subsets of neurons and assayed CO_2 response. We found that expressing *npr-1* in neuronal subsets that included the O_2-sensing URX neurons (Cheung et al., 2004; Gray et al., 2004) restored CO_2 response (Fig. 3*A*). These results suggest that NPR-1 activity in URX neurons is sufficient to enable CO_2 avoidance. However, we cannot exclude the possibility that NPR-1 function in other neurons also contributes to CO_2 avoidance.

To further investigate the role of the URX neurons in regulating CO_2 response, we ablated URX neurons in both the N2 and *npr-1*(*lf*) backgrounds and assayed CO_2 avoidance behavior. We found that either genetic ablation of a neuronal subset that includes URX or specific laser ablation of URX in the N2 background had no effect on CO_2 avoidance (Fig. 3*B*,*C*). However, both genetic and laser ablation of URX in *npr-1*(*lf*) mutants restored CO_2 avoidance (Fig. 3*B*,*C*). Moreover, the response of URX-ablated *npr-1*(*lf*) animals was not significantly different from the response of URX-ablated N2 animals in our laser ablation experiment (Fig. 3*C*). Thus, in *npr-1*(*lf*) mutants, URX neu-

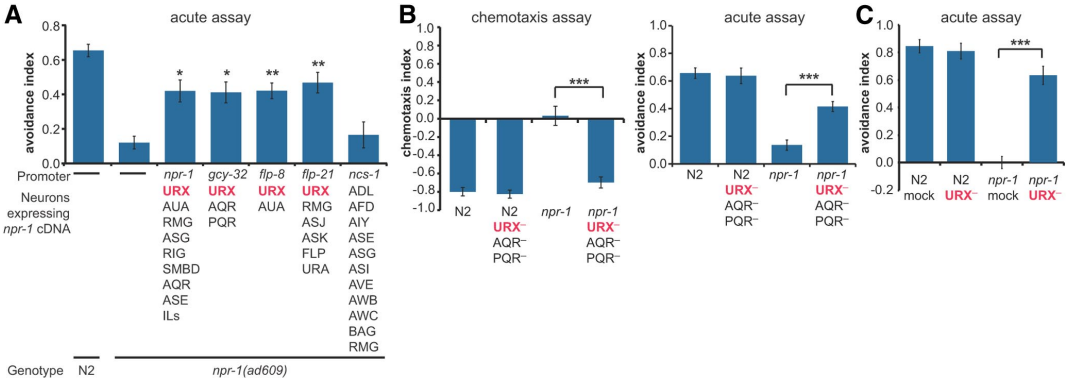

Figure 3. *npr-1* appears to act in URX neurons to regulate CO_2 avoidance. ***A***, Expression of *npr-1* cDNA from N2 animals in subsets of neurons that include URX restores CO_2 avoidance to *npr-1*(*lf*) mutants in an acute CO_2 avoidance assay. *$p < 0.05$, relative to the *npr-1*(*lf*) mutant (one-way ANOVA with Bonferroni post-test). **$p < 0.01$, relative to the *npr-1*(*lf*) mutant (one-way ANOVA with Bonferroni post-test). $n = 16–27$ trials for each genotype. Full expression patterns for each transgene were previously described (Macosko et al., 2009). ***B***, Genetic ablation of a subset of neurons that includes URX in *npr-1*(*lf*) mutants restores CO_2 avoidance. Left, CO_2 chemotaxis assay. Right, Acute CO_2 avoidance assay. ***$p < 0.001$, relative to the *npr-1*(*lf*) mutant (one-way ANOVA with Bonferroni post-test). $n = 7$ or 8 trials (chemotaxis assay) or 8–27 trials (acute assay) for each genotype. ***C***, Specific laser ablation of URX neurons in *npr-1*(*lf*) mutants restores CO_2 avoidance in an acute CO_2 avoidance assay. Ablations were performed on animals expressing a *gcy-36::GFP* transgene to verify the identity of the URX neurons. ***$p < 0.001$ (one-way ANOVA with Bonferroni post-test). The responses of mock-ablated N2 animals, URX-ablated N2 animals, and URX-ablated *npr-1* animals were not significantly different ($p > 0.05$). $n = 7–10$ trials for each treatment. For all graphs, error bars represent SEM.

rons inhibit CO_2 avoidance and removal of URX neurons is sufficient to restore CO_2 avoidance. Our results suggest a model in which CO_2 avoidance behavior is regulated by URX neuron activity. In N2 animals, NPR-1 reduces URX neuron activity, thereby enabling CO_2 avoidance. In *npr-1*(*lf*) animals, increased activity of URX neurons inhibits the CO_2 circuit, resulting in a loss of CO_2 avoidance.

URX neurons are not required for CO_2 attraction by dauers

In contrast to *C. elegans* adults and developing larvae, *C. elegans* dauer larvae are attracted to CO_2 (Fig. 4*A*) (Guillermin et al., 2011; Hallem et al., 2011a). The dauer is a developmentally arrested, alternative third larval stage that is thought to be analogous to the infective juvenile stage of parasitic nematodes (Hotez et al., 1993). The mechanism responsible for the change in CO_2 response valence that occurs at the dauer stage is not yet known. BAG neurons and the putative CO_2 receptor GCY-9 are required for CO_2 attraction by dauers (Fig. 4*A*) (Hallem et al., 2011a), suggesting that the same mechanism of CO_2 detection operates at the dauer and adult stages. However, *npr-1*(*lf*) and HW dauers are also attracted to CO_2, indicating that *npr-1* is not required for CO_2 attraction (Fig. 4*B*). The lack of requirement for *npr-1* at the dauer stage is not the result of altered *npr-1* expression in URX neurons because *npr-1* is expressed at comparable levels in N2 dauers and developing third-stage larvae (L3s) (Fig. 4*C*,*D*). To test whether URX neuron activity is required for CO_2 attraction by dauers, we tested whether dauers that lack URX neurons are still attracted to CO_2. We found that URX-ablated N2 and *npr-1*(*lf*) dauers display normal CO_2 attraction (Fig. 4*E*), indicating that URX neurons are not required to promote CO_2 attraction by dauers. Thus, URX neurons control whether CO_2 is a repulsive or neutral stimulus in adults, but other mechanisms are required to promote CO_2 attraction by dauers.

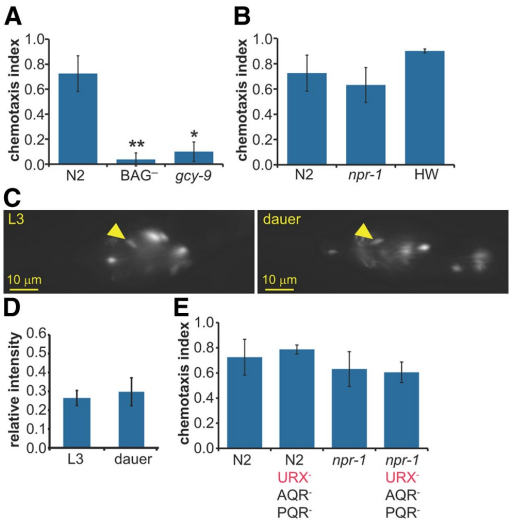

Figure 4. Mechanisms of CO_2 attraction by dauers. ***A***, BAG neurons and the receptor guanylate cyclase gene *gcy-9* are required for CO_2 attraction by dauers. *$p < 0.05$ (Kruskal–Wallis test with Dunn's post-test). **$p < 0.01$ (Kruskal–Wallis test with Dunn's post-test). $n = 4–12$ trials. ***B***, *npr-1* is not required for CO_2 attraction by dauers. $n = 4–8$ trials. ***C***, Epifluorescence images of *npr-1* expression in the URX neurons of L3 (left) and dauer (right) larvae in the N2 background. *npr-1* expression was assayed in *npr-1* animals containing an *npr-1::npr-1 SL2 GFP* transgene (Macosko et al., 2009). Arrowheads indicate the location of the URX neuron cell body. Anterior is to the left. ***D***, *npr-1* expression in the URX neurons of L3 and dauer larvae is not significantly different (unpaired *t* test). $n = 17–20$ animals. ***E***, URX neurons are not required for CO_2 attraction by dauers. Both N2 and *npr-1*(*lf*) dauers containing a genetic ablation of the URX, AQR, and PQR neurons display normal CO_2 attraction. $n = 4–8$ trials for each genotype. For all graphs, error bars represent SEM.

O_2 sensing by URX neurons is required for regulation of CO_2 avoidance

The URX neurons are O_2-sensing neurons that express O_2 receptors of the soluble guanylate cyclase (sGC) family (Cheung et al., 2004; Gray et al., 2004). Whether the URX neurons are also activated by CO_2 is unclear (Bretscher et al., 2011; Brandt et al., 2012). To test whether URX neurons regulate CO_2 response by directly responding to CO_2, we imaged

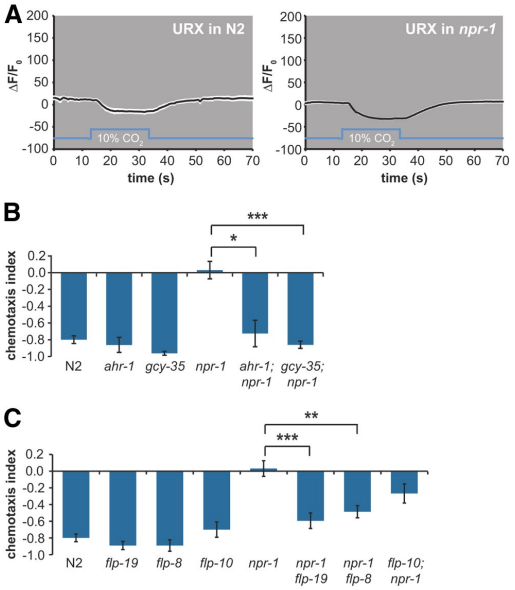

Figure 5. URX neurons mediate O_2-dependent regulation of CO_2 avoidance. ***A***, URX neurons do not respond to CO_2 in either N2 or *npr-1*(*lf*) animals under our imaging conditions. Calcium transients in URX neuron cell bodies were measured using G-CaMP3.0. Black lines indicate average calcium responses; white shading represents SEM. Blue lines below the traces indicate the timing of the CO_2 pulse. $n = 8$ or 9 animals for each genotype. To verify the lack of CO_2 response in URX neurons, we also imaged from N2 and *npr-1*(*lf*) animals containing an independently generated construct that expressed G-CaMP in URX (McGrath et al., 2009); these animals also did not display CO_2-evoked activity in URX (data not shown). ***B***, O_2 sensing by URX neurons is required for regulation of CO_2 avoidance. Mutation of *ahr-1* or *gcy-35* rescues the CO_2 response defect of *npr-1*(*lf*) mutants. $^*p < 0.05$ (Kruskal–Wallis test with Dunn's post-test). $^{***}p < 0.001$ (Kruskal–Wallis test with Dunn's post-test). $n = 4$–9 trials for each genotype. Error bars represent SEM. ***C***, Neuropeptide signaling regulates CO_2 avoidance. Mutation of the URX-expressed neuropeptide genes *flp-8* and *flp-19* significantly rescues the CO_2 response defect of *npr-1*(*lf*) mutants. $^{**}p < 0.01$, relative to the *npr-1*(*lf*) mutant (one-way ANOVA with Bonferroni post-test). $^{***}p < 0.001$, relative to the *npr-1*(*lf*) mutant (one-way ANOVA with Bonferroni post-test). $n = 6$–14 trials. Error bars represent SEM.

from the URX neurons of N2 and *npr-1*(*lf*) animals during CO_2 exposure using the calcium indicator G-CaMP3.0. We found that URX neurons are not activated by CO_2 (Fig. 5*A*). URX neurons did appear to show a slight decrease in calcium levels in response to CO_2, but whether this decrease is biologically relevant is not yet clear. These results indicate that URX neurons do not regulate CO_2 response as a result of CO_2-induced activation.

To test whether URX neurons instead regulate CO_2 response by responding to O_2, we examined the CO_2-evoked behavior of *aryl hydrocarbon receptor-1* (*ahr-1*) mutants. AHR-1 is a transcription factor that regulates aggregation behavior and that is required for normal expression of sGC O_2 receptors in URX neurons (Qin et al., 2006). We found that *ahr-1* mutants respond normally to CO_2 and that the *ahr-1* mutation rescues the CO_2 response defect of *npr-1*(*lf*) mutants (Fig. 5*B*). Thus, regulation of CO_2 avoidance by URX neurons of *npr-1*(*lf*) animals depends on their ability to sense O_2. Furthermore, mutation of the sGC gene *gcy-35*, which encodes an O_2 receptor that is expressed in URX and required for its O_2 response (Zimmer et al., 2009), also rescues the CO_2 response defect of *npr-1* mutants (Fig. 5*B*). Thus, GCY-35-mediated activation of URX neurons by ambient O_2 is required for regulation of CO_2 avoidance behavior. Together, these results demonstrate that CO_2 response is regulated by ambient O_2.

To investigate the mechanism by which URX neurons regulate CO_2 response in *npr-1* mutants, we examined the role of neuropeptide signaling in the regulation of CO_2 avoidance behavior. The URX neurons are known to express FMRFamide-related neuropeptide genes, including *flp-8*, *flp-10*, and *flp-19* (Li and Kim, 2008). To test whether these neuropeptide genes are required for the regulation of CO_2 response, we examined the CO_2-evoked behavior of neuropeptide mutants in the *npr-1*(*lf*) mutant background. We found that mutation of either *flp-8* or *flp-19*, but not *flp-10*, significantly rescued the CO_2 response defect of *npr-1* mutants (Fig. 5*C*). These results are consistent with the hypothesis that URX neurons modulate CO_2 response via a neuropeptide signaling pathway involving *flp-8* and *flp-19*. However, we cannot exclude the possibility that release of *flp-8* and *flp-19* from other neurons also contributes to the O_2-dependent regulation of CO_2 response.

npr-1(*lf*) and HW animals avoid CO_2 under low O_2 conditions

The URX neurons are activated when the ambient O_2 concentration increases from 10% to 21% (Zimmer et al., 2009; Busch et al., 2012). This response consists of both phasic and tonic components: a large initial increase in calcium transients is followed by a smaller sustained increase that continues until O_2 levels return to 10% (Busch et al., 2012). The fact that URX neurons remain active at high O_2 levels but are inactive at low O_2 levels led us to hypothesize that *npr-1*(*lf*) and HW animals might avoid CO_2 under low O_2 conditions, when URX neurons are inactive. We therefore examined the responses of *npr-1*(*lf*) and HW animals to CO_2 under low O_2 conditions by reducing the ambient O_2 concentration to 7% for the duration of the CO_2 chemotaxis assay. We found that, at 7% ambient O_2, both *npr-1*(*lf*) and HW animals displayed CO_2 avoidance behavior that was comparable with that of N2 animals (Fig. 6*A*). Thus, *npr-1*(*lf*) and HW animals are indeed capable of responding robustly to CO_2. However, CO_2 response in these animals is regulated by ambient O_2 such that CO_2 is repulsive at low O_2 concentrations and neutral at high O_2 concentrations.

The BAG neurons, which are activated by CO_2, are also activated by decreases in ambient O_2 from 21% to <10% (Zimmer et al., 2009). This raised the possibility that BAG neurons could cell-autonomously integrate responses to O_2 and CO_2, thus contributing to the O_2-dependent regulation of CO_2 response. To test this possibility, we examined the ability of animals that lack the soluble guanylate cyclase genes *gcy-31* and *gcy-33*, which are expressed in BAG neurons and are required for the O_2-evoked activity of BAG neurons (Zimmer et al., 2009), to respond to CO_2 at low ambient O_2. We found that *gcy-33; gcy-31* mutants responded normally to CO_2 at low ambient O_2 in both N2 and *npr-1*(*lf*) animals (Fig. 6*B*), indicating that the O_2-sensing ability of BAG is not required for the O_2-dependent regulation of CO_2 response. Consistent with these results, the BAG neurons were recently shown to play only a minor role in the chronic response to ambient O_2 (Busch et al., 2012). Thus, regulation of CO_2 response by ambient O_2 is not a result of cell-intrinsic signaling within BAG but instead requires a pair of designated O_2-sensing neurons.

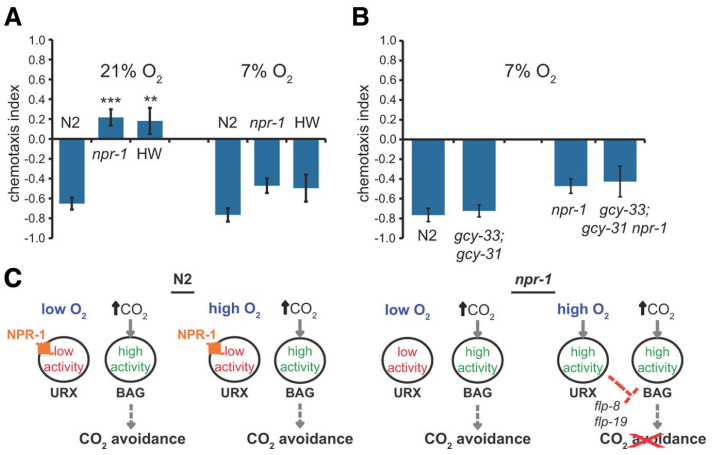

Figure 6. *npr-1(lf)* and HW animals avoid CO_2 under low O_2 conditions. ***A***, *npr-1(lf)* and HW animals do not respond to CO_2 at 21% ambient O_2 but avoid CO_2 at 7% ambient O_2. $^{**}p < 0.01$, relative to N2 control (Kruskal–Wallis test with Dunn's post-test). $^{***}p < 0.001$, relative to N2 control (Kruskal–Wallis test with Dunn's post-test). $n = 7$–26 trials for each genotype and condition. Error bars represent SEM. ***B***, CO_2 response at low ambient O_2 does not require O_2 sensing by BAG neurons. Animals that lack the soluble guanylate cyclase genes *gcy-31* and *gcy-33*, which are required for the O_2 response of BAG neurons (Zimmer et al., 2009), respond normally to CO_2 at 7% ambient O_2 in both the N2 and *npr-1(lf)* mutant backgrounds. The response of N2 animals is not significantly different from the response of *gcy-33; gcy-31* animals, and the response of *npr-1* animals is not significantly different from the response of *gcy-33; gcy-31 npr-1* animals (Kruskal–Wallis test with Dunn's post-test). $n = 8$–26 trials for each genotype. Error bars represent SEM. ***C***, A model for O_2-dependent regulation of CO_2 avoidance. Our results suggest that, in N2 animals, NPR-1 maintains URX in a low activity state, thus enabling CO_2 avoidance even at high ambient O_2. In *npr-1(lf)* mutant animals, reduced activity of URX at low ambient O_2 allows CO_2 avoidance, and increased activity of URX at high ambient O_2 inhibits CO_2 avoidance. Our results also suggest that CO_2 avoidance by URX neurons may be mediated by the URX-expressed neuropeptide genes *flp-8* and *flp-19*.

Discussion

Our results demonstrate that URX neurons control CO_2 response by coordinating the response to CO_2 with the response to ambient O_2. In *npr-1(lf)* animals, O_2-dependent activation of URX neurons determines CO_2 response such that CO_2 is repulsive at low ambient O_2 but neutral at high ambient O_2 (Fig. 6*C*). Moreover, our results are consistent with the hypothesis that URX neurons regulate the activity of the CO_2 circuit via a neuropeptide signaling pathway that involves the FMRFamide-related neuropeptide genes *flp-19* and *flp-8*. By contrast, in N2 animals, the URX neurons do not inhibit CO_2 avoidance at high ambient O_2 as a result of the presence of NPR-1 (Fig. 6*C*). NPR-1 does not constitutively silence the URX neurons of N2 animals because the URX neurons of N2 animals are activated by increases in ambient O_2 and ablation of URX in N2 animals alters O_2 response (Zimmer et al., 2009). However, our results suggest that NPR-1 may reduce URX neuron activity in N2 animals such that URX neurons no longer inhibit the CO_2 avoidance circuit. Alternatively, it is possible that NPR-1 activity is dynamically regulated by its neuropeptide ligands such that it is active under some conditions but not others, or that the URX neurons of N2 animals are sufficiently activated but are incapable of regulating CO_2 avoidance as a result of differences in neural connectivity or signaling between N2 and *npr-1(lf)* animals.

A recent survey of wild *C. elegans* strains revealed that the HW allele of *npr-1* is the natural variant, with the N2 allele having arisen during laboratory culturing (McGrath et al., 2009). HW animals were previously thought to be virtually insensitive to CO_2 (Hallem and Sternberg, 2008; McGrath et al., 2009), raising the question of whether CO_2 avoidance is exclusively a laboratory-derived behavior. Our results demonstrate that HW animals do indeed display robust CO_2 avoidance, but this behavior is restricted to low O_2 conditions. Wild *C. elegans* adults have been found in fallen rotting fruit and in the soil under rotting fruit, where O_2 levels are lower and CO_2 levels are higher than in the atmosphere (Felix and Duveau, 2012). Inside rotting fruit, *C. elegans* occupies microhabitats replete with bacteria, fungi, worms, insects, and other small invertebrates (Felix and Duveau, 2012). In this context, fluctuating levels of CO_2 and O_2 likely serve as important indicators of food availability, population density, and predator proximity (Bendesky et al., 2011; Milward et al., 2011; Scott, 2011). Suppression of CO_2 avoidance at high ambient O_2 may allow worms to migrate toward rotting fruit, which emits CO_2. Once inside the low O_2 environment of rotting fruit, CO_2 avoidance may allow worms to avoid cohabitating predators or overcrowding. Thus, O_2-dependent regulation of CO_2 avoidance is likely to be an ecologically relevant mechanism by which nematodes navigate gas gradients.

In addition to CO_2 response, a number of other chemosensory behaviors in *C. elegans* are subject to context-dependent changes in sensory valence (Sengupta, 2012). For example, olfactory and gustatory behavior exhibits experience-dependent plasticity, in which chemicals that are attractive to naive animals become neutral or repulsive after prolonged or repeated exposure in the absence of food (Sengupta, 2012). Olfactory plasticity occurs as a result of altered signaling in the AWC olfactory neurons (Tsunozaki et al., 2008), and salt plasticity occurs as a result of altered signaling in the ASE gustatory neurons and the downstream AIA and AIB interneurons (Tomioka et al., 2006; Adachi et al., 2010; Oda et al., 2011). Similarly, O_2 preference is modulated by prior O_2 exposure and the presence of bacterial food as a result of altered signaling in a distributed network of chemosensory neurons (Cheung et al., 2005; Chang et al., 2006). Our results suggest that CO_2 response is modulated by ambient O_2 via the activity of a pair of O_2-detecting neurons that interact with the CO_2 circuit downstream of CO_2 detection by BAG neurons (Fig. 6*C*). The neurons that act downstream of BAG and URX to control CO_2 response have not yet been identified. A number of interneurons receive synaptic input from both BAG and URX (White et al., 1986), and it will be interesting to determine whether any of them play a role in CO_2 avoidance.

CO_2-evoked behaviors in insects are also subject to context-dependent modulation. For example, the fruit fly *Drosophila melanogaster* is repelled by CO_2 when walking (Suh et al., 2004) but attracted to CO_2 in flight, a valence change that is modulated by octopamine signaling (Wasserman et al., 2013). In addition, both CO_2 repulsion by walking *D. melanogaster* and CO_2 attraction by mosquitoes can be suppressed by food odorants, which

directly alter the activity of the CO_2 receptor (Turner and Ray, 2009; Turner et al., 2011). Insects as well as many other animals, both free-living and parasitic, occupy microhabitats where environmental levels of O_2 and CO_2 vary greatly as a function of food or host availability, population density, and microorganism composition. Thus, it will be interesting to determine whether the control of CO_2 response by O_2-sensing neurons is a conserved feature of gas-sensing circuits.

References

Adachi T, Kunitomo H, Tomioka M, Ohno H, Okochi Y, Mori I, Iino Y (2010) Reversal of salt preference is directed by the insulin/PI3K and Gq/PKC signaling in *Caenorhabditis elegans.* Genetics 186:1309–1319. CrossRef Medline

Bargmann CI, Hartwieg E, Horvitz HR (1993) Odorant-selective genes and neurons mediate olfaction in *C. elegans.* Cell 74:515–527. CrossRef Medline

Bendesky A, Tsunozaki M, Rockman MV, Kruglyak L, Bargmann CI (2011) Catecholamine receptor polymorphisms affect decision-making in *C. elegans.* Nature 472:313–318. CrossRef Medline

Brandt JP, Aziz-Zaman S, Juozaityte V, Martinez-Velazquez LA, Petersen JG, Pocock R, Ringstad N (2012) A single gene target of an ETS-family transcription factor determines neuronal CO_2-chemosensitivity. PLoS One 7:e34014. CrossRef Medline

Brenner S (1974) The genetics of *Caenorhabditis elegans.* Genetics 77:71–94. Medline

Bretscher AJ, Busch KE, de Bono M (2008) A carbon dioxide avoidance behavior is integrated with responses to ambient oxygen and food in *Caenorhabditis elegans.* Proc Natl Acad Sci U S A 105:8044–8049. CrossRef Medline

Bretscher AJ, Kodama-Namba E, Busch KE, Murphy RJ, Soltesz Z, Laurent P, de Bono M (2011) Temperature, oxygen, and salt-sensing neurons in *C. elegans* are carbon dioxide sensors that control avoidance behavior. Neuron 69:1099–1113. CrossRef Medline

Buehlmann C, Hansson BS, Knaden M (2012) Path integration controls nest-plume following in desert ants. Curr Biol 22:645–649. CrossRef Medline

Busch KE, Laurent P, Soltesz Z, Murphy RJ, Faivre O, Hedwig B, Thomas M, Smith HL, de Bono M (2012) Tonic signaling from O_2 sensors sets neural circuit activity and behavioral state. Nat Neurosci 15:581–591. CrossRef Medline

Chaisson KE, Hallem EA (2012) Chemosensory behaviors of parasites. Trends Parasitol 28:427–436. CrossRef Medline

Chang AJ, Chronis N, Karow DS, Marletta MA, Bargmann CI (2006) A distributed chemosensory circuit for oxygen preference in *C. elegans.* PLoS Biol 4:e274. CrossRef Medline

Cheung BH, Arellano-Carbajal F, Rybicki I, de Bono M (2004) Soluble guanylate cyclases act in neurons exposed to the body fluid to promote *C. elegans* aggregation behavior. Curr Biol 14:1105–1111. CrossRef Medline

Cheung BH, Cohen M, Rogers C, Albayram O, de Bono M (2005) Experience-dependent modulation of *C. elegans* behavior by ambient oxygen. Curr Biol 15:905–917. CrossRef Medline

de Bono M, Bargmann CI (1998) Natural variation in a neuropeptide Y receptor homolog modifies social behavior and food response in *C. elegans.* Cell 94:679–689. CrossRef Medline

Dillman AR, Guillermin ML, Lee JH, Kim B, Sternberg PW, Hallem EA (2012) Olfaction shapes host-parasite interactions in parasitic nematodes. Proc Natl Acad Sci U S A 109:E2324–E2333. CrossRef Medline

Félix MA, Duveau F (2012) Population dynamics and habitat sharing of natural populations of *Caenorhabditis elegans* and *C. briggsae.* BMC Biol 10:59. CrossRef Medline

Glauser DA, Chen WC, Agin R, Macinnis BL, Hellman AB, Garrity PA, Tan MW, Goodman MB (2011) Heat avoidance is regulated by transient receptor potential (TRP) channels and a neuropeptide signaling pathway in *Caenorhabditis elegans.* Genetics 188:91–103. CrossRef Medline

Gray JM, Karow DS, Lu H, Chang AJ, Chang JS, Ellis RE, Marletta MA, Bargmann CI (2004) Oxygen sensation and social feeding mediated by a *C. elegans* guanylate cyclase homologue. Nature 430:317–322. CrossRef Medline

Guillermin ML, Castelletto ML, Hallem EA (2011) Differentiation of carbon dioxide-sensing neurons in *Caenorhabditis elegans* requires the ETS-5 transcription factor. Genetics 189:1327–1339. CrossRef Medline

Hallem EA, Sternberg PW (2008) Acute carbon dioxide avoidance in *Caenorhabditis elegans.* Proc Natl Acad Sci U S A 105:8038–8043. CrossRef Medline

Hallem EA, Dillman AR, Hong AV, Zhang Y, Yano JM, DeMarco SF, Sternberg PW (2011a) A sensory code for host seeking in parasitic nematodes. Curr Biol 21:377–383. CrossRef Medline

Hallem EA, Spencer WC, McWhirter RD, Zeller G, Henz SR, Ratsch G, Miller DM 3rd, Horvitz HR, Sternberg PW, Ringstad N (2011b) Receptor-type guanylate cyclase is required for carbon dioxide sensation by *Caenorhabditis elegans.* Proc Natl Acad Sci U S A 108:254–259. CrossRef Medline

Harris AL (2002) Hypoxia: a key regulatory factor in tumour growth. Nat Rev Cancer 2:38–47. CrossRef Medline

Hobert O. (2010) Neurogenesis in the nematode *Caenorhabditis elegans.* In: WormBook. www.WormBook.org. Accessed May 8th, 2013.

Hotez P, Hawdon J, Schad GA (1993) Hookworm larval infectivity, arrest and amphiparatenesis: the *Caenorhabditis elegans* Daf-c paradigm. Parasitol Today 9:23–26. CrossRef Medline

Langford NJ (2005) Carbon dioxide poisoning. Toxicol Rev 24:229–235. CrossRef Medline

Li C, Kim, K. (2008) Neuropeptides. In: WormBook, www.WormBook.org. Accessed May 8th, 2013.

Luo M, Sun L, Hu J (2009) Neural detection of gases—carbon dioxide, oxygen—in vertebrates and invertebrates. Curr Opin Neurobiol 19:354–361. CrossRef Medline

Macosko EZ, Pokala N, Feinberg EH, Chalasani SH, Butcher RA, Clardy J, Bargmann CI (2009) A hub-and-spoke circuit drives pheromone attraction and social behaviour in *C. elegans.* Nature 458:1171–1175. CrossRef Medline

McGrath PT, Rockman MV, Zimmer M, Jang H, Macosko EZ, Kruglyak L, Bargmann CI (2009) Quantitative mapping of a digenic behavioral trait implicates globin variation in *C. elegans* sensory behaviors. Neuron 61:692–699. CrossRef Medline

Milward K, Busch KE, Murphy RJ, de Bono M, Olofsson B (2011) Neuronal and molecular substrates for optimal foraging in *Caenorhabditis elegans.* Proc Natl Acad Sci U S A 108:20672–20677. CrossRef Medline

Morton DB (2011) Behavioral responses to hypoxia and hyperoxia in *Drosophila* larvae: molecular and neuronal sensors. Fly (Austin) 5:119–125. CrossRef Medline

Nagai T, Yamada S, Tominaga T, Ichikawa M, Miyawaki A (2004) Expanded dynamic range of fluorescent indicators for Ca^{2+} by circularly permuted yellow fluorescent proteins. Proc Natl Acad Sci U S A 101:10554–10559. CrossRef Medline

Oda S, Tomioka M, Iino Y (2011) Neuronal plasticity regulated by the insulin-like signaling pathway underlies salt chemotaxis learning in *Caenorhabditis elegans.* J Neurophysiol 106:301–308. CrossRef Medline

Persson A, Gross E, Laurent P, Busch KE, Bretes H, de Bono M (2009) Natural variation in a neural globin tunes oxygen sensing in wild *Caenorhabditis elegans.* Nature 458:1030–1033. CrossRef Medline

Qin H, Zhai Z, Powell-Coffman JA (2006) The *Caenorhabditis elegans* AHR-1 transcription complex controls expression of soluble guanylate cyclase genes in the URX neurons and regulates aggregation behavior. Dev Biol 298:606–615. CrossRef Medline

Reddy KC, Andersen EC, Kruglyak L, Kim DH (2009) A polymorphism in *npr-1* is a behavioral determinant of pathogen susceptibility in *C. elegans.* Science 323:382–384. CrossRef Medline

Rogers C, Persson A, Cheung B, de Bono M (2006) Behavioral motifs and neural pathways coordinating O_2 responses and aggregation in *C. elegans.* Curr Biol 16:649–659. CrossRef Medline

Satterlee JS, Sasakura H, Kuhara A, Berkeley M, Mori I, Sengupta P (2001) Specification of thermosensory neuron fate in *C. elegans* requires *ttx-1*, a homolog of *otd/Otx.* Neuron 31:943–956. CrossRef Medline

Scott K (2011) Out of thin air: sensory detection of oxygen and carbon dioxide. Neuron 69:194–202. CrossRef Medline

Sengupta P (2013) The belly rules the nose: feeding state-dependent modulation of peripheral chemosensory responses. Curr Opin Neurobiol 23:68–75. CrossRef Medline

Suh GS, Wong AM, Hergarden AC, Wang JW, Simon AF, Benzer S, Axel R, Anderson DJ (2004) A single population of olfactory sensory neurons mediates an innate avoidance behaviour in *Drosophila.* Nature 431:854–859. CrossRef Medline

Tian L, Hires SA, Mao T, Huber D, Chiappe ME, Chalasani SH, Petreanu L, Akerboom J, McKinney SA, Schreiter ER, Bargmann CI, Jayaraman V, Svoboda K, Looger LL (2009) Imaging neural activity in worms, flies and mice with improved GCaMP calcium indicators. Nat Methods 6:875–881. CrossRef Medline

Tomioka M, Adachi T, Suzuki H, Kunitomo H, Schafer WR, Iino Y (2006) The insulin/PI 3-kinase pathway regulates salt chemotaxis learning in *Caenorhabditis elegans*. Neuron 51:613–625. CrossRef Medline

Tsunozaki M, Chalasani SH, Bargmann CI (2008) A behavioral switch: cGMP and PKC signaling in olfactory neurons reverses odor preference in *C. elegans*. Neuron 59:959–971. CrossRef Medline

Turner SL, Ray A (2009) Modification of CO_2 avoidance behaviour in *Drosophila* by inhibitory odorants. Nature 461:277–281. CrossRef Medline

Turner SL, Li N, Guda T, Githure J, Cardé RT, Ray A (2011) Ultra-prolonged activation of CO_2-sensing neurons disorients mosquitoes. Nature 474:87–91. CrossRef Medline

Uchida O, Nakano H, Koga M, Ohshima Y (2003) The *C. elegans che-1* gene encodes a zinc finger transcription factor required for specification of the ASE chemosensory neurons. Development 130:1215–1224. CrossRef Medline

Vigne P, Frelin C (2010) Hypoxia modifies the feeding preferences of *Drosophila*: consequences for diet dependent hypoxic survival. BMC Physiol 10:8. CrossRef Medline

Wasserman S, Salomon A, Frye MA (2013) *Drosophila* tracks carbon dioxide in flight. Curr Biol 23:301–306. CrossRef Medline

West JB (2004) The physiologic basis of high-altitude diseases. Ann Intern Med 141:789–800. CrossRef Medline

White JG, Southgate E, Thomson JN, Brenner S (1986) The structure of the nervous system of the nematode *Caenorhabditis elegans*. Philos Trans R Soc Lond B Biol Sci 314:1–340. CrossRef Medline

Wingrove JA, O'Farrell PH (1999) Nitric oxide contributes to behavioral, cellular, and developmental responses to low oxygen in *Drosophila*. Cell 98:105–114. CrossRef Medline

Zimmer M, Gray JM, Pokala N, Chang AJ, Karow DS, Marletta MA, Hudson ML, Morton DB, Chronis N, Bargmann CI (2009) Neurons detect increases and decreases in oxygen levels using distinct guanylate cyclases. Neuron 61:865–879. CrossRef Medline

Follow up

Our results were later supported by published work from Mario de Bono's lab in which they also found ambient O_2 levels modulate CO_2 avoidance behavior mediated by *npr-1* (Kodama-Namba et al., 2013). In addition, they also showed that cultivation temperature can modulate CO_2 response, via the AFD thermosensory neurons. We tested whether AFD neurons are acting through its strongest post-synaptic target, the AIY interneurons, to promote CO_2 avoidance. We tested *ttx-1; ttx-3* double mutants that have both defective AFD and AIY interneurons. Disrupting AIY function in *ttx-1* mutants rescued the CO_2 avoidance behavior, suggesting that AFD neurons are promoting CO_2 avoidance by acting through AIY (Figure 2-1). It will be interesting to see if ablating AIY interneurons can inhibit temperature-dependent modulation of CO_2 response and whether we will see distinct calcium responses in AIY in an AFD mutant background in response to CO_2. This will shed light on the neuronal mechanisms behind the temperature-dependent modulation of the CO_2 circuit.

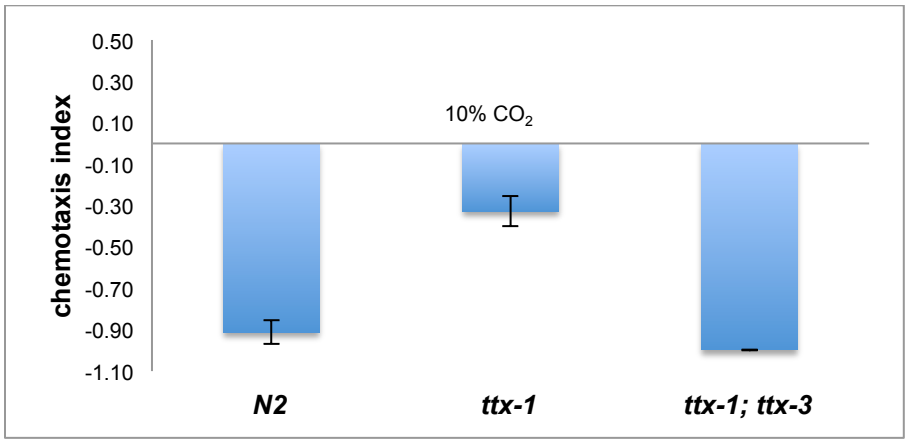

Fig. 2-1. Loss of AIY function in *ttx-1* mutants rescues CO_2 avoidance behavior. *ttx-1* mutants have a defect in AFD neurons and result in loss of CO_2 avoidance. *ttx-3* mutants have a defect in AIY function. Double mutants show disrupting AIY function in *ttx-1* mutants restores CO_2 avoidance. Results from chemotaxis assays in response to 10% CO_2 in 10% O_2 background. *n*=6-10 trials for each genotype.

As a follow up on the neuropeptide signaling pathway mediating O_2-dependent regulation of CO_2 avoidance behavior in *npr-1* mutants, we investigated whether *flp-8* or *flp-19* neuropeptides

are regulating CO_2 avoidance behavior through URX neurons. We expressed *flp-19* specifically in URX using a URX-specific promoter, *gcy-36*, in *npr-1flp19* double mutants. We found that expression of *flp-19* specifically in URX rescued inhibition of CO_2 avoidance in *npr-1flp-19* mutants (Figure 2-2). Therefore, *flp-19* is required in URX to regulate CO_2 response. We are currently working on rescuing *flp-8* in URX. Future experiments include identifying a neuropeptide receptor for *flp-19* and its neuronal targets.

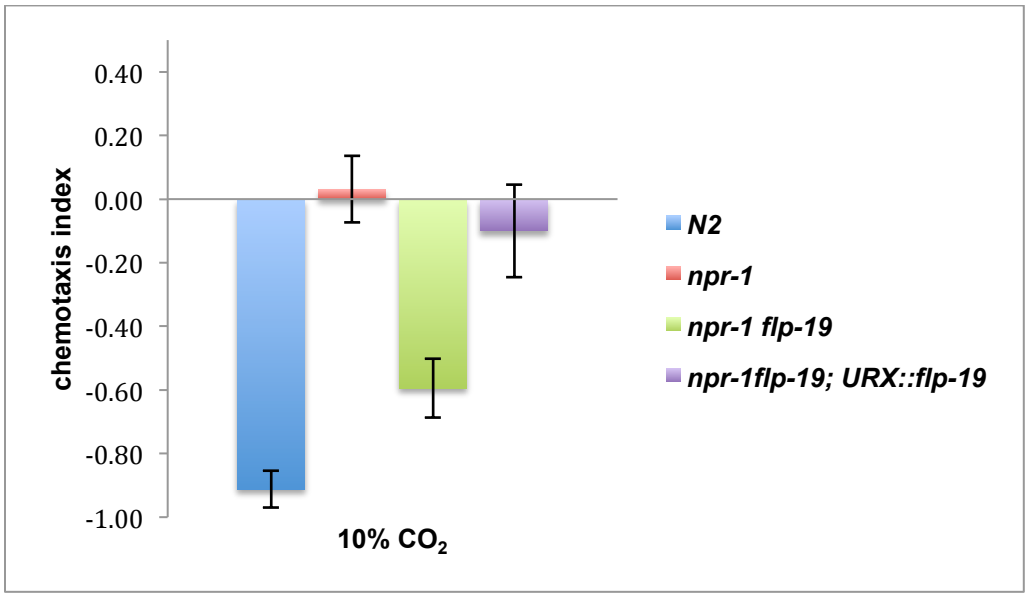

Fig. 2-2. Expression of *flp-19* in URX rescues *npr-1* phenotype. Expressed *flp-19* gDNA under URX promoter *gcy-36* in *npr-1flp-19* animals. *n*= 8-10 trials for each genotype. Chemotaxis assays were done using 10% CO_2 in an airstream containing 10% O_2.

Chapter 3:

Identifying the downstream interneurons required for CO_2 response

This work was done in collaboration with Manon L. Guillermin and is currently still in progress for submission to publication

To investigate how CO_2 response is modulated by O_2-sensing neurons, it is important to identify the interneurons acting downstream of the BAG neurons to mediate CO_2 response. It is possible that the URX neurons are acting on one or more of the interneurons downstream of BAG to regulate the CO_2 circuit. We first identified all interneurons that receive direct synaptic input from BAG using the *C. elegans* wiring diagram (Figure 3-1) (White et al., 1986). We identified 7 interneurons that are directly post-synaptic to BAG. The interneurons RIG, RIA, and AVE are also directly post-synaptic to the URX neurons, thus identifying a possible site of action for CO_2 regulation. However, it is also possible that URX can regulate the CO_2 circuit through extrasynaptic signaling to other BAG targets, possibly via the neuropeptides FLP-19 and FLP-8 (Carrillo et al., 2013).

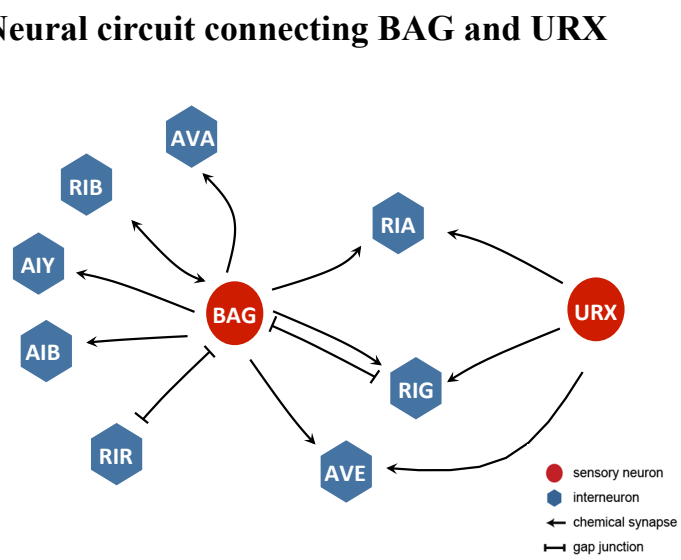

Fig. 3-1. BAG is presynaptic to 7 interneurons. URX has 3 common downstream interneurons with BAG. RIA, RIG, and AVE may be targets for O_2-dependent regulation of CO_2 avoidance.

To test which of these interneurons are important for CO_2 avoidance behavior, we genetically ablated them individually using cell-specific caspase expression (Chelur and Chalfie, 2007; the original caspase plasmids was a gift from Daniel Colon-Ramos, Yale University) and tested ablated animals across a range of CO_2 concentrations in a chemotaxis assay. We found that ablation of AIY interneurons resulted in increased CO_2 avoidance behavior in 1% and 2.5% CO_2 compared to N2 wild-type animals (Figure 3-2). This was also confirmed using animals that

have a mutation in *ttx-3*, a LIM homeodomain protein that is required for specification and function of AIY interneurons (Hobert et al., 1997). *ttx-3* mutants showed significantly increased CO_2 avoidance across the same concentration range (data not shown). This suggests that AIY interneurons have an inhibitory or opposing effect on CO_2 avoidance behavior. We also saw that RIG- ablated animals have reduced avoidance behavior at 2.5% CO_2 compared to N2 wild type (Figure 3-2). This suggests RIG interneurons have a role in promoting CO_2 avoidance. Ablation of RIG did not completely abolish avoidance behavior, which suggests it acts redundantly to promote CO_2 avoidance. These results indicate behavioral sensitivity to CO_2 is mediated by opposing interneurons. We are still currently investigating the role of other targets of BAG in CO_2 response.

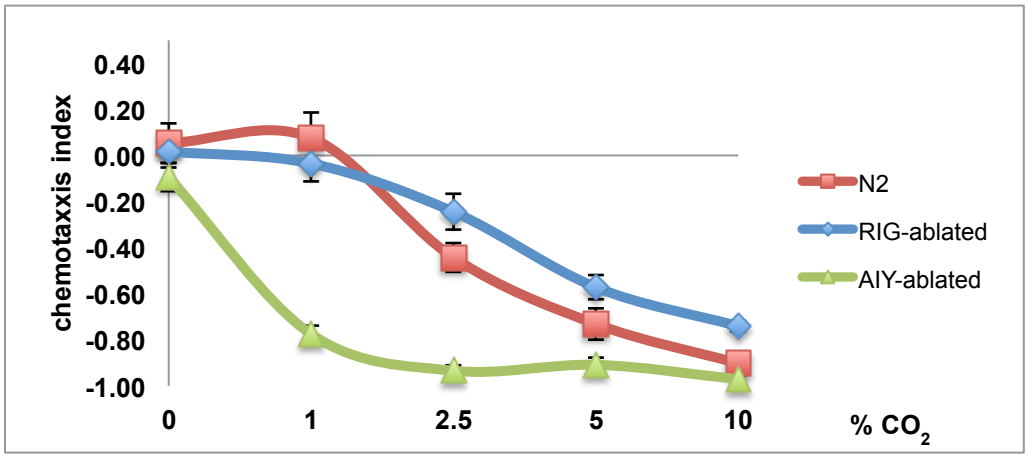

Fig. 3-2. Responses of RIG and AIY-ablated animals across CO_2 concentrations. Ablation of RIG interneurons results in decrease in CO_2 avoidance behavior at 2.5% CO_2 ($p < 0.05$, two-way ANOVA). Ablation of AIY interneurons results in increased CO_2 avoidance at 1% and 2.5% CO_2 concentrations (1% and 2.5% $p<0.0001$; two-way ANOVA). Chemotaxis assays were performed in a 21% O_2 background for each CO_2 concentration tested. Data generated by M.L.G.

If AIY interneurons have an inhibitory effect on the CO_2 circuit, then enhancing AIY synaptic output should result in a decrease in CO_2 avoidance. Likewise, if the role of RIG is to promote CO_2 avoidance, then enhancing RIG output should result in increase in CO_2 avoidance. To test this, we utilized a constitutively active form of protein kinase c homolog, *pkc-1(gf),* that promotes neuropeptide release (Sieburth et al., 2007). We expressed *pkc-1(gf)* specifically in AIY

interneurons and found that animals have reduced avoidance behavior in response to 2.5%, 5%, and 10% CO_2 (Figure 3-3). When we expressed *pkc-1(gf)* specifically in RIG, we saw increased avoidance in response to 2.5% and 5% CO_2 compared to N2. This supports our hypothesis that AIY activity opposes and RIG activity promotes CO_2 avoidance behavior, respectively.

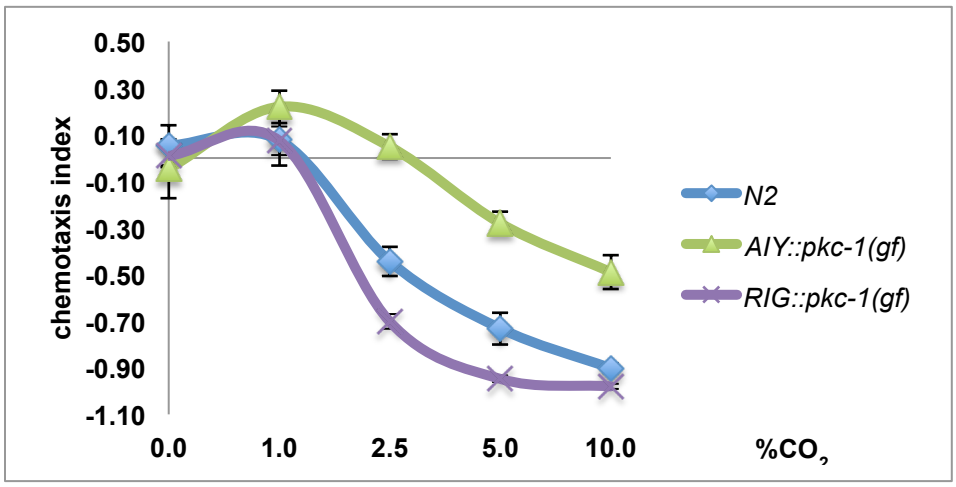

Fig. 3-3. Increasing synaptic transmission in AIY and RIG reveal antagonistic roles in CO_2 response. A constitutively active protein kinase c homolog *pkc-1(gf)* results in increased synaptic transmission. Expression of *pkc-1(gf)* in AIY resulted in decreased CO_2 avoidance at 2.5%, 5%, and 10% CO_2 concentrations (2.5% $p<0.0001$; 5% $p<0.001$; 10% $p<0.0001$, two-way ANOVA). Expressing *pkc-1(gf)* in RIG resulted in increased CO_2 avoidance in 2.5% and 5% CO_2 concentrations (2.5% $p<0.01$; 5% $p<0.05$, two-way ANOVA). All CO_2 chemotaxis assays were tested in a 21% O_2 background. Data generated by M.L.G.

We next asked whether AIY or RIG are targets of URX-mediated inhibition of CO_2 avoidance in *npr-1* mutants. We genetically ablated AIY in the *npr-1* loss of function *(lf)* background and tested for rescue of CO_2 avoidance behavior in response to 10% CO_2. We found that ablating AIY interneurons in *npr-1(lf)* restored CO_2 avoidance (Figure 3-4). Thus, *npr-1* modulates CO_2 response at or above the first-order interneuron level of the CO_2 circuit. We are currently working on testing RIG-ablated *npr-1(lf)* animals in response to CO_2. We are also going to image AIY interneurons in *npr-1*(*lf)* animals in response to CO_2 under high and low O_2 conditions to see if there is a difference in AIY activity compared to N2 animals.

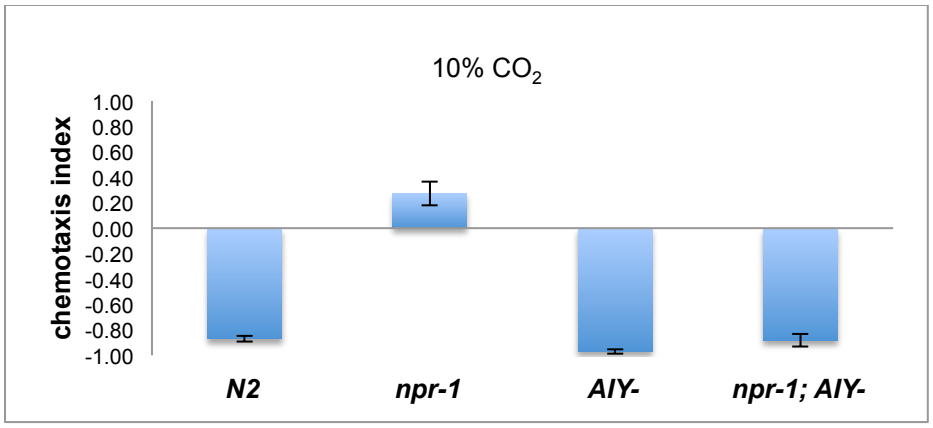

Fig. 3-4. Ablation of AIY interneurons rescues CO_2 avoidance in *npr-1* mutants. Animals were tested under 10% CO_2 in a 21% O_2 background in chemotaxis assays. *n*=8-14 for each genotype.

Our behavioral experiments suggest that AIY and RIG interneurons respond to CO_2 to modulate avoidance behavior. We used calcium imaging to evaluate AIY and RIG calcium activity in response to CO_2 using the calcium indicator yellow cameleon YC3.60. RIG activity increased in response to a 20 second pulse of 10% CO_2 (Figure 3-5). This CO_2-evoked activity was BAG-dependent as RIG activity was lost in BAG-ablated animals in response to 10% CO_2 (Figure 3-5). This suggests RIG interneurons are part of the CO_2 circuit.

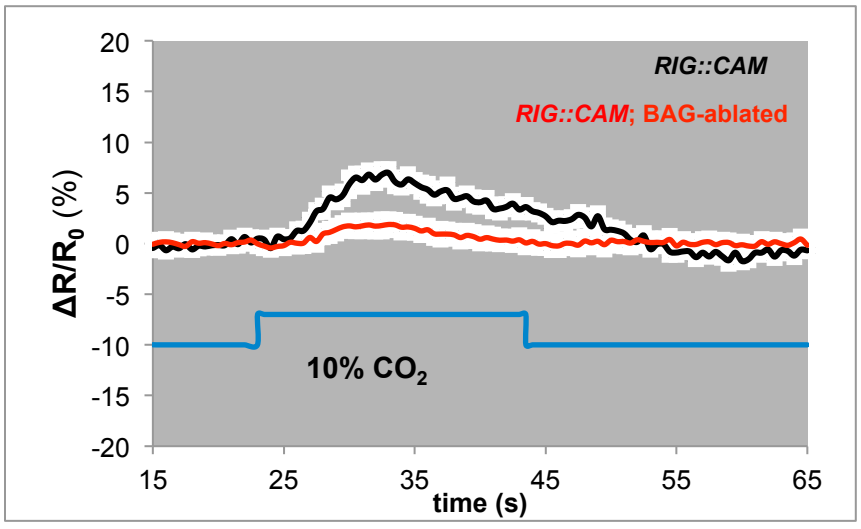

Fig. 3-5. RIG interneurons show CO_2-evoked activity that is BAG-dependent. RIG cell bodies were imaged in animals expressing ratiometric yellow calcium indicator YC3.60. Black traces indicate average calcium responses in N2 background. Red traces indicate average calcium responses in BAG-ablated background. White shading represents SEM. Blue line indicates timing of CO_2 pulse. Data generated by M.L.G.

We next imaged from AIY processes in response to 10% CO_2. We did not observe depolarization in response to 10% CO_2 pulse. Instead we saw a hyperpolarization response indicating AIY is inhibited by CO_2 (Figure 3-6). The CO_2-evoked inhibition was also BAG-dependent (Figure 3-6). Hence, opposite calcium activities in AIY and RIG mirror our behavioral results. These results suggest BAG neurons inhibit AIY and activate RIG to generate appropriate avoidance behavior to CO_2.

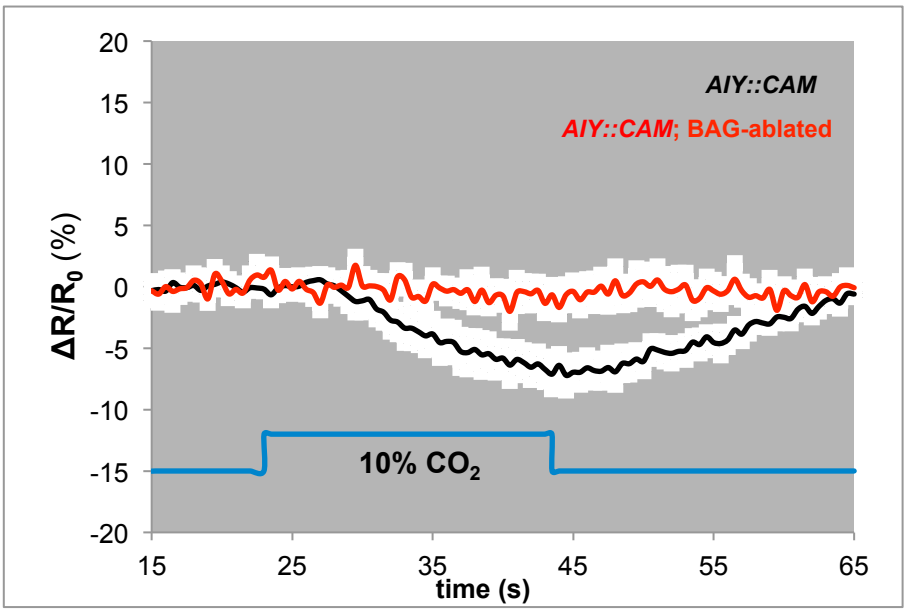

Fig. 3-6. AIY shows CO_2-evoked inhibition that is BAG-dependent. AIY processes were imaged in animals expressing the ratiometric calcium indicator yellow cameleon YC3.60. Black traces indicate average calcium responses in N2 background. Red traces indicate average calcium responses in BAG-ablated background. White shading represents SEM. Blue line indicates the timing of the CO_2 pulse. Data generated by M.L.G.

Food modulates a number of behaviors including thermotaxis, salt-sensing, oxygen, and CO_2 responses (de Bono et al., 2002; Bretscher et al., 2008, 2011; Chang et al., 2006; Cheung et al., 2005; Saeki et al., 2001; Sasakura and Mori, 2013). In *Drosophila*, the presence of food odors inhibits CO_2-evoked avoidance behavior (Turner and Ray, 2009). We asked whether an attractive food-related odorant could modulate CO_2 response in N2 and *npr-1(lf)* animals. We chose isoamyl alcohol because it is well-studied and characterized as a chemoattractant odorant (Bargmann et al., 1993). We diluted isoamyl alcohol (IAA) in paraffin oil (1:10) and

dipped the odorant on a filter paper and placed it on a lid of a 6 cm NGM plate. This chemotaxis setup is the same as described in Carrillo et al., 2013, except that the air and 10% CO_2 tubes were inserted on the sides of the NGM plate instead of the lid. We used paraffin oil as a control. We found that the presence of IAA had no effect on CO_2 avoidance behavior in N2 animals (Figure 3-7).

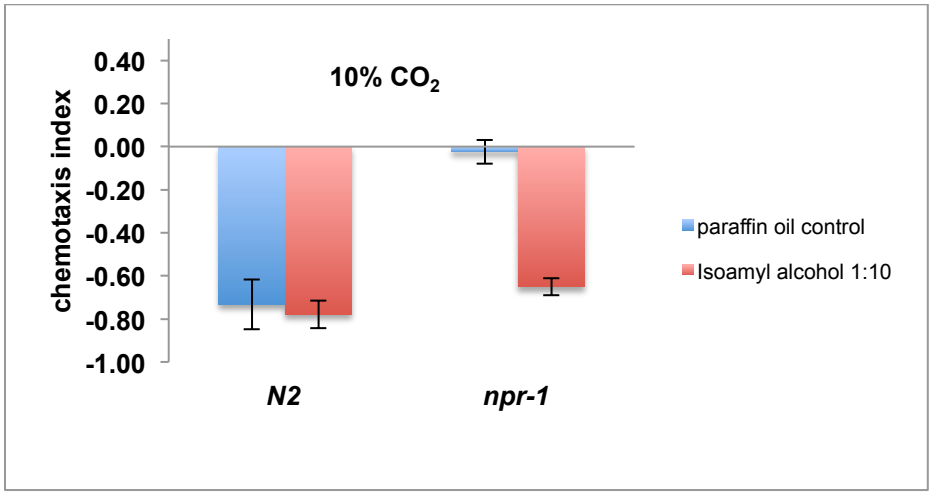

Fig. 3-7. Presence of isoamyl alcohol restores CO_2 avoidance in *npr-1* mutants. Chemotaxis assays were done using 6cm NGM plates with either filter paper dipped in paraffin oil or diluted odorant and placed on lid of assay plates. CO_2 stimulus consisted of 10% CO_2 in an air stream containing 21% O_2. *n*= 8-16 trials (paraffin oil control) for each genotype. *n*= 8-14 trials (IAA) for each genotype.

However, presence of the odorant did rescue CO_2 avoidance in *npr-1(lf)* animals *(*Figure 3-7). AWC neurons respond to IAA and have an odor-OFF response, where they are inhibited in presence of the odor and activated by removal of the odor (Chalasani et al., 2007). We wondered whether inhibition of AWC neurons by IAA was mediating the rescue of CO_2 avoidance in *npr-1(lf)* mutants. To investigate this, we tested AWC-ablated animals in the N2 and *npr-1(lf)* backgrounds in response to 10% CO_2. Ablation of AWC neurons in *npr-1(lf)* animals rescued CO_2 avoidance behavior (Figure 3-8).

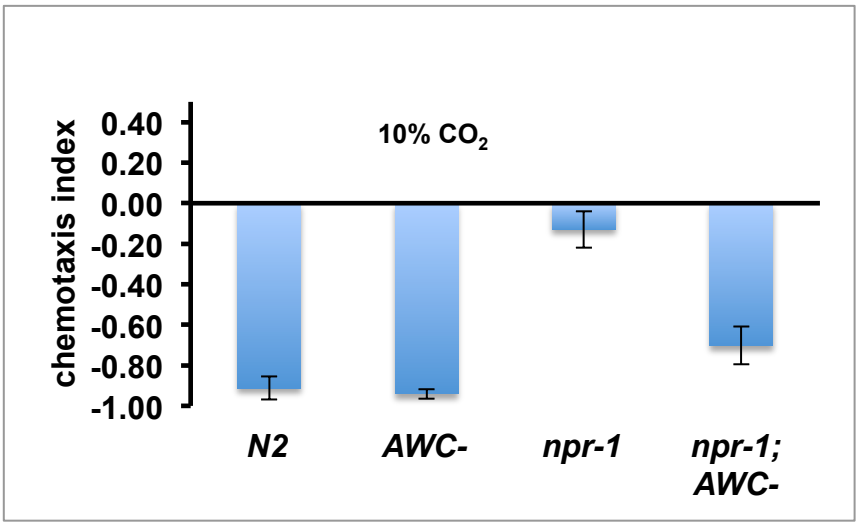

Fig.3-8. Ablation of AWC neurons restores CO_2 avoidance in *npr-1* mutants. Chemotaxis assays were done using 10% CO_2 with 10% O_2 background. *n*= 6-22 trials for each genotype. AWC-ablated animals express a transgene that specifically kills AWC neurons (a gift from Piali Sengupta lab, Brandeis University).

Although AWC-ablated N2 animals showed normal CO_2 avoidance at 10% CO_2, we observed an increase in CO_2 avoidance in these animals at lower CO_2 concentrations, similar to AIY-ablated animals at 2.5% and 5% CO_2 (data not shown). These results suggest that context-dependent modulation of CO_2 response includes food odor sensory neurons among thermosensory, oxygen, and salt sensory neurons (Bretscher et al., 2011; Carrillo et al., 2013; Kodama-Namba et al., 2013). Further experiments still need to be done to investigate how AWC neurons can modulate the CO_2 circuit and whether it does this through its strongest post-synaptic interneuron, AIY.

Materials and methods

CO_2 chemotaxis assays. All chemotaxis assays were performed as described in Carrillo et al., 2013.

Isoamyl alcohol CO_2 assay. Similar to chemotaxis assay, except small 6cm NGM plates were used as assay plates. To measure CO_2 avoidance in presence of odor, we dipped odor or paraffin oil in 6cm Whatman paper (odor diluted 1:10 in paraffin oil). Paraffin oil was used as a control. Animals were washed and prepared as described in Carrillo et al., 2013. To establish a CO_2 gradient, holes were made on opposite sides of the small NGM plate above agar level. Air

control and CO_2 gas tubes were then inserted. CO_2 stimuli consisted of 10% CO_2 and 21% O_2 and the rest was balanced with N_2.

Calcium imaging. Imaging was performed as described in Carrillo et al., 2013.

Ablation of interneurons. Cell-specific ablations were done using the two-component caspase-3 system developed by Dr. Martin Chalfie (Dattananda et al., 2007). In short, using transcriptional promoters whose expression patterns overlap uniquely in the cell of interest, we coexpressed inactive caspase-3 subunits, which together generate constitutively active caspase activity leading to cell death. This method is incredibly effective, therefore we also used it in cases where we had cell-specific promoters and did not necessarily need to employ an intersectional strategy. To genetically ablate the AIY interneuron we injected the following two plasmids into N2 worms, and generated stable transgenic lines: *Pttx-3 cz::caspase-3(p17)* and *Pttx-3 caspase-3(p12)::nz*

These plasmids were a gift from Daniel Colón-Ramos. Both plasmids were injected at a concentration of 50ng/uL along with the co-injection marker *myo-2::DsRed*. We verified that AIY was successfully ablated by crossing the transgenic lines expressing caspase-3 subunits to OH99. OH99 contains an integrated array expressing GFP in AIY. Presence of the *myo-2::DsRed* and loss of GFP confirmed the successful ablation of AIY.

To genetically ablate RIG, we replaced the *ttx-3* promoter in the two aforementioned plasmids with the RIG-specific promoter *twk-3*. The *Ptwk-3 cz::caspase-3(p17)* and *Ptwk-3 caspase-3(p-12)::nz* plasmids were injected at a concentration of 35ng/uL along with the co-injection marker *myo-2::DsRed*. To confirm the successful ablation of RIG we crossed the transgenic line expressing caspase-3 subunits to EAH269. EAH269 contains *twk-3::SL2 GFP*, which expresses GFP in RIG, due to the *twk-3* promoter, and GFP in the tail due to a basal promoter within the

SL2 GFP plasmid. Presence of *myo-2::DsRed* along with GFP in the tail, and loss of GFP in the head neuron, confirmed the successful ablation of RIG.

Generation of pkc-1(gf) lines. To express the Protein Kinase C gain of function mutation *pkc-1(gf)* in BAG, AIY and RIG, we used the cell-specific promoters *flp-17, ttx-3* and *twk-3*, respectively. We obtained the *pkc-1(gf) SL2 GFP* sequence from the PEM_15 plasmid sent to us from the Bargmann lab. All three resulting *pkc-1(gf) SL2 GFP* plasmids were injected at a concentration of 50ng/uL.

Chapter 4:

The immune response of *Drosophila* to entomopathogenic nematodes

This is a separate project I worked on with an undergraduate student in our lab, Jenny Peña.

IAI
Journals.ASM.org

Variation in the Susceptibility of *Drosophila* to Different Entomopathogenic Nematodes

Jennifer M. Peña, Mayra A. Carrillo, Elissa A. Hallem

Department of Microbiology, Immunology, and Molecular Genetics, University of California, Los Angeles, Los Angeles, California, USA

Entomopathogenic nematodes (EPNs) in the genera *Heterorhabditis* and *Steinernema* are lethal parasites of insects that are of interest as models for understanding parasite-host interactions and as biocontrol agents for insect pests. EPNs harbor a bacterial endosymbiont in their gut that assists in insect killing. EPNs are capable of infecting and killing a wide range of insects, yet how the nematodes and their bacterial endosymbionts interact with the insect immune system is poorly understood. Here, we develop a versatile model system for understanding the insect immune response to parasitic nematode infection that consists of seven species of EPNs as model parasites and five species of *Drosophila* fruit flies as model hosts. We show that the EPN *Steinernema carpocapsae*, which is widely used for insect control, is capable of infecting and killing *D. melanogaster* larvae. *S. carpocapsae* is associated with the bacterium *Xenorhabdus nematophila*, and we show that *X. nematophila* induces expression of a subset of antimicrobial peptide genes and suppresses the melanization response to the nematode. We further show that EPNs vary in their virulence toward *D. melanogaster* and that *Drosophila* species vary in their susceptibilities to EPN infection. Differences in virulence among different EPN-host combinations result from differences in both rates of infection and rates of postinfection survival. Our results establish a powerful model system for understanding mechanisms of host-parasite interactions and the insect immune response to parasitic nematode infection.

Entomopathogenic nematodes (EPNs) of the genera *Steinernema* and *Heterorhabditis* are insect-parasitic nematodes that are phylogenetically distant but share a similar life cycle as a result of convergent evolution (1). EPNs offer numerous advantages as model parasitic nematodes, including small size, short generation time, and amenability to *in vitro* culturing (2). EPN infective larvae are associated with bacterial endosymbionts: *Steinernema* species are associated with bacteria in the genus *Xenorhabdus*, and *Heterorhabditis* species are associated with bacteria in the genus *Photorhabdus* (1). At least some EPNs are capable of infecting the fruit fly *Drosophila melanogaster*, providing a genetically tractable system for understanding the immune response to parasitic nematodes and their bacterial endosymbionts (3–6). However, the insect immune response to EPN infection is poorly understood.

During a particular developmental stage called the infective juvenile (IJ), EPNs infect insects (Fig. 1A). IJs are developmentally arrested, third-stage larvae analogous to the dauer stage of free-living nematodes (7). IJs actively seek out insect hosts using chemosensory cues (8–10) and infect either by entering through natural body openings or by penetrating the insect cuticle (11). IJs harbor their bacterial endosymbiont in their gut and deposit it into the insect upon infection, where it assists the nematode in killing the insect, digesting insect tissues, and inhibiting the growth of other microorganisms (12–14). Following infection, the nematodes reproduce in the insect cadaver and feed on the bacterium-infested tissue until resources are depleted, at which point new IJs form and emerge from the cadaver to search for new hosts (Fig. 1B) (15).

In response to EPN infection, insects mount an innate immune response that involves antimicrobial peptide (AMP) expression as well as activation of the melanization and encapsulation reactions (11). At the same time, the nematodes attempt to evade or suppress the insect immune response through a process that remains poorly understood. Both the nematode and its bacterial endosymbiont appear to inhibit some aspects of AMP production, melanization, encapsulation, and phagocytosis (11, 16–18). Studies using *D. melanogaster* larvae as a model host for the EPN *Heterorhabditis bacteriophora* and its endosymbiont *Photorhabdus luminescens* have shown that infection induces expression of a large number of immune genes, including AMPs, and that AMP expression is primarily a response to the bacterial endosymbiont rather than to the nematode (4, 19). Infection also stimulates clotting, and clotting mutants show decreased survival in response to *H. bacteriophora-P. luminescens* infection (20, 21). However, studies of the immune response of *D. melanogaster* to EPN infection have so far been limited to *H. bacteriophora-P. luminescens*, and the extent to which the immune response differs for different EPNs is unclear.

Here, we demonstrate that the distantly related EPN *Steinernema carpocapsae* and its bacterial endosymbiont *Xenorhabdus nematophila* are capable of infecting *D. melanogaster* larvae and are more virulent toward *D. melanogaster* than *H. bacteriophora-P. luminescens*. Infection with *S. carpocapsae* symbiont IJs (i.e., IJs harboring *X. nematophila* in their gut) induced expression of a subset of AMP genes. *S. carpocapsae* infection also activated the

Received 6 October 2014 **Returned for modification** 21 November 2014
Accepted 29 December 2014
Accepted manuscript posted online 5 January 2015
Citation Peña JM, Carrillo MA, Hallem EA. 2015. Variation in the susceptibility of *Drosophila* to different entomopathogenic nematodes. Infect Immun 83:1130–1138. doi:10.1128/IAI.02740-14.
Editor: J. A. Appleton
Address correspondence to Elissa A. Hallem, ehallem@microbio.ucla.edu.
Supplemental material for this article may be found at http://dx.doi.org/10.1128/IAI.02740-14.

doi:10.1128/IAI.02740-14

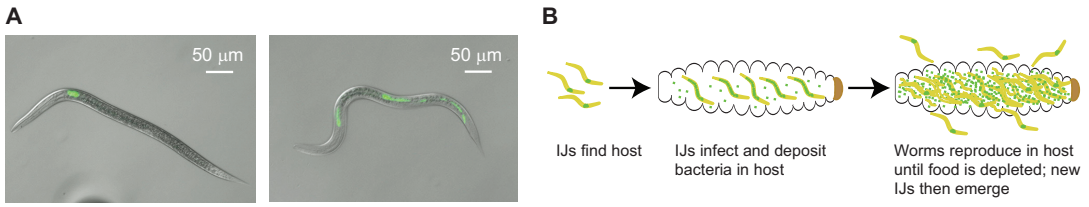

FIG 1 Life cycle of *S. carpocapsae*. (A) Photomicrographs of *S. carpocapsae* infective juveniles (IJs) with GFP-expressing *X. nematophila*. The left frame shows an IJ outside the host, and the right frame shows an IJ that was extracted from a host and that is defecating *X. nematophila*. (B) The life cycle of *S. carpocapsae*. IJs in the soil find a host, enter through a natural body opening, and defecate their symbiotic bacteria into the host. The bacteria play an important role in overcoming the host immune system (1). The nematodes develop and reproduce in the insect cadaver until resources are depleted. New IJs then form and exit the cadaver. Green dots represent the bacterial endosymbiont.

melanization pathway, and a higher rate of melanization occurred following infection with axenic IJs than with symbiont IJs, suggesting that *X. nematophila* suppresses the melanization response. Finally, exposure of *D. melanogaster* larvae to seven different EPN species revealed that EPNs vary in their virulence levels toward *D. melanogaster*, and exposure of five different *Drosophila* species to *S. carpocapsae* symbiont IJs revealed that *Drosophila* species vary in their susceptibilities to EPN infection. Our results establish the EPN-*Drosophila* system as a powerful model for investigating the insect immune response to nematode infection.

MATERIALS AND METHODS

Nematode strains. The following EPN strains were used: *S. carpocapsae* ALL (8, 9), *H. bacteriophora* Baine (22), *Steinernema glaseri* NC (23), *Steinernema scapterisci* FL (24), *Steinernema riobrave* TX (25), *Heterorhabditis indica* HOM1 (22), and *Steinernema feltiae* SN (26).

***Drosophila* stocks.** Wild-type *D. melanogaster* larvae were from the Canton-S strain. Studies of AMP expression were conducted with strains of *D. melanogaster* containing either an *attacinA*::*GFP*, *cecropinA1*::*GFP*, *metchnikowin*::*GFP*, *drosocin*::*GFP*, *drosomycin*::*GFP*, *diptericin*::*GFP*, or *defensin*::*GFP* transgene (where GFP is green fluorescent protein) (27). Wild-type *Drosophila virilis*, *Drosophila simulans*, *Drosophila yakuba*, and *Drosophila pseudoobscura* were stocks 15010-1051.00, 14021-0251.006, 14021-0261.00, and 14011-0121.104 from the *Drosophila* Species Stock Center, respectively. We note that all *D. melanogaster* strains, as well as the wild-type *Drosophila simulans* strain, were confirmed to be infected with *Wolbachia* by PCR using previously described primers (28). However, *Wolbachia* status is unlikely to affect susceptibility to EPNs or their bacterial endosymbionts: although *Wolbachia* infection may protect against some viral infections (29, 30), it does not appear to protect against other types of infections and has little or no effect on AMP expression (29, 31–33).

Bacterial strains. The following bacterial strains were used: wild-type *X. nematophila* HGB800 (34), GFP-expressing *X. nematophila* HGB340 (13), colonization-defective *X. nematophila* HGB777 (35), *Escherichia coli* OP50-GFP, *P. luminescens* TT01-GFP (36), *Photorhabdus temperata* NC1-GFP (36), and colonization-defective *P. temperata* NC1-GFP TRN16 (36). *Xenorhabdus* was grown in LB broth containing 0.1% sodium pyruvate, and *Photorhabdus* was grown in PP3 broth as previously described (8).

Nematode culturing. To generate symbiont IJs, nematodes were cultured in either the waxworm *Galleria mellonella* (for all species except *S. scapterisci*) or the house cricket *Acheta domestica* (for *S. scapterisci*) as previously described (8, 9). Briefly, five last-instar waxworms or one medium-sized cricket (American Cricket Ranch, Lakeside, CA) was placed in a 5-cm petri dish with a 55-mm Whatman 1 filter paper in the bottom of the dish. Approximately 500 to 1,000 IJs suspended in water were distributed on the filter paper and on the insects. Petri dishes were stored either at 25°C in the case of *H. bacteriophora* and *S. riobrave* or at room temperature (22 to 23°C) in the case of all other species. *H. bacteriophora* and *S. riobrave* infections were performed at 25°C because these species are found primarily in warm climates (37) and infect insects more efficiently at 25°C than at room temperature. Infections for the other species were performed at room temperature because these species infect more efficiently at room temperature than at 25°C. After ~10 days the insect cadavers were placed on White traps (38) or, in the case of *S. glaseri*, on modified White traps containing plaster of Paris (9). Symbiont IJs were collected from traps within 10 days, stored at 15°C, and tested within 1 month of collection.

To generate axenic *S. carpocapsae* IJs, symbiont *S. carpocapsae* IJs were surface sterilized by incubation in 1% commercial bleach for 5 min. IJs were then rinsed three times in distilled H_2O (dH_2O), incubated in antibiotic solution (10 μg/ml gentamicin, 100 μg/ml streptomycin, 100 μg/ml carbenicillin, and 20 μg/ml kanamycin in dH_2O) for 48 h, and plated onto 1× lipid agar-cholesterol plates (39) (final concentration of cholesterol, 5 mg/liter) containing 0.1% sodium pyruvate and seeded with *X. nematophila* HGB777 bacteria (35). Axenic nematodes were maintained on lipid agar-cholesterol plates seeded with HGB777, and IJs were collected from plates as previously described (8). IJs were incubated in 1% commercial bleach for 5 min and then rinsed three times in dH_2O to surface sterilize them prior to testing. To verify that the IJs were axenic, 5 μl of IJ pellet was plated onto a lipid agar-cholesterol plate and incubated at 25°C. The absence of bacteria on the plate was confirmed after 2 to 3 days.

To generate symbiont *S. carpocapsae* IJs containing GFP-expressing *X. nematophila*, axenic IJs were plated onto lipid agar-cholesterol plates seeded with *X. nematophila* HGB340 bacteria. Nematodes were maintained on lipid agar-cholesterol plates seeded with HGB340, and IJs were collected from plates as previously described (8).

To generate symbiont *H. bacteriophora* IJs containing GFP-expressing *P. luminescens*, symbiont *H. bacteriophora* IJs that had emerged from waxworms were plated onto 1× lipid agar-cholesterol plates (39) containing 0.1% sodium pyruvate seeded with *P. temperata* NC1 TRN16 bacteria (36). IJs were collected from plates as previously described (8) and plated onto 1× lipid agar-cholesterol plates seeded with *P. luminescens* TT01-GFP bacteria (36). Nematodes were maintained on 1× lipid agar-cholesterol plates seeded with TT01-GFP, and IJs were collected from plates as previously described (8). Axenic *H. bacteriophora* IJs were generated as described above for axenic *S. carpocapsae* IJs, except that they were plated onto and maintained on TRN16.

Infection of *Drosophila* larvae with EPNs. IJs used to assay survival were grown in waxworms; IJs used to assay infection were grown on GFP-expressing bacteria. IJs were rinsed three times in dH_2O, and 10 μl of water containing 500 IJs was pipetted onto the center of a 5-cm petri dish containing nematode growth medium (NGM). For each trial, 20 third-instar *Drosophila* larvae were rinsed twice in 1× phosphate-buffered saline (PBS) and placed onto the NGM plate containing IJs. *Drosophila*

larvae infected with *H. bacteriophora* and *S. riobrave* were kept in a 25°C incubator; larvae infected with all other strains were kept at room temperature. Different temperatures were used for *H. bacteriophora* and *S. riobrave* because these species are adapted for infection and growth at warmer temperatures than the other species, as described above. Metal rings were placed onto the plate lids as weights to prevent fly larvae from escaping. Infection and survival were scored at 24 and 48 h postexposure to IJs. Melanization was scored at 48 h postexposure to IJs to ensure that a majority of the population had been infected.

To score infection, fly larvae or pupae (in cases where the fly larvae pupated during the course of the experiment) were assayed under an epifluorescence dissecting microscope. IJs grown on GFP-expressing symbiotic bacteria were used to facilitate detection of worms inside the fly host. Fly larvae or pupae were considered infected if worms were visible inside the body. Although worms could be seen inside the host even without the presence of GFP-expressing symbiotic bacteria, worms could be identified more efficiently when they had GFP-expressing symbiotic bacteria. To score survival, fly larvae or pupae were assayed under a dissecting microscope at ×50 magnification. Animals were determined to be alive if they had a visible heartbeat or responded to gentle prodding.

To score melanization, fly larvae or pupae were first scored under a dissecting microscope at ×50 magnification for black spots on the cuticle and then dissected to determine whether they were infected. For each trial, the percentage of infected fly larvae or pupae with visible melanization was quantified. A value of 100% would indicate that all of the infected *D. melanogaster* larvae showed visible melanization; a value of 0% would indicate that none of the infected *D. melanogaster* larvae showed visible melanization.

Infection of *Drosophila* larvae with bacteria. GFP-expressing *X. nematophila*, *E. coli*, or *P. luminescens* cells were used for infection assays; wild-type bacteria were used for all other assays. To generate each assay plate, 100 μl of a bacterial suspension (for *X. nematophila* and *E. coli*) or 200 μl of bacterial suspension (for *P. luminescens*) from a 1- or 2-day culture was spread onto a 5-cm plate containing LB supplemented with 100 μg/ml carbenicillin and 0.1% sodium pyruvate (*X. nematophila*), LB alone (*E. coli*), or 1× lipid agar with cholesterol plus 0.1% sodium pyruvate (*P. luminescens*). Plates were incubated at 25°C for 1 to 2 days (*X. nematophila* and *P. luminescens*) or at 37°C overnight (*E. coli*) to create a bacterial lawn. For each trial, 20 second-instar or early-third-instar *D. melanogaster* larvae were rinsed in 1× PBS and placed onto a plate containing a bacterial lawn. A second plate containing a bacterial lawn was then secured upside down on top of the first plate to prevent the fly larvae from avoiding the bacteria by crawling onto the plate lid. Survival was scored at 24, 48, and 72 h as described above. To assay infection, fly larvae were washed twice in 1×PBS, placed onto unseeded NGM plates, and scored for GFP expression under an epifluorescence dissecting microscope after 24 and 48 h. All flies with visible GFP expression inside the body were scored as GFP positive. The percentages of GFP-positive fly larvae were then calculated. Fly larvae that were GFP negative at 24 h were placed onto new plates seeded with bacteria and scored again at 48 h. No GFP expression was observed in control experiments where fly larvae were not exposed to bacteria.

AMP expression assay. AMP expression was assayed in *D. melanogaster* larvae following infection with symbiont IJs, axenic IJs, or bacteria. For these experiments, both symbiont IJs and axenic IJs were grown *in vitro* on plates containing lawns of *X. nematophila* to eliminate any potential differences in *D. melanogaster* AMP expression resulting from differences in nematode culturing conditions. We used seven different transgenic *D. melanogaster* strains as hosts, each of which expressed a reporter construct in which GFP expression was driven by the promoter of a different AMP gene (27). Details of the transgenic *D. melanogaster* larvae expressing the AMP reporter constructs are described above under "*Drosophila* stocks." We note that no GFP-expressing *X. nematophila* was present in this experiment; symbiont IJs contained bacteria that did not express GFP, and the bacteria used for bacterial infections also did not express GFP. Thus, the GFP expression observed in these experiments was from the transgenic *D. melanogaster* hosts and was a reflection of AMP gene expression.

Infection of transgenic *D. melanogaster* larvae was performed as described above; each trial consisted of 20 fly larvae. For the uninfected controls, fly larvae were placed onto either NGM plates without IJs (controls for infection with symbiont or axenic IJs) or LB plates without bacteria (control for infection with *X. nematophila*). AMP expression was scored at 24 h postexposure to IJs. We note that in initial experiments, AMP expression was scored at 8, 24, and 48 h postexposure to IJs. AMP expression levels at 8 h postexposure were low because most fly larvae had not yet been infected, and no difference was observed between AMP expression levels at 24 and 48 h postexposure (data not shown). We therefore focused on the 24-h time point for further experiments.

To score AMP expression, larvae were removed from the plates, rinsed twice in 1× PBS, placed onto unseeded NGM plates, and observed using the GFP filter of an epifluorescence dissecting microscope. For the *attacin*, *cecropin*, *defensin*, *drosocin*, and *metchnikowin* genes, fly larvae were scored as GFP positive if any GFP expression was observed. For the *diptericin* and *drosomycin* genes, fly larvae were scored as GFP positive if diffuse GFP expression was observed because small spots of GFP expression were often observed under normal culturing conditions. The percentage of fly larvae expressing GFP was then calculated. We note that we previously validated our visual GFP scoring method for these reporter lines by comparing expression data obtained by visual scoring versus quantification in ImageJ and determining that expression data obtained by both methods were consistent (4). To control for GFP expression not due to infection with IJs or bacteria, the percentage of GFP-positive fly larvae obtained from the uninfected control experiments was subtracted from the percentage of GFP-positive fly larvae obtained from the infection experiments. Thus, Fig. 3 reports the background-subtracted values for the percentage of fly larvae that express the indicated AMP reporter construct.

For the bacterial infection experiment, plates were observed at 24 and 48 h postexposure to *X. nematophila*. On plates where some or all of the fly larvae had burrowed into the agar by the 24-h time point, all larvae on that plate were transferred to a new *X. nematophila* plate to ensure that the fly larvae remained in contact with the bacteria for the duration of the experiment.

Examining the time course for infection and survival following EPN exposure. For each trial, ~20 fly larvae were exposed to symbiont IJs containing GFP-expressing *X. nematophila* or *P. temperata*. IJs were used within 1 week of collection. Infection was scored at 2, 4, 6, 8, 24, and 48 h postexposure to IJs and was visualized using the GFP filter on an epifluorescence microscope. At each time point, larvae were rinsed twice in 1×PBS and placed onto unseeded NGM plates prior to scoring. After scoring, infected larvae were placed onto unseeded NGM plates that did not contain IJs, while uninfected larvae were placed back onto the original plate containing IJs so that they could be scored for infection at later time points. To examine postinfection survival, all larvae infected by 8 h were scored for survival at 24 and 48 h. Trials in which fewer than three fly larvae became infected by 8 h were not included in the analysis. To assay long-term survival, animals were scored for infection and survival as described above, except that any animals still alive at 48 h were placed onto new unseeded NGM plates and monitored for survival to adulthood.

Statistical analysis. Statistical analysis was performed using GraphPad Instat or Prism software. Standard statistical tests were used for all experiments, as described in the figure legends. All statistical comparisons are described in the relevant figure legends and supplemental tables. The value for sample size (*n*) used for statistical analysis refers to the number of trials performed for each treatment, condition, or genotype; each trial consisted of ~20 fly larvae.

RESULTS AND DISCUSSION

***S. carpocapsae* infects and kills *D. melanogaster*.** *S. carpocapsae* has a wide geographical distribution and a broad host range and is

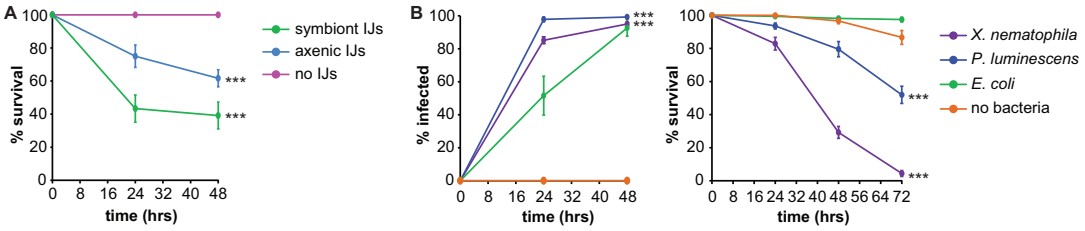

FIG 2 *S. carpocapsae* and its bacterial endosymbiont *X. nematophila* are pathogenic toward *D. melanogaster*. (A) Survival of *D. melanogaster* larvae exposed to symbiont *S. carpocapsae* IJs, axenic S. *carpocapsae* IJs, or no IJs. All three survival curves are significantly different ($P < 0.0001$, log rank test). ***, $P < 0.001$ relative to the no-IJ control (log rank test with Bonferroni correction; $n = 6$ trials for each condition). (B) Infection (left) and survival (right) of *D. melanogaster* larvae exposed to either *X. nematophila*, *P. luminescens*, *E. coli*, or no bacteria. All three species of bacteria successfully infected *D. melanogaster* (left graph) although infection rates were significantly different for each species ($P < 0.01$, log rank test). ***, $P < 0.001$ for *X. nematophila* and *P. luminescens* relative to *E. coli* (log rank test with Bonferroni correction). The survival curve for fly larvae exposed to *E. coli* was not significantly different from the survival curve for the no-bacteria control (right graph); all other survival curves were significantly different from each other ($P < 0.001$, log rank test with Bonferroni correction). ***, $P < 0.001$ relative to *E. coli* and the no-bacteria control (log rank test with Bonferroni correction). The no-bacteria control shown in the graph was performed on LB plates; a no-bacteria control was also performed on lipid-agar plates (for comparison to *P. luminescens*), and results were not significantly different from those of the control on LB plates ($P = 0.2728$, log rank test; $n = 5$ to 9 trials for each condition). For all graphs, the *x* axis refers to time postexposure, and error bars represent standard errors of the means. In some cases, error bars are too small to be visible.

used as a biocontrol agent for numerous insect pests (40). To determine whether *S. carpocapsae* is pathogenic for *D. melanogaster*, we used an infection assay in which we exposed third-instar fly larvae to symbiont IJs. Third-instar larvae were used for this assay because EPNs typically infect late-stage insect larvae (41). We scored infection and survival at 24 and 48 h postexposure since EPNs generally kill hosts within 48 h (41). We found that approximately 60% of the fly larvae exposed to symbiont IJs died within 24 h (Fig. 2A). Thus, *S. carpocapsae* is capable of infecting and killing *D. melanogaster* larvae. To determine whether pathogenicity was conferred primarily by *S. carpocapsae* or *X. nematophila*, we exposed fly larvae to axenic IJs. We found that axenic IJs were also capable of infecting and killing *D. melanogaster* larvae, although with less efficiency than symbiont IJs (Fig. 2A). Thus, *S. carpocapsae* IJs are pathogenic for *D. melanogaster* even in the absence of *X. nematophila*, consistent with previous studies of *S. carpocapsae* infection in larger insects, such as *Galleria mellonella* (42).

We then examined the pathogenicity of *X. nematophila* in the absence of its nematode vector by exposing fly larvae to agar plates containing lawns of *X. nematophila*. For comparison, we also exposed fly larvae to lawns of *P. luminescens* and *E. coli*. We found that exposure to all three bacteria resulted in infection of fly larvae, as determined by counting the number of GFP-positive fly larvae postexposure to GFP-labeled bacteria (Fig. 2B, left graph). *X. nematophila* was pathogenic for *D. melanogaster* larvae: 95% of fly larvae exposed to *X. nematophila* were dead by 72 h (Fig. 2B, right graph). *X. nematophila* was significantly more virulent than *P. luminescens*, which killed only approximately 50% of fly larvae by 72 h (Fig. 2B). In contrast, *E. coli* was not pathogenic for *D. melanogaster* larvae. These results are consistent with a previous study which found that *X. nematophila* is more virulent than *P. luminescens* when injected into *D. melanogaster* adults (43). Taken together, these results suggest that both *P. luminescens* and *X. nematophila* are pathogenic for *D. melanogaster* larvae but differ in their virulence levels.

Infection of fly larvae with *X. nematophila* most likely occurred by ingestion since GFP-expressing bacteria appeared to localize initially to the digestive tract (see Fig. S1 in the supplemental material). This is consistent with our previous observations of exposure of fly larvae to *Photorhabdus* bacteria (4). Susceptibility to *X. nematophila* is not likely to be the result of exposure to external toxins, since nonfeeding third-instar larvae did not become infected with *X. nematophila* in our assay. However, we cannot exclude the possibility that *X. nematophila* secretes toxins that have external effects on second- and early-third-instar larvae but not older third-instar larvae.

Infection induces expression of antimicrobial peptide (AMP) genes. A major component of the insect innate immune response is AMP production by the fat body, a structure similar to the mammalian liver and adipose tissue (44). Studies of a number of insects, including the cecropia moth *Hyalophora cecropia*, the beet armyworm *Spodoptera exigua*, and the tobacco hornworm *Manduca sexta* have shown that EPN infection can induce expression of AMP genes and that both the nematode and the bacteria can suppress AMP activity (45–49). We previously showed that infection of *D. melanogaster* larvae with *H. bacteriophora* symbiont IJs resulted in expression of four AMP genes, *attacin*, *diptericin*, *drosomycin*, and *metchnikowin*, and that this expression was a specific response to *P. luminescens* (4). Similar results were subsequently observed for infection of *M. sexta* with *H. bacteriophora* symbiont IJs, thus validating *D. melanogaster* as a model for other insect hosts (45). The AMP genes *diptericin* and *drosomycin* have also been shown to be upregulated following direct injection of either *P. luminescens* or *X. nematophila* into *D. melanogaster* adults (43). However, the AMP response of *D. melanogaster* to infection with *S. carpocapsae* symbiont IJs had not yet been examined, and the extent to which AMP expression is induced by EPNs versus their bacterial endosymbionts remains unclear (4, 6, 45).

To determine whether infection of *D. melanogaster* larvae with *S. carpocapsae-X. nematophila* induces AMP expression, we exposed both second-instar and third-instar fly larvae to symbiont IJs and monitored AMP expression at 24 h postexposure. To monitor AMP expression, we used seven different transgenic fly lines, each of which contained a reporter construct that expressed GFP under the control of a different AMP gene promoter. For each transgenic line, AMP expression was determined by scoring the fly larvae or pupae (in cases where the fly larvae pupated during the

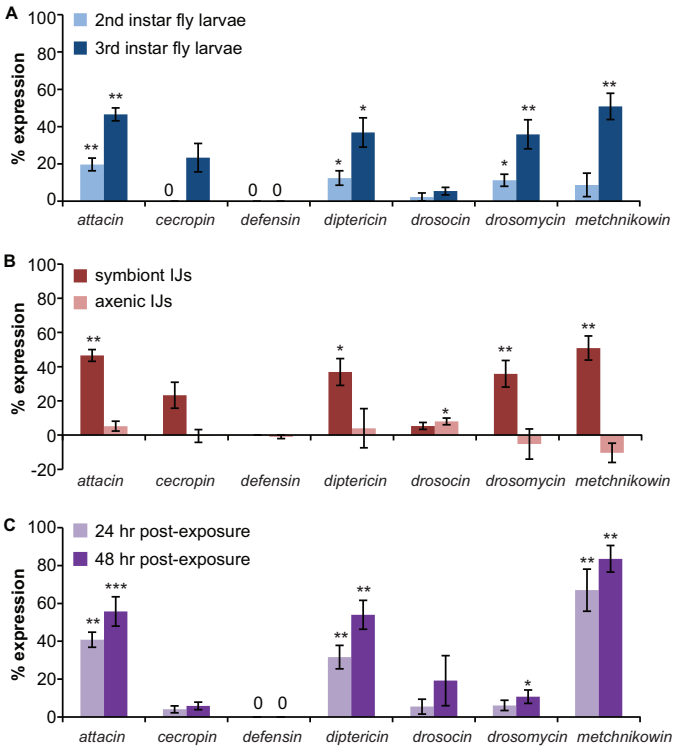

FIG 3 Infection of *D. melanogaster* larvae with symbiont *S. carpocapsae* IJs or *X. nematophila* induces a humoral immune response. (A) AMP expression following infection with symbiont *S. carpocapsae* IJs. Infection of second- or third-instar *D. melanogaster* larvae with symbiont *S. carpocapsae* IJs induces expression of a subset of AMP genes. (B) AMP expression following infection with symbiont versus axenic *S. carpocapsae* IJs. Infection of third-instar *D. melanogaster* larvae with symbiont *S. carpocapsae* IJs results in AMP expression, while infection with axenic *S. carpocapsae* IJs results in little or no AMP expression. Data for symbiont IJ exposure are from panel A. For panels A and B, AMP expression was examined at 24 h postexposure to IJs using transgenic fly larvae containing reporter constructs in which an AMP gene promoter was used to drive expression of GFP (27). (C) Infection of second-instar *D. melanogaster* larvae with *X. nematophila* results in AMP expression. AMP expression was examined at 24 and 48 h postexposure to bacteria using the same transgenic fly larvae as used in the experiments described in panels A and B. *, $P < 0.05$; **, $P < 0.01$; ***, $P < 0.001$, unpaired *t* test or Mann-Whitney test (infected larvae versus uninfected control larvae of the same genotype; $n = 5$ to 12 trials for each condition). For all graphs, error bars represent standard errors of the means.

course of the experiment) for GFP expression at 24 h postexposure to IJs and quantifying the percentage of fly larvae or pupae expressing GFP. We found that exposure of third-instar fly larvae to symbiont IJs induced significant expression of four AMP genes: *attacin*, *diptericin*, *drosomycin*, and *metchnikowin* (Fig. 3A). Thus, the same subset of AMP genes is induced by exposure to *S. carpocapsae* symbiont IJs and *H. bacteriophora* symbiont IJs (4). The percentage of animals showing AMP expression was higher for third-instar larvae exposed to symbiont IJs than for second-instar larvae exposed to symbiont IJs (Fig. 3A), most likely because symbiont IJs were more effective at killing third-instar than second-instar larvae (see Fig. S2 in the supplemental material).

To determine whether AMP expression is a response to the nematode or the bacteria, we first exposed fly larvae to axenic IJs. Third-instar fly larvae were used for this experiment since a higher rate of AMP expression was observed with third-instar larvae than with second-instar larvae (Fig. 3A). We found that whereas fly larvae exposed to symbiont IJs showed AMP expression, fly larvae exposed to axenic IJs showed little or no AMP expression (Fig. 3B). Thus, the AMP response observed upon infection with symbiont IJs is not observed upon infection with axenic IJs.

We then exposed fly larvae to bacteria alone by placing fly larvae on a plate containing a lawn of *X. nematophila*. Second-instar or early-third-instar larvae were used for these experiments since older third-instar larvae did not become infected with bacteria in this assay. Exposure to *X. nematophila* induced expression of the same four AMP genes that were induced by infection with symbiont IJs (Fig. 3C). The routes of infection differ for fly larvae exposed to symbiont IJs and bacteria, and we cannot exclude the possibility that AMP expression might vary based on the route of infection. However, our results suggest that AMP expression is primarily a response to *X. nematophila* rather than *S. carpocapsae*.

We note that for comparison of AMP expression following infection of *D. melanogaster* larvae with either symbiont IJs or axenic IJs, we used nematodes grown *in vitro* on plates containing

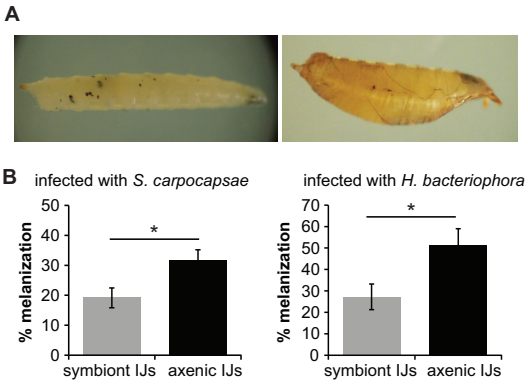

FIG 4 *X. nematophila* and *P. luminescens* partially suppress the melanization response of *D. melanogaster*. (A) Melanization from *S. carpocapsae* infection. The panel shows a representative *D. melanogaster* larva (left) and pupa (right) melanized by axenic *S. carpocapsae* IJs. (B) *X. nematophila* and *P. luminescens* inhibit melanization. Infection of *D. melanogaster* larvae with axenic *S. carpocapsae* (left graph) or *H. bacteriophora* (right graph) IJs resulted in a higher percentage of melanized fly larvae or pupae than infection with symbiont IJs. *, $P < 0.05$, unpaired *t* test. No melanization was observed in fly larvae not exposed to IJs. Melanization was scored at 48 h postexposure to IJs. Error bars represent standard errors of the means ($n = 7$ to 8 trials).

lawns of *X. nematophila* rather than nematodes grown in waxworms (see Materials and Methods). Growing nematodes *in vitro* was necessary to obtain axenic IJs, and thus both symbiont IJs and axenic IJs were grown *in vitro* for these experiments so that differences in AMP expression between axenic IJs and symbiont IJs could not be attributed to differences in nematode culturing conditions. However, we also directly tested whether AMP expression levels in fly larvae differed following infection with IJs cultured *in vitro* versus *in vivo*. We compared AMP expression in third-instar fly larvae infected with symbiont IJs grown on plates of *X. nematophila* and symbiont IJs grown in waxworms. No significant differences in AMP expression levels were observed following infection with IJs cultured *in vitro* versus *in vivo* (see Fig. S3 in the supplemental material), suggesting that the *D. melanogaster* immune response to *S. carpocapsae* symbiont IJs is similar, regardless of whether the IJs are cultured *in vitro* versus *in vivo*.

***X. nematophila* and *P. luminescens* suppress the melanization response of *D. melanogaster*.** Melanization is a cellular immune response of arthropods that results in melanin production at the wound site and that contributes to pathogen killing and wound healing (11, 50). Previous studies have shown that EPN infection of some insects results in rapid melanization and encapsulation of IJs although in permissive hosts IJs can escape the capsule and kill the insect (51–53). Both *Xenorhabdus* and *Photorhabdus* produce specific inhibitors of phospholipase A_2, a key component of the melanization and encapsulation reactions, suggesting that the bacterial endosymbionts of EPNs promote nematode survival by suppressing these reactions (54, 55). To test whether infection with *S. carpocapsae*-*X. nematophila* or *H. bacteriophora*-*P. luminescens* activates the melanization response, we exposed fly larvae to either symbiont or axenic IJs and scored infected larvae for the presence of visible melanin spots (Fig. 4A). We found that both symbiont and axenic IJs induced melanization but that axenic IJs induced a higher rate of melanization than symbiont IJs (Fig. 4B). These results suggest that *X. nematophila* and *P. luminescens* facilitate the killing of *D. melanogaster* larvae by partially suppressing the melanization response.

Virulence differs for different EPN-*Drosophila* combinations. To examine the versatility of the fruit fly-EPN model system, we compared the ability of symbiont IJs from seven EPN species—*S. carpocapsae*, S. *scapterisci*, *S. riobrave*, *S. glaseri*, *S. feltiae*, *H. bacteriophora*, and *H. indica*—to infect and kill *D. melanogaster* larvae. These EPN species differ dramatically in their host ranges: *S. carpocapsae* and *S. feltiae* have broad host ranges that include insects from multiple orders, *S. scapterisci* has a narrow host range that is limited to orthopterans, and the other species have intermediate host ranges (24, 56–59). *S. feltiae* was also recently shown to be virulent toward *D. melanogaster* (3). We exposed *D. melanogaster* larvae to symbiont IJs of the different EPN species and scored survival at 24 and 48 h. We found that virulence differed greatly among species: *S. scapterisci* and *S. riobrave* were not virulent toward *D. melanogaster* larvae, *S. carpocapsae* and *S. feltiae* were highly virulent, and the other species displayed intermediate virulence (Fig. 5A). Thus, EPNs vary in their virulence toward *D. melanogaster* larvae.

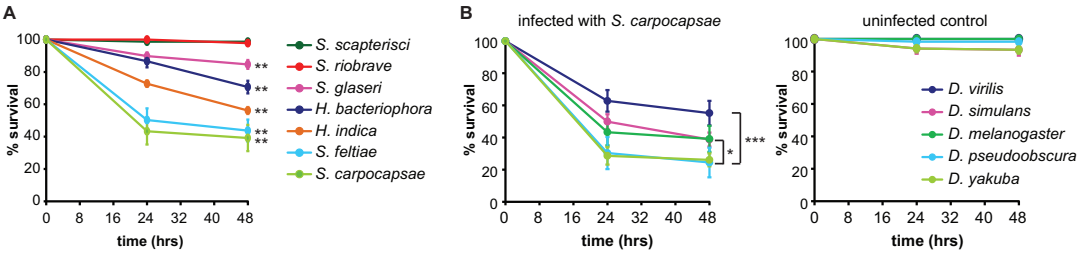

FIG 5 Species specificity of *Drosophila*-EPN interactions. (A) Infection of *D. melanogaster* with EPNs. EPNs vary in their virulence toward *D. melanogaster* larvae. Fly larvae were infected with symbiont IJs. Survival curves are significantly different ($P < 0.0001$, log rank test). Posttest results for each pairwise comparison are shown in Table S1 in the supplemental material. **, $P < 0.01$ relative to *S. scapterisci* (log rank test with Bonferroni correction; $n = 6$ to 8 trials for each condition). (B) *Drosophila* species vary in their susceptibility to *S. carpocapsae* symbiont IJ infection. Survival curves (left graph) are significantly different ($P < 0.01$, log rank test). Posttest results for each pairwise comparison are shown in Table S2 in the supplemental material. ***, $P < 0.001$ for *D. virilis* versus *D. pseudoobscura* and *D. virilis* versus *D. yakuba*; *, $P < 0.05$ for *D. pseudoobscura* versus *D. simulans*. The right graph shows survival curves of uninfected control larvae ($n = 6$ to 7 trials for each condition). For all graphs, the *x* axis refers to time postexposure, and error bars represent standard errors of the means.

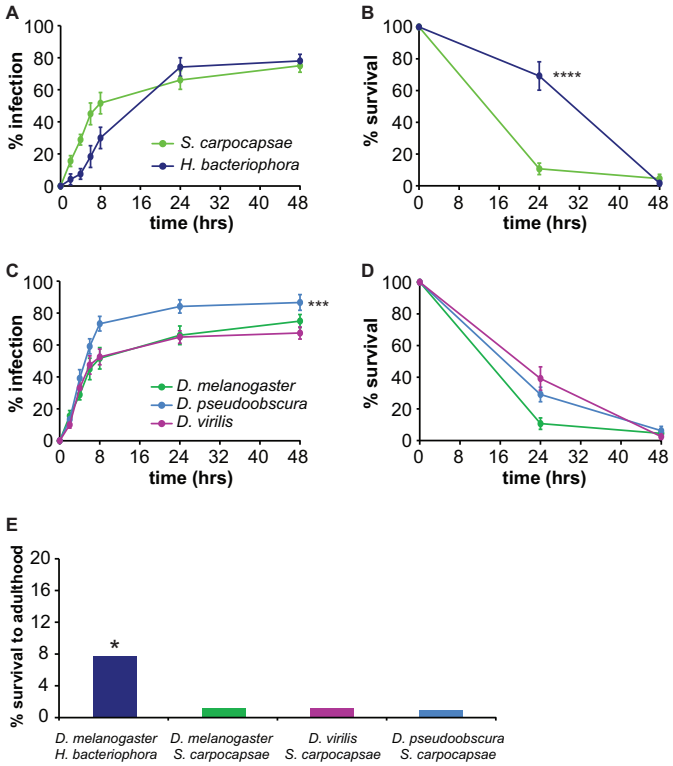

FIG 6 Virulence of EPNs for *Drosophila* species. (A) *D. melanogaster* infection. *S. carpocapsae* and *H. bacteriophora* symbiont IJs infect *D. melanogaster* larvae at the same rate ($P > 0.05$, log rank test; $n = 6$ to 9 trials for each condition). (B) Survival of *D. melanogaster*. *S. carpocapsae* symbiont IJs kill *D. melanogaster* larvae more rapidly than *H. bacteriophora* symbiont IJs. ****, $P < 0.0001$, log rank test. Survival was scored for fly larvae that became infected within 8 h of exposure to IJs ($n = 4$ to 9 trials for each condition). (C) Infection with *S. carpocapsae*. *S. carpocapsae* symbiont IJs infect *D. pseudoobscura* larvae more rapidly than *D. melanogaster* and *D. virilis* larvae. ***, $P < 0.001$ for *D. pseudoobscura* relative to *D. melanogaster* and *D. virilis* (log rank test with Bonferroni correction; $n = 6$ to 9 trials for each condition). (D) Survival from *S. carpocapsae* infection. *S. carpocapsae* symbiont IJs kill *D. melanogaster*, *D. pseudoobscura*, and *D. virilis* larvae at the same rate ($P > 0.05$, log rank test; $n = 6$ to 9 trials for each condition). Note that panels B and D show survival rates only of infected fly larvae rather than of all fly larvae exposed to EPNs. (E) Long-term survival of EPN-infected fly larvae. *D. melanogaster* larvae infected with *H. bacteriophora* symbiont IJs show a higher rate of long-term survival than the other *Drosophila*-EPN combinations. *, $P < 0.05$, chi-square test ($n = 52$ to 104 fly larvae for each condition). For graphs in panels A to D, error bars show standard errors of the means.

We then examined the ability of *S. carpocapsae*, one of the most virulent EPNs for *D. melanogaster*, to infect and kill four phylogenetically and ecologically diverse *Drosophila* species: *D. virilis*, *D. simulans*, *D. pseudoobscura*, and *D. yakuba*. We found that *S. carpocapsae* symbiont IJs were capable of infecting and killing all *Drosophila* species tested (Fig. 5B). However, survival rates following exposure to *S. carpocapsae* symbiont IJs varied across species, with *D. virilis* showing the highest survival rate and *D. pseudoobscura* and *D. yakuba* showing the lowest survival rates (Fig. 5B). Thus, *Drosophila* species vary in their susceptibility to EPN infection.

Studies of larger insects, such as the Japanese beetle *Popillia japonica*, the house cricket *Acheta domesticus*, and the Colorado potato beetle *Leptinotarsa decemlineata*, have suggested that differences in virulence among EPNs can be attributed to differences in the abilities of EPNs to infect different hosts as well as differences in the host immune response to infection (51–53). To investigate the cause of differences in survival rates among *Drosophila* species exposed to different EPNs, we examined infection rates and postinfection survival rates of selected *Drosophila*-EPN combinations. Infection rates were examined by using IJs containing GFP-expressing endosymbionts to facilitate detection of IJs within the host. Fly larvae were considered infected if nematodes were visible inside the body. We found that different *Drosophila*-EPN combinations varied in both the rates at which the fly larvae became infected and the rates at which they succumbed to the infection (Fig. 6). For example, although *S. carpocapsae* symbiont IJs and *H. bacteriophora* symbiont IJs infected *D. melanogaster* at the same rate, *S. carpocapsae* symbiont IJs killed *D. melanogaster* more rapidly than *H. bacteriophora* symbiont IJs (Fig. 6A and B). In contrast, *S. carpocapsae* symbiont IJs infected *D. pseudoobscura* more rapidly than *D. melanogaster* or *D. virilis*, but all three fly species succumbed to infection at the same rate (Fig. 6C and D). Thus, the *Drosophila*-EPN model system can be used to study

differences in both nematode infectivity and the host immune response to nematode infection.

We also assayed the long-term survival of EPN-infected *Drosophila* larvae by exposing fly larvae to symbiont IJs, separating out all fly larvae that became infected by 8 h postexposure to IJs, and monitoring their survival until death or adulthood. We found that *Drosophila* larvae were capable of surviving EPN infection at low levels (Fig. 6E). Moreover, survival rates varied for different EPN species: the long-term survival rate was 1% for *D. melanogaster*, *D. virilis*, and *D. pseudoobscura* infected with *S. carpocapsae* but 8% for *D. melanogaster* infected with *H. bacteriophora* (Fig. 6E). Thus, *Drosophila* larvae are more successful at overcoming some EPN infections than others. Whether long-term survival occurs because nematodes exit the host shortly after infection or because the host immune system overcomes the infection remains to be determined.

Conclusions. Our results demonstrate that both *S. carpocapsae* and its bacterial endosymbiont *X. nematophila* are pathogenic for *D. melanogaster* larvae. We also show that EPN species vary in their virulence toward *D. melanogaster* and that *Drosophila* species vary in their susceptibility to EPN infection. These differences in virulence reflect differences in both the rates at which fly larvae become infected with EPNs and the rates at which infected fly larvae succumb to the infection. All five of the *Drosophila* species tested have sequenced genomes (60), and six of the seven nematode species tested have sequenced or nearly sequenced genomes (61, 62). A comparison of *Drosophila* genomes revealed that many immune-related genes evolve more rapidly than other genes and identified numerous species-specific differences in immune-related genes, including copy number differences in AMP genes (63). Our results establish a versatile model system for investigating at a genome-wide level how genetic differences contribute to the diverse immune responses of insects to parasitic nematode infection.

ACKNOWLEDGMENTS

We thank Heidi Goodrich-Blair, David Shapiro-Ilan, Adler Dillman, Paul Sternberg, Utpal Banerjee, Cathy Clarke, and the *Drosophila* Species Stock Center for nematode, fly, and bacterial strains. We also thank Adler Dillman, Michelle Castelletto, Joon Ha Lee, Manon Guillermin, and Kristen Yankura for comments on the manuscript.

J.M.P. was a Howard Hughes Undergraduate Research Program Scholar and was supported by National Institute of General Medical Sciences grant R25GM055052. M.A.C. is an NSF Predoctoral Fellow and a Eugene V. Cota-Robles Fellow. E.A.H. is a MacArthur Fellow, a McKnight Scholar, a Rita Allen Foundation Scholar, and a Searle Scholar.

REFERENCES

1. **Dillman AR, Sternberg PW.** 2012. Entomopathogenic nematodes. Curr Biol **22:**R430–R431. http://dx.doi.org/10.1016/j.cub.2012.03.047.
2. **Ciche, T.** 20 February 2007. The biology and genome of *Heterorhabditis bacteriophora*. *In* The *C. elegans* Research Community (ed), WormBook. http://dx.doi.org/10.1895/wormbook.1.135.1.
3. **Dobes P, Wang Z, Markus R, Theopold U, Hyrsl P.** 2012. An improved method for nematode infection assays in *Drosophila* larvae. Fly **6:**75–79. http://dx.doi.org/10.4161/fly.19553.
4. **Hallem EA, Rengarajan M, Ciche TA, Sternberg PW.** 2007. Nematodes, bacteria, and flies: a tripartite model for nematode parasitism. Curr Biol **17:**898–904. http://dx.doi.org/10.1016/j.cub.2007.04.027.
5. **Castillo JC, Shokal U, Eleftherianos I.** 2012. A novel method for infecting *Drosophila* adult flies with insect pathogenic nematodes. Virulence **3:**339–347. http://dx.doi.org/10.4161/viru.20244.
6. **Castillo JC, Shokal U, Eleftherianos I.** 2013. Immune gene transcription in *Drosophila* adult flies infected by entomopathogenic nematodes and their mutualistic bacteria. J Insect Physiol **59:**179–185. http://dx.doi.org/10.1016/j.jinsphys.2012.08.003.
7. **Hotez P, Hawdon J, Schad GA.** 1993. Hookworm larval infectivity, arrest and amphiparatenesis: the *Caenorhabditis elegans* Daf-c paradigm. Parasitol Today **9:**23–26. http://dx.doi.org/10.1016/0169-4758(93)90159-D.
8. **Hallem EA, Dillman AR, Hong AV, Zhang Y, Yano JM, DeMarco SF, Sternberg PW.** 2011. A sensory code for host seeking in parasitic nematodes. Curr Biol **21:**377–383. http://dx.doi.org/10.1016/j.cub.2011.01.048.
9. **Dillman AR, Guillermin ML, Lee JH, Kim B, Sternberg PW, Hallem EA.** 2012. Olfaction shapes host-parasite interactions in parasitic nematodes. Proc Natl Acad Sci U S A **109:**E2324–E2333. http://dx.doi.org/10.1073/pnas.1211436109.
10. **Rasmann S, Ali JG, Helder J, van der Putten WH.** 2012. Ecology and evolution of soil nematode chemotaxis. J Chem Ecol **38:**615–628. http://dx.doi.org/10.1007/s10886-012-0118-6.
11. **Castillo JC, Reynolds SE, Eleftherianos I.** 2011. Insect immune responses to nematode parasites. Trends Parasitol **27:**537–547. http://dx.doi.org/10.1016/j.pt.2011.09.001.
12. **Ciche TA, Ensign JC.** 2003. For the insect pathogen *Photorhabdus luminescens*, which end of a nematode is out? Appl Environ Microbiol **69:**1890–1897. http://dx.doi.org/10.1128/AEM.69.4.1890-1897.2003.
13. **Martens EC, Heungens K, Goodrich-Blair H.** 2003. Early colonization events in the mutualistic association between *Steinernema carpocapsae* nematodes and *Xenorhabdus nematophila* bacteria. J Bacteriol **185:**3147–3154. http://dx.doi.org/10.1128/JB.185.10.3147-3154.2003.
14. **Akhurst RJ.** 1982. Antibiotic activity of *Xenorhabdus* spp., bacteria symbiotically associated with insect pathogenic nematodes of the families Heterorhabditidae and Steinernematidae. J Gen Microbiol **128:**3061–3065.
15. **Adams BJ, Nguyen KB.** 2002. Taxonomy and systematics, p 1–33. *In* Gaugler R (ed), Entomopathogenic nematology. CABI Publishing, New York, NY.
16. **Eleftherianos I, ffrench-Constant RH, Clarke DJ, Dowling AJ, Reynolds SE.** 2010. Dissecting the immune response to the entomopathogen *Photorhabdus*. Trends Microbiol **18:**552–560. http://dx.doi.org/10.1016/j.tim.2010.09.006.
17. **Richards GR, Goodrich-Blair H.** 2009. Masters of conquest and pillage: *Xenorhabdus nematophila* global regulators control transitions from virulence to nutrient acquisition. Cell Microbiol **11:**1025–1033. http://dx.doi.org/10.1111/j.1462-5822.2009.01322.x.
18. **Brivio MF, Mastore M, Nappi AJ.** 2010. A pathogenic parasite interferes with phagocytosis of insect immunocompetent cells. Dev Comp Immunol **34:**991–998. http://dx.doi.org/10.1016/j.dci.2010.05.002.
19. **Arefin B, Kucerova L, Dobes P, Markus R, Strnad H, Wang Z, Hyrsl P, Zurovec M, Theopold U.** 2014. Genome-wide transcriptional analysis of *Drosophila* larvae infected by entomopathogenic nematodes shows involvement of complement, recognition and extracellular matrix proteins. J Innate Immun **6:**192–204. http://dx.doi.org/10.1159/000353734.
20. **Hyrsl P, Dobes P, Wang Z, Hauling T, Wilhelmsson C, Theopold U.** 2011. Clotting factors and eicosanoids protect against nematode infections. J Innate Immun **3:**65–70. http://dx.doi.org/10.1159/000320634.
21. **Wang Z, Wilhelmsson C, Hyrsl P, Loof TG, Dobes P, Klupp M, Loseva O, Morgelin M, Ikle J, Cripps RM, Herwald H, Theopold U.** 2010. Pathogen entrapment by transglutaminase—a conserved early innate immune mechanism. PLoS Pathog **6:**e1000763. http://dx.doi.org/10.1371/journal.ppat.1000763.
22. **Shapiro-Ilan DI, Mizell RF.** 2012. Laboratory virulence of entomopathogenic nematodes to two ornamental plant pests, *Corythucha ciliata* (Hemiptera: Tingidae) and *Stethobaris nemesis* (Coleoptera: Curculionidae). Fla Entomol **95:**922–927. http://dx.doi.org/10.1653/024.095.0415.
23. **Li XY, Cowles EA, Cowles RS, Gaugler R, Cox-Foster DL.** 2009. Characterization of immunosuppressive surface coat proteins from *Steinernema glaseri* that selectively kill blood cells in susceptible hosts. Mol Biochem Parasitol **165:**162–169. http://dx.doi.org/10.1016/j.molbiopara.2009.02.001.
24. **Nguyen KB, Smart GC.** 1991. Pathogenicity of *Steinernema scapterisci* to selected invertebrate hosts. J Nematol **23:**7–11.
25. **Canhilal R, Reid W, Kutuk H, El-Bouhssini M.** 2007. Susceptibility of sunn pest, *Eurygaster integriceps* Puton (Hemiptera: Scutelleridae), to various entomopathogenic nematodes (Rhabditida: Steinernematidae and Heterorhabditidae). J Agric Urban Entomol **24:**19–26. http://dx.doi.org/10.3954/1523-5475-24.1.19.
26. **Campbell JF, Gaugler R.** 1997. Inter-specific variation in entomopatho-

genic nematode foraging strategy: dichotomy or variation along a continuum? Fundam Appl Nematol **20:**393–398.
27. **Tzou P, Ohresser S, Ferrandon D, Capovilla M, Reichhart JM, Lemaitre B, Hoffmann JA, Imler JL.** 2000. Tissue-specific inducible expression of antimicrobial peptide genes in *Drosophila* surface epithelia. Immunity **13:** 737–748. http://dx.doi.org/10.1016/S1074-7613(00)00072-8.
28. **O'Neill SL, Giordano R, Colbert AM, Karr TL, Robertson HM.** 1992. 16S rRNA phylogenetic analysis of the bacterial endosymbionts associated with cytoplasmic incompatibility in insects. Proc Natl Acad Sci U S A **89:**2699–2702. http://dx.doi.org/10.1073/pnas.89.7.2699.
29. **Hamilton PT, Perlman SJ.** 2013. Host defense via symbiosis in *Drosophila*. PLoS Pathog **9:**e1003808. http://dx.doi.org/10.1371/journal.ppat.1003808.
30. **Martinez J, Longdon B, Bauer S, Chan Y-S, Miller WJ, Bourtzis K, Teixeira L, Jiggins FM.** 2014. Symbionts commonly provide broad spectrum resistance to viruses in insects: a comparative analysis of *Wolbachia* strains. PLoS Pathog **10:**e1004369. http://dx.doi.org/10.1371/journal.ppat.1004369.
31. **Bourtzis K, Pettigrew MM, O'Neill SL.** 2000. *Wolbachia* neither induces nor suppresses transcripts encoding antimicrobial peptides. Insect Mol Biol **9:**635–639. http://dx.doi.org/10.1046/j.1365-2583.2000.00224.x.
32. **Chrostek E, Marialva MSP, Yamada R, O'Neill SL, Teixeira L.** 2014. High anti-viral protection without immune upregulation after interspecies *Wolbachia* transfer. PLoS One **9:**e99025. http://dx.doi.org/10.1371/journal.pone.0099025.
33. **Wong ZS, Hedges LM, Brownlie JC, Johnson KN.** 2011. *Wolbachia*-mediated antibacterial protection and immune gene regulation in *Drosophila*. PLoS One **6:**e25430. http://dx.doi.org/10.1371/journal.pone.0025430.
34. **Richards GR, Vivas EI, Andersen AW, Rivera-Santos D, Gilmore S, Suen G, Goodrich-Blair H.** 2009. Isolation and characterization of *Xenorhabdus nematophila* transposon insertion mutants defective in lipase activity against Tween. J Bacteriol **191:**5325–5331. http://dx.doi.org/10.1128/JB.00173-09.
35. **Cowles CE, Goodrich-Blair H.** 2004. Characterization of a lipoprotein, NilC, required by *Xenorhabdus nematophila* for mutualism with its nematode host. Mol Microbiol **54:**464–477. http://dx.doi.org/10.1111/j.1365-2958.2004.04271.x.
36. **Ciche TA, Kim KS, Kaufmann-Daszczuk B, Nguyen KC, Hall DH.** 2008. Cell invasion and matricide during *Photorhabdus luminescens* transmission by *Heterorhabditis bacteriophora* nematodes. Appl Environ Microbiol **74:**2275–2287. http://dx.doi.org/10.1128/AEM.02646-07.
37. **Hominick WM.** 2002. Biogeography, p 115–143. *In* Gaugler R (ed), Entomopathogenic nematology. CABI Publishing, New York, NY.
38. **White GF.** 1927. A method for obtaining infective nematode larvae from cultures. Science **66:**302–303. http://dx.doi.org/10.1126/science.66.1709.302.
39. **Vivas EI, Goodrich-Blair H.** 2001. *Xenorhabdus nematophilus* as a model for host-bacterium interactions: *rpoS* is necessary for mutualism with nematodes. J Bacteriol **183:**4687–4693. http://dx.doi.org/10.1128/JB.183.16.4687-4693.2001.
40. **Shapiro-Ilan DI, Gouge DH, Koppenhofer AM.** 2002. Factors affecting commercial success: case studies in cotton, turf, and citrus, p 333–355. *In* Gaugler R (ed), Entomopathogenic nematology. CABI Publishing, New York, NY.
41. **Kaya HK, Gaugler R.** 1993. Entomopathogenic nematodes. Annu Rev Entomol **38:**181–206. http://dx.doi.org/10.1146/annurev.en.38.010193.001145.
42. **Dowds BC, Peters A.** 2002. Virulence mechanisms, p 79–98. *In* Gaugler R (ed), Entomopathogenic nematology. CABI Publishing, New York, NY.
43. **Aymeric JL, Givaudan A, Duvic B.** 2010. Imd pathway is involved in the interaction of *Drosophila melanogaster* with the entomopathogenic bacteria, *Xenorhabdus nematophila* and *Photorhabdus luminescens*. Mol Immunol **47:**2342–2348. http://dx.doi.org/10.1016/j.molimm.2010.05.012.
44. **Liu Y, Liu H, Liu S, Wang S, Jiang RJ, Li S.** 2009. Hormonal and nutritional regulation of insect fat body development and function. Arch Insect Biochem Physiol **71:**16–30. http://dx.doi.org/10.1002/arch.20290.
45. **Eleftherianos I, Joyce S, Ffrench-Constant RH, Clarke DJ, Reynolds SE.** 2010. Probing the tri-trophic interaction between insects, nematodes and *Photorhabdus*. Parasitol **137:**1695–1706. http://dx.doi.org/10.1017/S0031182010000508.
46. **Gotz P, Boman A, Boman HG.** 1981. Interactions between insect immunity and an insect-pathogenic nematode with symbiotic bacteria. Proc R Soc Lond B **212:**333–350. http://dx.doi.org/10.1098/rspb.1981.0043.
47. **Ji D, Kim Y.** 2004. An entomopathogenic bacterium, *Xenorhabdus nematophila*, inhibits the expression of an antibacterial peptide, cecropin, of the beet armyworm, *Spodoptera exigua*. J Insect Physiol **50:**489–496. http://dx.doi.org/10.1016/j.jinsphys.2004.03.005.
48. **Park Y, Herbert EE, Cowles CE, Cowles KN, Menard ML, Orchard SS, Goodrich-Blair H.** 2007. Clonal variation in *Xenorhabdus nematophila* virulence and suppression of *Manduca sexta* immunity. Cell Microbiol **9:**645–656. http://dx.doi.org/10.1111/j.1462-5822.2006.00815.x.
49. **Hwang J, Park Y, Kim Y, Hwang J, Lee D.** 2013. An entomopathogenic bacterium, *Xenorhabdus nematophila*, suppresses expression of antimicrobial peptides controlled by Toll and Imd pathways by blocking eicosanoid biosynthesis. Arch Insect Biochem Physiol **83:**151–169. http://dx.doi.org/10.1002/arch.21103.
50. **Cerenius L, Lee BL, Soderhall K.** 2008. The proPO-system: pros and cons for its role in invertebrate immunity. Trends Immunol **29:**263–271. http://dx.doi.org/10.1016/j.it.2008.02.009.
51. **Ebrahimi L, Niknam G, Dunphy GB.** 2011. Hemocyte responses of the Colorado potato beetle, *Leptinotarsa decemlineata*, and the greater wax moth, *Galleria mellonella*, to the entomopathogenic nematodes, *Steinernema feltiae* and *Heterorhabditis bacteriophora*. J Insect Sci **11:**75. http://dx.doi.org/10.1673/031.011.7501.
52. **Li X-Y, Cowles RS, Cowles EA, Gaugler R, Cox-Foster DL.** 2007. Relationship between the successful infection by entomopathogenic nematodes and the host immune response. Int J Parasitol **37:**365–374. http://dx.doi.org/10.1016/j.ijpara.2006.08.009.
53. **Wang Y, Gaugler R, Cui L.** 1994. Variations in immune response of *Popillia japonica* and *Acheta domesticus* to *Heterorhabditis bacteriophora* and *Steinernema* species. J Nematol **26:**11–18.
54. **Song CJ, Seo S, Shrestha S, Kim Y.** 2011. Bacterial metabolites of an entomopathogenic bacterium, *Xenorhabdus nematophila*, inhibit a catalytic activity of phenoloxidase of the diamondback moth, *Plutella xylostella*. J Microbiol Biotechnol **21:**317–322.
55. **Seo S, Lee S, Hong Y, Kim Y.** 2012. Phospholipase A2 inhibitors synthesized by two entomopathogenic bacteria, *Xenorhabdus nematophila* and *Photorhabdus temperata* subsp. *temperata*. Appl Environ Microbiol **78:** 3816–3823. http://dx.doi.org/10.1128/AEM.00301-12.
56. **Poinar GO, Jr.** 1979. Nematodes for biological control of insects. CRC Press, Boca Raton, FL.
57. **Hodson AK, Friedman ML, Wu LN, Lewis EE.** 2011. European earwig (*Forficula auricularia*) as a novel host for the entomopathogenic nematode *Steinernema carpocapsae*. J Invertebr Pathol **107:**60–64. http://dx.doi.org/10.1016/j.jip.2011.02.004.
58. **Nguyen KB, Smart GC.** 1990. *Steinernema scapterisci* n. sp (Rhabditida: Steinernematidae). J Nematol **22:**187–199.
59. **Frank JH.** 2009. *Steinernema scapterisci* as a biological control agent of *Scapteriscus* mole crickets, p115–132. *In* Hajek AE, Glare TR, O'Callaghan M (ed), Use of microbes for control and eradication of invasive arthropods. Springer, Dordrecht, The Netherlands.
60. **Lin MF, Carlson JW, Crosby MA, Matthews BB, Yu C, Park S, Wan KH, Schroeder AJ, Gramates LS, St Pierre SE, Roark M, Wiley KL, Jr, Kulathinal RJ, Zhang P, Myrick KV, Antone JV, Celniker SE, Gelbart WM, Kellis M.** 2007. Revisiting the protein-coding gene catalog of *Drosophila melanogaster* using 12 fly genomes. Genome Res **17:**1823–1836. http://dx.doi.org/10.1101/gr.6679507.
61. **Dillman AR, Mortazavi A, Sternberg PW.** 2012. Incorporating genomics into the toolkit of nematology. J Nematol **44:**191–205.
62. **Bai X, Adams BJ, Ciche TA, Clifton S, Gaugler R, Kim KS, Spieth J, Sternberg PW, Wilson RK, Grewal PS.** 2013. A lover and a fighter: the genome sequence of an entomopathogenic nematode *Heterorhabditis bacteriophora*. PLoS One **8:**e69618. http://dx.doi.org/10.1371/journal.pone.0069618.
63. **Sackton TB, Lazzaro BP, Schlenke TA, Evans JD, Hultmark D, Clark AG.** 2007. Dynamic evolution of the innate immune system in *Drosophila*. Nat Genet **39:**1461–1468. http://dx.doi.org/10.1038/ng.2007.60.

Variation in the susceptibility of *Drosophila* to different entomopathogenic nematodes: supplemental information

Jennifer M. Peña, Mayra A. Carrillo, and Elissa A. Hallem

Supplemental Figure Legends

Figure S1. Infection of 2nd instar *D. melanogaster* larvae by exposure to *X. nematophila* bacteria. Representative images of *D. melanogaster* larvae exposed to *X. nematophila*. 2nd instar fly larvae were placed on a lawn of GFP-expressing *X. nematophila.* Fly larvae were observed at 24 hours (A) or 48 hours (B) post-exposure to *X. nematophila*. *X. nematophila* appeared to localize primarily to the digestive tract, suggesting that larvae became infected by ingestion of *X. nematophila*.

Figure S2. *S. carpocapsae* is more effective at killing 3rd instar fly larvae than 2nd instar fly larvae. Average survival of 2nd instar vs. 3rd instar *D. melanogaster* larvae infected with *S. carpocapsae* symbiont IJs at 24 hours post-exposure to IJs. Data are from Figure 3A. Survival was scored in parallel to AMP expression, and survival data for the different AMP expression lines was pooled. n = 37-47 trials. Error bars show SEM. ***, $P<0.001$, Mann-Whitney test.

Figure S3. Infection of 3rd instar *D. melanogaster* larvae with symbiont IJs cultured *in vitro* vs. *in vivo.* Symbiont IJs were cultured either on plates containing lawns of *X. nematophila* (*in vitro* method) or in waxworms (*in vivo* method). No significant differences in AMP expression were observed following exposure to

symbiont IJs cultured on plates vs. in waxworms (P>0.05, two-way ANOVA). n = 5-6 trials for each condition.

Supplemental Tables

Table S1. Pathogenicity of different EPN species toward *D. melanogaster* larvae. Pairs of survival curves were compared using a log-rank test with Bonferroni correction. "ns," not significant. Data are from Figure 5A.

Pair	***P* value**
S. carpocapsae vs. *S. riobrave*	*P*<0.01
S. carpocapsae vs. *S. scapterisci*	*P*<0.01
S. carpocapsae vs. *S. glaseri*	*P*<0.01
S. carpocapsae vs. *S. feltiae*	ns
S. carpocapsae vs. *H. bacteriophora*	*P*<0.01
S. carpocapsae vs. *H. indica*	ns
S. riobrave vs. *S. scapterisci*	ns
S. riobrave vs. *S. glaseri*	*P*<0.01
S. riobrave vs. *S. feltiae*	*P*<0.01
S. riobrave vs. *H. bacteriophora*	*P*<0.01
S. riobrave vs. *H. indica*	*P*<0.01
S. scapterisci vs. *S. glaseri*	*P*<0.01
S. scapterisci vs. *S. feltiae*	*P*<0.01
S. scapterisci vs. *H. bacteriophora*	*P*<0.01
S. scapterisci vs. *H. indica*	*P*<0.01
S. glaseri vs. *S. feltiae*	*P*<0.01
S. glaseri vs. *H. bacteriophora*	*P*<0.01
S. glaseri vs. *H. indica*	*P*<0.01
S. feltiae vs. *H. bacteriophora*	*P*<0.05
S. feltiae vs. *H. indica*	ns
H. bacteriophora vs. *H. indica*	ns

Table S2. Pathogenicity of *S. carpocapsae* symbiont IJs for different *Drosophila* species. Pairs of survival curves were compared using a log-rank test with Bonferroni correction. “ns,” not significant. Data are from Figure 5B.

Pair	***P* value**
D. melanogaster vs. *D. virilis*	ns
D. melanogaster vs. *D. yakuba*	ns
D. melanogaster vs. *D. pseudoobscura*	ns
D. melanogaster vs. *D. simulans*	ns
D. virilis vs. *D. yakuba*	*P*<0.001
D. virilis vs. *D. pseudoobscura*	*P*<0.001
D. virilis vs. *D. simulans*	ns
D. yakuba vs. *D. pseudoobscura*	ns
D. yakuba vs. *D. simulans*	ns
D. pseudoobscura vs. *D. simulans*	*P*<0.05

Figure S1

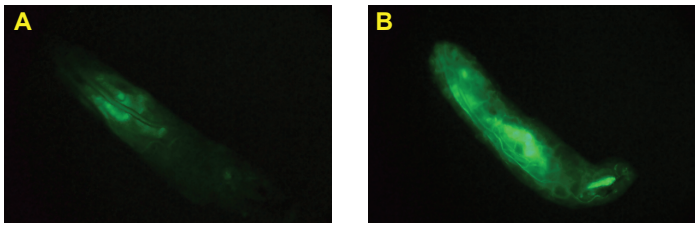

Figure S2

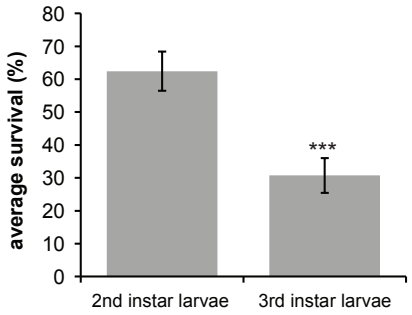
average survival (%)
80
70
60
50
40
30
20
10
0
***
2nd instar larvae
3rd instar larvae

Figure S3

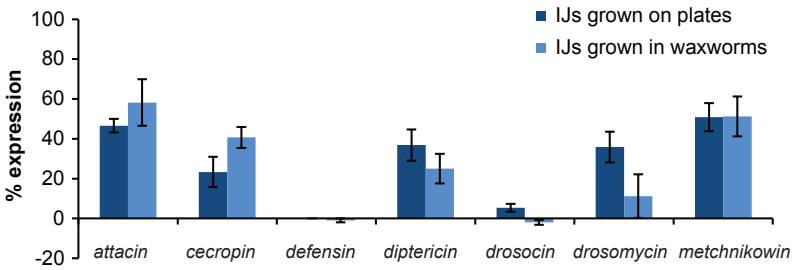
IJs grown on plates
IJs grown in waxworms
% expression
100
80
60
40
20
0
-20
attacin
cecropin
defensin
diptericin
drosocin
drosomycin
metchnikowin

Discussion

We set out to investigate the neural basis for carbon dioxide avoidance in *C. elegans.* Our results demonstrate that CO_2 avoidance behavior undergoes context-dependent modulation and reveal a distributed network of sensory neurons integrated in the CO_2 circuit that includes thermosensory, oxygen, and odor-sensing neurons (Figure D-1).

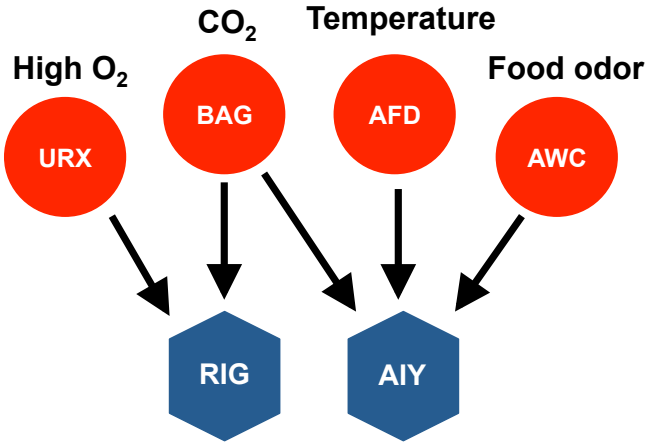

Fig. D-1. A distributed network of sensory neurons regulate the CO_2 circuit. Diverse sensory neurons regulate CO_2 response according to high O_2, temperature, and attractive food odor. URX synapses onto RIG, a possible target for CO_2 avoidance inhibition. AIY interneurons have been found to act downstream of BAG, AFD, and high O_2 to regulate CO_2 response. AFD and AWC directly synapse onto AIY. Sensory neurons are indicated as red circles. Interneurons are pictured as blue hexagons. Black arrows indicate chemical synapses.

We have shown that CO_2 sensitivity is modulated by two opposing interneurons, AIY and RIG. We propose a model whereby upon CO_2 exposure, the BAG sensory neurons are activated leading to increased activity of the RIG interneuron and decreased activity of the AIY interneuron to promote appropriate CO_2 avoidance behavior (Figure D-2).

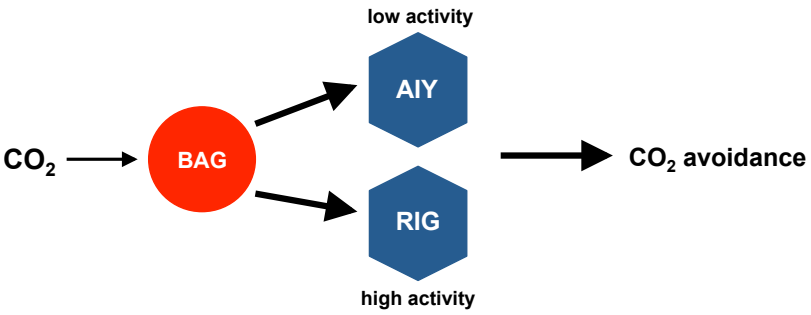

Fig. D-2. Antagonistic roles by RIG and AIY mediate CO_2 avoidance behavior. Behavioral and calcium imaging data suggests when BAG is activated by CO_2, it activates RIG and inhibits AIY. AIY opposes and RIG promotes avoidance of CO_2, respectively. Thus, low activity in AIY and high activity in RIG together mediate appropriate response to CO_2 levels.

Overall, our findings suggest that multiple sensory neurons can modulate a behavioral response mediated by another sensory neuron most likely due to synaptic outputs integrated by common

downstream interneurons. This is consistent with studies examining other chemosensory behaviors such as salt-sensing, temperature-sensing, and oxygen-sensing, which have been shown to be regulated by networks of sensory neurons (Aoki and Mori, 2015; Chang et al., 2006; Leinwand and Chalasani, 2013). Continuing studies on the composition of the CO_2 circuit will reveal exactly how the circuit can be reconfigured to generate context- dependent CO_2 responses. This includes identifying the neuromodulators acting on the circuit to mediate behavioral plasticity.

Opposing first-order interneurons regulate CO_2 sensitivity

Using cell specific genetic ablation, manipulation of neurotransmission using molecular biology, and calcium imaging to observe neuronal activity, we have shown that the AIY and RIG interneurons have antagonistic roles in generating CO_2-evoked behavior. First, ablation of the AIY interneurons resulted in increased CO_2 avoidance behavior across CO_2 concentrations (Figure 3-2). Conversely, ablation of the RIG interneurons resulted in decreased CO_2 avoidance (Figure 3-2). Second, increasing synaptic output from AIY and RIG reversed the ablation behavior phenotype. Increasing AIY and RIG output resulted in decreased and increased CO_2 avoidance, respectively (Figure 3-3). Lastly, calcium imaging reflects AIY and RIG roles in CO_2 avoidance. AIY interneurons showed hyperpolarization, indicating inhibition, in response to a 10% CO_2 pulse. In contrast, RIG neurons showed a depolarization response to a 10% CO_2 pulse. From these results we infer that context-dependent regulation of AIY and RIG's antagonistic activities generates a coordinated behavioral response to CO_2. Opposing interneurons are also a feature for olfactory behavior where AIY neurons are activated upon odor stimulation and AIB interneurons are inhibited (Chalasani et al., 2007).

RIG interneurons have been found to be important in mediating CO_2 avoidance behavior in this study. However, ablation of these interneurons alone did not eliminate CO_2 avoidance behavior,

which suggests it acts redundantly with another or other interneurons downstream of BAG. Double ablations of a combination of these interneurons will address which other interneurons are important in mediating avoidance behavior in response to CO_2.

How would AIY and RIG CO_2-evoked activities lead to generation of avoidance behavior in a CO_2 gradient? Studies in thermotaxis, salt-sensing, and food odor-sensing have addressed a similar question of how animals use sensory neurons to move towards or away from a stimulus. Animals use locomotion behavior to navigate towards favorable conditions. The behavioral mechanism of chemotaxis consists of two strategies, klinokinesis and klinotaxis. Klinokinesis, also called biased random walk, involves undergoing turns and reversals (pirouettes) to reorient and move in a different direction. If the animal is going up a gradient of an attractant, turns become less frequent and therefore the animal will move forward ("run") primarily in the direction of the stimulus. If the worm is going down the gradient of an attractant, turns become more frequent and this eventually biases the locomotion toward the higher concentration of the attractant (Pierce-Shimomura et al., 1999). In klinotaxis, also called weathervaning, animals curve toward the higher concentration of a stimulus during forward locomotion (Iino and Yoshida, 2009). Salt chemotaxis and thermotaxis has been shown to use klinokinesis and klinotaxis strategies (Iino and Yoshida, 2009; Luo et al., 2014; Ramot et al., 2008; Ryu and Samuel, 2002). These strategies have not yet been investigated in CO_2 avoidance behavior in a gradient assay.

AIY interneurons are required to suppress reversals and turns (Gray et al., 2005; Wakabayashi et al., 2004). AIY has also been shown to evoke weathervane behavior for animals to migrate towards lower salt concentrations (Satoh et al., 2014). A recent study investigated how a versatile interneuron such as AIY can modulate multiple behavior outputs such as speed, reversals, and turns (Li et al., 2014). AIY can regulate both speed and reversals by recruiting two distinct circuits. One circuit is inhibitory; AIY suppresses reversal by suppressing AIZ interneurons. The other is excitatory; AIY modulates speed by activating RIB interneurons (Li et

al., 2014). We hypothesize that AIY interneurons will function to modulate speed and reversals when navigating a CO_2 gradient through AIZ and RIB interneurons (Figure D-3).

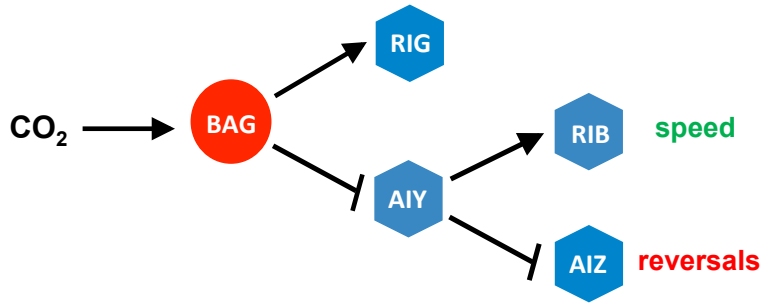

Fig. D-3. Model for CO_2-evoked locomotor activity. In presence of high CO_2, we hypothesize that BAG will inhibit AIY to promote reversals and turns. As the animals navigate away from high CO_2 to low CO_2 BAG inhibition on AIY will decrease and this results in increase in speed and decrease in turns as a way to escape high CO_2 levels. RIG also directly synapses onto AIY and RIB, thus possibly modulating reversals and speed as well.

It is possible that when animals are navigating up a CO_2 gradient, we may see an increase in reversals/turns and decrease in speed. This will show the importance of AIY inhibition. Conversely, when animals are moving away from CO_2, we may see a decrease in reversals/turns and an increase in speed. In future experiments, we will test whether AIZ interneurons ablation will give a behavioral phenotype in CO_2 avoidance behavior. Studying klinokinesis and klinotaxis behavior in a CO_2 gradient will enable us to dissect how AIY, RIG, and perhaps other downstream interneurons from BAG play a role in encoding a behavioral output to generate avoidance or attraction to CO_2. We are planning to use a worm tracking system that has been used to study locomotor strategies in other sensory behaviors (Daniel Ramot, 2008; Husson et al., 2012).

Multimodal integration in the CO_2 circuit modulates avoidance behavior

One of the main goals of neuroscience is to understand how sensory inputs are integrated to generate a behavior. Studying circuits and behavior in *C. elegans* have revealed the complexity of neural circuits, even with a connectome consisting of only 302 neurons. Part of this complexity is due to a sensory neuron being capable of responding to multiple stimuli and multiple sensory neurons responding to the same stimulus (Bargmann, 2012; Komuniecki et al.,

2014). Multiple circuits have been shown to regulate one behavior in *C. elegans*. For example, in aerotaxis behavior, animals avoid high O_2 and migrate to a lower preferred O_2 concentration. This behavior involves a distributed network of sensory neurons, although only AQR, PQR, and URX are the direct oxygen sensors in this network (Chang et al., 2006). Thermotaxis behavior also involves multiple sensory neurons (Aoki and Mori, 2015). Likewise, we found that CO_2 behavior can also be regulated by multiple sensory neurons: BAG, URX, AFD, and AWC. Our work suggests the CO_2 circuit is flexible, which most likely functions to increase adaptation to a changing environment. The role of each neuron in the CO_2 circuit is further discussed below.

BAG neurons are the primary CO_2 sensors and are required for CO_2 response

Wild-type N2 animals show CO_2 avoidance when well fed and CO_2 attraction when developmentally arrested in the dauer stage (Carrillo et al., 2013; Hallem et al., 2011a). BAG neurons are required for CO_2 avoidance and CO_2 attraction in these conditions. URX neurons have been shown to have CO_2-evoked activity, however these neurons are not required for CO_2 attraction in dauers (Bretscher et al., 2011; Carrillo et al., 2013). This indicates that BAG neurons are the primary sensory neurons required for all CO_2-evoked behavior.

One of the biggest questions we have yet to address is what is the neurotransmitter and/or neuropeptide/s that BAG uses to signal to downstream neurons in the CO_2 circuit? BAG neurons express a number of different neuropeptides (Hallem et al., 2011b). Whether any of these neuropeptides are required for CO_2 avoidance or attraction in a chemotaxis assay has not yet been investigated. A study using isolated BAG neurons in culture showed that a BAG-enriched FMRF-amide like neuropeptide *flp-17* is released upon CO_2 stimuli (Smith et al., 2013). *flp-17* mutants showed normal acute avoidance to CO_2, however they have not yet been tested in a gradient assay (Hallem and Sternberg, 2008). BAG neurons are characterized as glutamatergic. Interestingly, AFD and AWC both modulate AIY interneurons through glutamate

signaling. AIY is inhibited by AFD and activated by AWC through different glutamate receptors (Aoki and Mori, 2015). It will be interesting to see if BAG inhibits AIY through glutamate signaling and whether it uses similar receptors. RIG interneurons are known to express at least two glutamate receptors. Imaging from AIY and RIG interneurons in a *flp-17* mutant or AIY and RIG glutamate receptor mutant backgrounds should give us insight into how neurotransmitter and neuropeptide signaling affect CO_2-evoked activity in these interneurons.

Oxygen sensing neurons regulate CO_2 avoidance behavior mediated by npr-1

CO_2 avoidance behavior requires the activity of neuropeptide Y-like receptor NPR-1 (Bretscher et al., 2008; Carrillo et al., 2013; Hallem and Sternberg, 2008). Our study led to the discovery that NPR-1 acts to inhibit the oxygen sensing URX neurons to mediate CO_2 avoidance behavior. Therefore, the CO_2 circuit is modulated by ambient O_2 levels through a neuropeptide signaling pathway. Our results were later confirmed by another study also showing ambient O_2 levels inhibit CO_2 avoidance behavior (Kodama-Namba et al., 2013). We hypothesized that URX neurons would modulate the CO_2 circuit directly since URX neurons share common downstream interneurons with BAG. RIG interneurons are one common target between BAG and URX, and RIG has shown a phenotype in CO_2 avoidance behavior in our assays. Thus, RIG could be a potential synaptic target of URX to regulate CO_2 avoidance behavior. Imaging from RIG interneurons in the *npr-1* mutant background under low and high O_2 concentrations would address this.

We also evaluated whether AIY might be mediating inhibition of CO_2 avoidance in *npr-1* mutants. AIY-ablated *npr-1* mutants showed wild type 10% CO_2 avoidance, suggesting AIY interneurons are acting downstream of *npr-1* regulation. URX neurons do not have a direct synapse onto AIY. However, it has been recently shown that AIY interneurons are required for O_2-evoked behaviors in *npr-1* mutants, indicating that AIY interneurons also integrate sensory information

from the O_2 sensing circuit to modulate CO_2 response (Laurent et al., 2015). The mechanism of how AIY can respond to inputs from the O_2 circuit is unknown. It is possible that AIY can receive input through extrasynaptic signaling from URX or through another interneuron that is directly downstream of URX and synapses onto AIY. In the latter case, one such interneuron would be AUA, which has been shown to have O_2-evoked Ca^{2+} activity and is also required for O_2 behavior (Busch et al., 2012). Calcium imaging in AIY in N2 and *npr-1* mutant background under high and low O_2 conditions should reveal how AIY activity is altered in response to a CO_2 stimulus. It is possible that O_2 input in *npr-1* mutants might relieve CO_2–evoked inhibition in AIY, which can lead to loss of CO_2 avoidance behavior. At the other end of the oxygen spectrum, hypoxia can also inhibit CO_2 avoidance behavior through the hypoxia inducible factor 1 (*hif-1*) pathway (Bretscher et al., 2008). The mechanism of how *hif-1* inhibits CO_2 response and whether AIY also integrates hypoxia response into the CO_2 circuit remains to be elucidated.

AFD sensory neurons are required for CO_2 avoidance

One of the surprising results of our study was that animals that lacked functional AFD neurons showed loss of CO_2 avoidance behavior. AIY interneurons are a primary target of AFD. We found that animals lacking both AIY and AFD rescued CO_2 avoidance behavior, suggesting that AFD can modulate the CO_2 circuit by targeting a common downstream interneuron with BAG. Studies from Mario de Bono's lab, whose research also focuses on CO_2 behavior in *C. elegans*, provided further evidence that temperature is another environmental factor that modulates CO_2 avoidance behavior (Bretscher et al., 2011; Kodama-Namba et al., 2013). Although his studies show that AFD are direct CO_2 sensors, we and others were not able to confirm this, perhaps due to different imaging techniques (Brandt et al., 2012; Carrillo et al., 2013; Smith et al., 2013). Nevertheless, Kodama-Namba et al showed that cultivation temperature could modify CO_2 avoidance behavior at low CO_2 concentration and this requires AFD neurons. If CO_2 response

can be modulated by acclimation temperature, then it would be interesting to see if CO_2 itself can be used as an environmental context cue that modulates thermotaxis behavior.

Food odor sensory neurons modulate CO_2 avoidance behavior

AWC neurons respond to food odor and drive food-seeking behavior (Chalasani et al., 2007; Gray et al., 2005). CO_2 can also be used as a sensory cue for the presence of food, as it is expelled as a respiratory byproduct in bacteria, the main food source of *C. elegans*. Thus, CO_2 and food odorants are likely to be integrated by common neuronal pathways to signal the presence of food or a nearby food source. However, in a case like this, AWC neurons would mediate attraction to the food source but the presence of CO_2 would mediate avoidance from the food source depending on the animal's starvation state. In *Drosophila*, flies have an innate avoidance behavior to CO_2, a component of an odor emitted by stressed flies (Suh et al., 2004). However, like *C. elegans*, the location of their food source is in fruit compost, where CO_2 levels tend to be high. To overcome CO_2 avoidance, food odors act on the CO_2 receptors to inhibit CO_2 avoidance behavior (Turner and Ray, 2009).

We also tested whether CO_2 avoidance can be modulated by the presence of an attractant food odorant, isoamyl alcohol. The presence of this attractant odorant in our assay did not affect N2 CO_2 avoidance but did rescue CO_2 avoidance behavior in *npr-1* mutants. AWC neurons are inhibited by the presence of isoamyl alcohol and ablation of AWC neurons mimicked the rescue of CO_2 avoidance in *npr-1* mutants. When we tested AWC-ablated N2 animals across CO_2 concentrations, we saw a slight increase in CO_2 avoidance, suggesting AWC neurons modulate CO_2 avoidance behavior in both N2 and *npr-1* mutants similar to AIY. We have yet to image from AWC neurons to see if it shows any CO_2-evoked Ca^{2+} activity. AWC neurons also share AIY as a common downstream interneuron with BAG, and AWC can have both excitatory and inhibitory inputs to AIY (Chalasani et al., 2007; Ohnishi et al., 2011). One key experiment is to

image from AIY in AWC-ablated animals and evaluate any change in Ca^{2+} activity in response to CO_2. This could give us further insight of whether AIY also integrates AWC input to modulate CO_2-evoked behavior. BAG neurons have been found to have an inhibitory role in AWC-mediated olfactory preference to the bacterial pathogen *Pseudomonas aeruginosa* PA14 (Harris et al., 2014). Thus, it is possible that CO_2 sensing in BAG might regulate AWC responses to food odors and/or its downstream circuit. Together, this suggests that animals integrate both CO_2 and food odor cues using a common neuronal pathway to produce behavioral flexibility to both behaviors.

Concluding remarks

Why does temperature, oxygen, and food odor modulate CO_2 response in *C. elegans*? *C. elegans* is predominantly found in decomposing plant material such as fruits and stems that provide an abundant source of bacterial food (Frézal and Félix, 2015). In this environment, temperature, CO_2, O_2, and food levels are likely to fluctuate. Animals thrive at temperatures ranging from 15°C-25°C (Hedgecock and Russell, 1975). CO_2 and O_2 levels can indicate the presence of pathogens, mates, predators, and population density. Food odor gradients generated in rotting fruits are likely to be used by animals to locate food. Hence, *C. elegans* would need to integrate all these sensory cues to modulate behavior in such a diverse environment to ensure survival.

Our work suggests that modulation of CO_2 response happens at the interneuron level, through AIY and RIG activity. AIY interneurons have been shown to integrate multiple sensory inputs including temperature and odor, to generate appropriate locomotory responses (Chalasani et al., 2007; Luo et al., 2014; Satoh et al., 2014). AIY receives strong synaptic input from AFD and AWC neurons (White et al., 1986). Hence, these neurons likely modulate the CO_2 circuit through AIY. Multisensory integration has also been characterized in mammals where neurons in the

superior colliculus integrate visual, auditory, and somatosensory inputs (Meredith and Stein, 1986). The yellow fever mosquito *Aedes aegypti* has been shown to use multimodal integration of CO_2, heat, and odor to drive host-seeking and blood-feeding behavior (McMeniman et al., 2014). More work needs to be done to identify other interneurons downstream of BAG required to promote CO_2 avoidance and the neuromodulators behind CO_2 behavioral plasticity.

Drosophila can also respond to thermal, oxygen, and food odor cues (Khurana and Siddiqi, 2013; Luo et al., 2010; Morton, 2011). It would be interesting to see if an insect that shares a similar habitat with *C. elegans* can also use thermal and oxygen level cues to modify CO_2-evoked behavior. The presence of food odor has already been shown to modulate CO_2 avoidance behavior in *Drosophila* (Turner and Ray, 2009).

C. elegans is a free-living nematode that shares conserved neural anatomy and function across nematode species including parasitic nematodes (Bumbarger et al., 2007; Forbes et al., 2004). Although they have the same neural anatomy they have different behavioral life styles and different behavioral responses to the same sensory cue. For example, *C. elegans* dauers are attracted to CO_2 but human-parasitic nematode *Strongyloides stercoralis* infective juveniles, a developmental stage similar to dauers, is repelled by CO_2 (Castelletto et al., 2014). It is possible that *Strongyloides stercoralis* is repelled by CO_2 alone, but might switch to attraction if CO_2 is presented with an odorant or warmer temperature. Future studies on the CO_2 circuit and behavior in *C. elegans* would reveal whether BAG, AIY, and RIG, have conserved roles for CO_2-evoked behaviors in parasitic nematodes and whether it can be modulated by temperature, odors, and ambient oxygen. We hope this work can lead to an understanding of how neural circuits can undergo context-dependent modulation to generate behavioral plasticity and whether the mechanisms of this plasticity are conserved across species.

***Drosophila* immune response to entomopathogenic nematodes (EPNs)**

Drosophila melanogaster as a model system has made many contributions in the field of immunology, most notably the discovery of Toll-like receptors (Lemaitre et al., 1996). Most recently, it has become a useful tool to study host-parasite interactions (Keebaugh and Schlenke, 2014). *Drosophila* has been shown to be susceptible to the EPN *Heterorhabditis bacteriophora* and its symbiotic bacteria *Photorhabdus luminescens* and infection generated a specific immune response to *P. luminescens* (Hallem et al., 2007). In this study, we tested the versatility of *Drosophila* as a model system to study the immune response to other EPN species. We found that *Drosophila melanogaster* is susceptible to the EPN *Steinernema carpocapsae* and its bacterial symbiont *Xenorhabdus nematophila.* Different species of EPNs vary in their virulence toward *D. melanogaster*. We also show that several species of *Drosophila* can vary in their susceptibility to *S. carpocapsae*. These findings establish *Drosophila* as an ideal model system to study differences in EPN virulence and differences in host immune response to infection.

The key outcome of this study is the opportunity to use other *Drosophila* species that varied in their susceptibility to *S. carpocapsae* and compare their immune response with that of the more susceptible *D. melanogaster.* All *Drosophila* species used in this study have sequenced genomes. Future studies should make use of this and generate transgenic flies to study AMP expression following EPN infection. This will give insight into the difference in susceptibility between *Drosophila* species to the same EPN. Another interesting result was the finding that *S. carpocapsae* is more virulent than *H. bacteriophora*. We also found that its symbiont bacteria *X. nematophila* is also more virulent than the *H. bacteriophora* symbiont *P. luminescens,* which is consistent with results using adult flies (Aymeric et al., 2010). Using genome-wide transcriptional analysis of *Drosophila* infection with *S. carpocapsae* will reveal important target genes that may be mediating immunity or susceptibility to infection. Transcriptional analysis has

already been done for *H. bacteriophora* infection in *Drosophila* (Arefin et al., 2014). Comparison of transcription responses between *H. bacteriophora* and *S. carpocapsae* infections will further reveal differences in virulence factors of both EPNs.

Other future experiments include elucidating the immune pathways that might be generating some protection against EPN infection that can be contributing to the differences in susceptibility. For example, clotting factors that help sequester bacteria, such as transglutaminase and eicosanoids, have been shown to protect against *H. bacteriophora* infection in *D. melanogaster* (Hyrsl et al., 2011; Wang et al., 2010). Whether clotting factors mediate protection against *S. carpocapsae* in *D. melanogaster* or other *Drosophila* species remains to be determined. The Toll/Imd pathways mediate expression of AMPs in response to various pathogens (Lemaitre and Hoffmann, 2007). The Toll pathway also plays a role in the cellular immune response including encapsulating and killing of parasites (Valanne et al., 2011). The Imd and Toll pathways were dispensable for the response against *H. bacteriophora* infection in *D. melanogaster* (Hallem et al., 2007). Whether this holds true for *S. carpocapsae* infection in *D. melanogaster* and other *Drosophila* species remains to be seen. Making use of the versatility of *Drosophila* as a model system for EPN infections can lead to novel pest control agents and a better understanding of the immune response to parasitic nematodes.

REFERENCES

Aoki, I., and Mori, I. (2015). Molecular biology of thermosensory transduction in C. elegans. Curr. Opin. Neurobiol. *34*, 117–124.

Arefin, B., Kucerova, L., Dobes, P., Markus, R., Strnad, H., Wang, Z., Hyrsl, P., Zurovec, M., and Theopold, U. (2014). Genome-wide transcriptional analysis of Drosophila larvae infected by entomopathogenic nematodes shows involvement of complement, recognition and extracellular matrix proteins. J. Innate Immun. *6*, 192–204.

Aymeric, J.-L., Givaudan, A., and Duvic, B. (2010). Imd pathway is involved in the interaction of Drosophila melanogaster with the entomopathogenic bacteria, Xenorhabdus nematophila and Photorhabdus luminescens. Mol. Immunol. *47*, 2342–2348.

Bargmann, C.I. (2012). Beyond the connectome: how neuromodulators shape neural circuits. BioEssays News Rev. Mol. Cell. Dev. Biol. *34*, 458–465.

Bargmann, C.I., Hartwieg, E., and Horvitz, H.R. (1993). Odorant-selective genes and neurons mediate olfaction in C. elegans. Cell *74*, 515–527.

De Bono, M., Tobin, D.M., Davis, M.W., Avery, L., and Bargmann, C.I. (2002). Social feeding in Caenorhabditis elegans is induced by neurons that detect aversive stimuli. Nature *419*, 899–903.

Brandt, J.P., Aziz-Zaman, S., Juozaityte, V., Martinez-Velazquez, L.A., Petersen, J.G., Pocock, R., and Ringstad, N. (2012). A single gene target of an ETS-family transcription factor determines neuronal CO2-chemosensitivity. PloS One *7*, e34014.

Bretscher, A.J., Busch, K.E., and de Bono, M. (2008). A carbon dioxide avoidance behavior is integrated with responses to ambient oxygen and food in Caenorhabditis elegans. Proc. Natl. Acad. Sci. U. S. A. *105*, 8044–8049.

Bretscher, A.J., Kodama-Namba, E., Busch, K.E., Murphy, R.J., Soltesz, Z., Laurent, P., and de Bono, M. (2011). Temperature, oxygen, and salt-sensing neurons in C. elegans are carbon dioxide sensors that control avoidance behavior. Neuron *69*, 1099–1113.

Bumbarger, D.J., Crum, J., Ellisman, M.H., and Baldwin, J.G. (2007). Three-dimensional fine structural reconstruction of the nose sensory structures of Acrobeles complexus compared to Caenorhabditis elegans (Nematoda: Rhabditida). J. Morphol. *268*, 649–663.

Busch, K.E., Laurent, P., Soltesz, Z., Murphy, R.J., Faivre, O., Hedwig, B., Thomas, M., Smith, H.L., and de Bono, M. (2012). Tonic signaling from O_2 sensors sets neural circuit activity and behavioral state. Nat. Neurosci. *15*, 581–591.

Carrillo, M.A., Guillermin, M.L., Rengarajan, S., Okubo, R.P., and Hallem, E.A. (2013). O2-sensing neurons control CO2 response in C. elegans. J. Neurosci. Off. J. Soc. Neurosci. *33*, 9675–9683.

Castelletto, M.L., Gang, S.S., Okubo, R.P., Tselikova, A.A., Nolan, T.J., Platzer, E.G., Lok, J.B., and Hallem, E.A. (2014). Diverse Host-Seeking Behaviors of Skin-Penetrating Nematodes. PLoS Pathog *10*, e1004305.

Chalasani, S.H., Chronis, N., Tsunozaki, M., Gray, J.M., Ramot, D., Goodman, M.B., and Bargmann, C.I. (2007). Dissecting a circuit for olfactory behaviour in Caenorhabditis elegans. Nature *450*, 63–70.

Chang, A.J., Chronis, N., Karow, D.S., Marletta, M.A., and Bargmann, C.I. (2006). A distributed chemosensory circuit for oxygen preference in C. elegans. PLoS Biol. *4*, e274.

Chelur, D.S., and Chalfie, M. (2007). Targeted cell killing by reconstituted caspases. Proc. Natl. Acad. Sci. U. S. A. *104*, 2283–2288.

Cheung, B.H.H., Cohen, M., Rogers, C., Albayram, O., and de Bono, M. (2005). Experience-dependent modulation of C. elegans behavior by ambient oxygen. Curr. Biol. CB *15*, 905–917.

Daniel Ramot, B.E.J. (2008). The Parallel Worm Tracker: A Platform for Measuring Average Speed and Drug-Induced Paralysis in Nematodes. PloS One *3*, e2208.

Forbes, W.M., Ashton, F.T., Boston, R., Zhu, X., and Schad, G.A. (2004). Chemoattraction and chemorepulsion of Strongyloides stercoralis infective larvae on a sodium chloride gradient is mediated by amphidial neuron pairs ASE and ASH, respectively. Vet. Parasitol. *120*, 189–198.

Frézal, L., and Félix, M.-A. (2015). C. elegans outside the Petri dish. eLife *4*.

Gray, J.M., Hill, J.J., and Bargmann, C.I. (2005). A circuit for navigation in Caenorhabditis elegans. Proc. Natl. Acad. Sci. U. S. A. *102*, 3184–3191.

Hallem, E.A., and Sternberg, P.W. (2008). Acute carbon dioxide avoidance in Caenorhabditis elegans. Proc. Natl. Acad. Sci. U. S. A. *105*, 8038–8043.

Hallem, E.A., Rengarajan, M., Ciche, T.A., and Sternberg, P.W. (2007). Nematodes, bacteria, and flies: a tripartite model for nematode parasitism. Curr. Biol. CB *17*, 898–904.

Hallem, E.A., Dillman, A.R., Hong, A.V., Zhang, Y., Yano, J.M., DeMarco, S.F., and Sternberg, P.W. (2011a). A sensory code for host seeking in parasitic nematodes. Curr. Biol. CB *21*, 377–383.

Hallem, E.A., Spencer, W.C., McWhirter, R.D., Zeller, G., Henz, S.R., Rätsch, G., Miller, D.M., 3rd, Horvitz, H.R., Sternberg, P.W., and Ringstad, N. (2011b). Receptor-type guanylate cyclase is required for carbon dioxide sensation by Caenorhabditis elegans. Proc. Natl. Acad. Sci. U. S. A. *108*, 254–259.

Harris, G., Shen, Y., Ha, H., Donato, A., Wallis, S., Zhang, X., and Zhang, Y. (2014). Dissecting the Signaling Mechanisms Underlying Recognition and Preference of Food Odors. J. Neurosci. *34*, 9389–9403.

Hedgecock, E.M., and Russell, R.L. (1975). Normal and mutant thermotaxis in the nematode Caenorhabditis elegans. Proc. Natl. Acad. Sci. U. S. A. *72*, 4061–4065.

Hobert, O., Mori, I., Yamashita, Y., Honda, H., Ohshima, Y., Liu, Y., and Ruvkun, G. (1997). Regulation of interneuron function in the C. elegans thermoregulatory pathway by the ttx-3 LIM homeobox gene. Neuron *19*, 345–357.

Husson, S.J., Costa, W.S., Schmitt, C., and Gottschalk, A. (2012). Keeping track of worm trackers. WormBook Online Rev. C Elegans Biol. 1–17.

Hyrsl, P., Dobes, P., Wang, Z., Hauling, T., Wilhelmsson, C., and Theopold, U. (2011). Clotting factors and eicosanoids protect against nematode infections. J. Innate Immun. *3*, 65–70.

Iino, Y., and Yoshida, K. (2009). Parallel use of two behavioral mechanisms for chemotaxis in Caenorhabditis elegans. J. Neurosci. Off. J. Soc. Neurosci. *29*, 5370–5380.

Keebaugh, E.S., and Schlenke, T.A. (2014). Insights from natural host–parasite interactions: The Drosophila model. Dev. Comp. Immunol. *42*, 111–123.

Khurana, S., and Siddiqi, O. (2013). Olfactory Responses of Drosophila Larvae. Chem. Senses bjs144.

Kodama-Namba, E., Fenk, L.A., Bretscher, A.J., Gross, E., Busch, K.E., and de Bono, M. (2013). Cross-Modulation of Homeostatic Responses to Temperature, Oxygen and Carbon Dioxide in C. elegans. PLoS Genet. *9*, e1004011.

Komuniecki, R., Hapiak, V., Harris, G., and Bamber, B. (2014). Context-dependent modulation reconfigures interactive sensory-mediated microcircuits in Caenorhabditis elegans. Curr. Opin. Neurobiol. *29*, 17–24.

Laurent, P., Soltesz, Z., Nelson, G., Chen, C., Arellano-Carbajal, F., Levy, E., and Bono, M. de (2015). Decoding a neural circuit controlling global animal state in C. elegans. eLife e04241.

Leinwand, S.G., and Chalasani, S.H. (2013). Neuropeptide signaling remodels chemosensory circuit composition in Caenorhabditis elegans. Nat. Neurosci. *16*, 1461–1467.

Lemaitre, B., and Hoffmann, J. (2007). The host defense of Drosophila melanogaster. Annu. Rev. Immunol. *25*, 697–743.

Lemaitre, B., Nicolas, E., Michaut, L., Reichhart, J.M., and Hoffmann, J.A. (1996). The dorsoventral regulatory gene cassette spätzle/Toll/cactus controls the potent antifungal response in Drosophila adults. Cell *86*, 973–983.

Li, Z., Liu, J., Zheng, M., and Xu, X.Z.S. (2014). Encoding of both analog- and digital-like behavioral outputs by one C. elegans interneuron. Cell *159*, 751–765.

Luo, L., Gershow, M., Rosenzweig, M., Kang, K., Fang-Yen, C., Garrity, P.A., and Samuel, A.D.T. (2010). Navigational decision making in Drosophila thermotaxis. J. Neurosci. Off. J. Soc. Neurosci. *30*, 4261–4272.

Luo, L., Cook, N., Venkatachalam, V., Martinez-Velazquez, L.A., Zhang, X., Calvo, A.C., Hawk, J., MacInnis, B.L., Frank, M., Ng, J.H.R., et al. (2014). Bidirectional thermotaxis in Caenorhabditis elegans is mediated by distinct sensorimotor strategies driven by the AFD thermosensory neurons. Proc. Natl. Acad. Sci. *111*, 2776–2781.

McMeniman, C.J., Corfas, R.A., Matthews, B.J., Ritchie, S.A., and Vosshall, L.B. (2014). Multimodal integration of carbon dioxide and other sensory cues drives mosquito attraction to humans. Cell *156*, 1060–1071.

Meredith, M.A., and Stein, B.E. (1986). Visual, auditory, and somatosensory convergence on cells in superior colliculus results in multisensory integration. J. Neurophysiol. *56*, 640–662.

Morton, D.B. (2011). Behavioral responses to hypoxia and hyperoxia in Drosophila larvae. Fly (Austin) *5*, 119–125.

Ohnishi, N., Kuhara, A., Nakamura, F., Okochi, Y., and Mori, I. (2011). Bidirectional regulation of thermotaxis by glutamate transmissions in Caenorhabditis elegans. EMBO J. *30*, 1376–1388.

Pierce-Shimomura, J.T., Morse, T.M., and Lockery, S.R. (1999). The fundamental role of pirouettes in Caenorhabditis elegans chemotaxis. J. Neurosci. Off. J. Soc. Neurosci. *19*, 9557–9569.

Ramot, D., MacInnis, B.L., Lee, H.-C., and Goodman, M.B. (2008). Thermotaxis is a Robust Mechanism for Thermoregulation in Caenorhabditis elegans Nematodes. J. Neurosci. *28*, 12546–12557.

Ryu, W.S., and Samuel, A.D.T. (2002). Thermotaxis in Caenorhabditis elegans Analyzed by Measuring Responses to Defined Thermal Stimuli. J. Neurosci. *22*, 5727–5733.

Saeki, S., Yamamoto, M., and Iino, Y. (2001). Plasticity of chemotaxis revealed by paired presentation of a chemoattractant and starvation in the nematode Caenorhabditis elegans. J. Exp. Biol. *204*, 1757–1764.

Sasakura, H., and Mori, I. (2013). Behavioral plasticity, learning, and memory in C. elegans. Curr. Opin. Neurobiol. *23*, 92–99.

Satoh, Y., Sato, H., Kunitomo, H., Fei, X., Hashimoto, K., and Iino, Y. (2014). Regulation of Experience-Dependent Bidirectional Chemotaxis by a Neural Circuit Switch in Caenorhabditis elegans. J. Neurosci. *34*, 15631–15637.

Sieburth, D., Madison, J.M., and Kaplan, J.M. (2007). PKC-1 regulates secretion of neuropeptides. Nat. Neurosci. *10*, 49–57.

Smith, E.S.J., Martinez-Velazquez, L.A., and Ringstad, N. (2013). A chemoreceptor that detects molecular carbon dioxide. J. Biol. Chem. jbc.M113.517367.

Suh, G.S.B., Wong, A.M., Hergarden, A.C., Wang, J.W., Simon, A.F., Benzer, S., Axel, R., and Anderson, D.J. (2004). A single population of olfactory sensory neurons mediates an innate avoidance behaviour in Drosophila. Nature *431*, 854–859.

Turner, S.L., and Ray, A. (2009). Modification of CO2 avoidance behaviour in Drosophila by inhibitory odorants. Nature *461*, 277–281.

Valanne, S., Wang, J.-H., and Rämet, M. (2011). The Drosophila Toll Signaling Pathway. J. Immunol. *186*, 649–656.

Wakabayashi, T., Kitagawa, I., and Shingai, R. (2004). Neurons regulating the duration of forward locomotion in Caenorhabditis elegans. Neurosci. Res. *50*, 103–111.

Wang, Z., Wilhelmsson, C., Hyrsl, P., Loof, T.G., Dobes, P., Klupp, M., Loseva, O., Mörgelin, M., Iklé, J., Cripps, R.M., et al. (2010). Pathogen entrapment by transglutaminase--a conserved early innate immune mechanism. PLoS Pathog. *6*, e1000763.

White, J.G., Southgate, E., Thomson, J.N., and Brenner, S. (1986). The structure of the nervous system of the nematode Caenorhabditis elegans. Philos. Trans. R. Soc. Lond. B. Biol. Sci. *314*, 1–340.